

# Modelling biologically important NH... $\pi$ interactions

Alexander F. Pozharskii,<sup>1</sup> Olga V. Dyablo,<sup>1</sup> Valery A. Ozeryanskii,<sup>1</sup> Olga G. Pogosova

Department of Organic Chemistry, Southern Federal University,  
ul. Zorge 7, 344090 Rostov-on-Don, Russian Federation

The review summarizes the information accumulated to date on NH... $\pi$  interactions, which represent an unconventional type of hydrogen bonding between the NH-donor (most often amines, carboxamides or NH heterocycles) and a proton acceptor (usually an electron-rich aromatic or heteroaromatic rings). The importance of NH... $\pi$  interactions stems mainly from their involvement in the structuring of proteins and some other biomolecules, as well as in molecular recognition processes. The growth of knowledge on NH... $\pi$  interactions contributes to a better understanding of complex biochemical processes, stimulates the development of new drugs and improved methods of their targeted delivery. Since the study of NH... $\pi$  interactions on living tissues is rather difficult, their modelling on various synthetic objects has become widespread. In the review, various types of such models are systematized and compared in regard of their geometry, stereo dynamics, and NH... $\pi$  binding energy. Examples of reactions driven by NH... $\pi$  interaction are given, as well as examples of practical use. A rational classification of existing models is proposed, which facilitates their convenient consideration. The bibliography includes 196 references.

## Contents

1. Introduction	1	5. Folded/unfolded models	24
2. Research methods	4	5.1. Short peptide and diketopiperazine models	24
3. Unfolded models	4	5.2. Modelling neurotransmitters	27
3.1. NH... $\pi$ complexes of benzene with ammonia, amines and ammonium ions	4	6. Reactions driven by NH... $\pi$ interactions	31
3.2. NH... $\pi$ complexes of simple benzene derivatives	6	7. Miscellaneous issues	32
3.3. NH... $\pi$ complexes of condensed arenes	7	7.1. NH... $\pi$ interaction and recognition of $\alpha$ -amino acids	32
3.4. NH... $\pi$ complexes of arenes with (thio)carboxamides	8	7.2. NH... $\pi$ interaction and urea-assisted protein denaturation	32
3.5. NH... $\pi$ complexes with sulfonamides	9	7.3. NH... $\pi$ interaction in vitamin B <sub>12</sub> coenzyme	32
3.6. NH... $\pi$ complexes of arenes with NH-heterocycles	10	8. Practical applications of NH... $\pi$ interactions	33
3.7. NH... $\pi$ self-association of aniline and NH-heterocycles	13	9. Conclusion	35
3.8. <i>peri</i> -Disubstituted naphthalenes as NH... $\pi$ models	14	10. List of acronyms	35
4. Folded and caged models	18	11. References	36
4.1. One-component NH... $\pi$ systems	23		
4.2. Two-component NH... $\pi$ host-guest systems	23		
4.2.1. NH-Donor as a guest	23		
4.2.2. Benzene and other aromatics as guests	24		
4.3. Zip-complexes	24		

## 1. Introduction

One of the most important discoveries of the 20th century in the field of chemistry and molecular biology was the establishment of the structure of proteins, their functions in the body, the mechanism of biosynthesis and methods of synthetic production.<sup>1–3</sup> Proteins are polymer molecules formed during the sequential condensation of  $\alpha$ -amino acids, which is accompanied by elimination of water. In nature, this process, which involves 20 so-called proteinogenic acids, is controlled by genes. A variety of genes and countless amino acid sequences determine the intra- and interspecies differences in living organisms. The nature of proteins as linear polyamides (polypeptides) was established in 1902 by E. Fisher, and the specific sequence of amino acid

residues was called the primary structure of proteins (Fig. 1).

Half a century later, based on the data of X-ray diffraction analysis (XRD), Pauling and Corey<sup>4,5</sup> came to

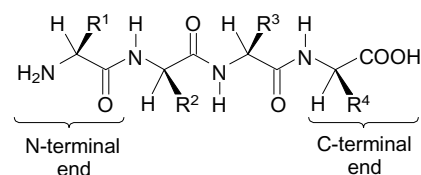


**Figure 1.** Fragment of polypeptide chain (primary protein structure) with amino acid residues containing different side groups R<sup>1</sup>–R<sup>4</sup>.



sine, and phenylalanine is 5:1.5:1, respectively.<sup>11</sup> It is believed that this sequence is determined by a decrease in the surface of the  $\pi$ -system in the given series and, consequently, by an increase in its first ionization potential (IP<sub>1</sub>).

One of the key issues concerns parameters of the XH $\cdots\pi$  bond and the directionality of the X–H vector to the aromatic ring face. As applied to NH donors, these parameters include the NH $\cdots$ M and N $\cdots$ M distances, where M is the centroid of the ring, the linearity of the HB (NHM angle), and the angle  $\omega$  between the perfectly linear HB and the normal to the ring plane (Fig. 4). In cases where the N–H vector is more oriented to one of the ring C<sub>*i*</sub> atoms or to middle of the ring C–C bond than to the centroid, the corresponding N $\cdots$ C<sub>*i*</sub> and NH $\cdots$ C<sub>*i*</sub> distances are also considered.

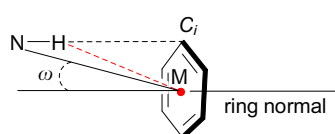


**Figure 4.** Schematic representation showing orientation of N–H vector to the aromatic ring centroid (M) and the nearest carbon atom (C<sub>*i*</sub>). The figure was created by the authors using data of Ref. 11.

In reality, the NH $\cdots\pi$  bond is rarely linear and the NHM angle is almost always less than 180°. This is explained by the fact that the NH proton is also attracted to other nearby electronegative atoms, primarily to the oxygen of the OH, C=O groups or water molecules (Fig. 5*a*). Another common factor distorting the geometry of NH $\cdots\pi$  bonds is the pronounced tendency of the aromatic ring planes to stack with NH-donor groups.

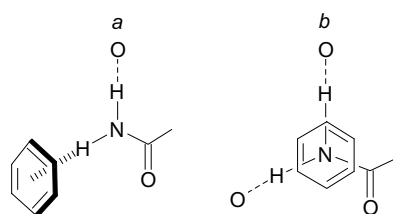


**Figure 5.** NH $\cdots\pi$  bond (*a*) and stacking (*b*) with participation of carboxamide group. The figure was created by the authors using data of Refs 11, 17.

This type of interaction is especially characteristic of planar NH donors with a sp<sup>2</sup>-hybridized nitrogen atom and a sufficiently large surface.<sup>11, 17</sup> These include the carboxamide group in asparagine and glutamine (Fig. 5*b*), the indole system in tryptophan, as well as guanidinium and imidazolium cations in protonated arginine and histidine. Analysis of a large number of XRD protein structures showed that the border between stacking and NH $\cdots\pi$  interaction is rather blurred. Conventionally, the latter include clusters with an angle  $\omega < 25^\circ$ , while stacking occurs with  $\omega$  near 90° and slightly lower.<sup>11, 17</sup> For the absolute majority of the studied proteins, the  $\omega$  value lies in the range of 45–60°. In fact, stacking and NH $\cdots\pi$  interactions are superimposed on each other, with the former

dominating in a ratio of  $\sim 2.5:1$ .<sup>11</sup> It is believed that due to stacking, the potential of NH bonds is partially released for interaction with other partners, including aromatic nuclei, which gives an additional gain in energy.<sup>11, 17</sup> As Table 1 shows, for uncharged NH donors (carboxamide groups), the average interaction energy is about 4.4 kcal mol<sup>-1</sup>, while for the positively charged guanidinium and imidazolium systems of arginine and histidine, it is almost twice as large (8.0 kcal mol<sup>-1</sup>). These values include both the electrostatic and dispersion components, which can be separated in the calculation.<sup>17</sup> As for the NH $\cdots$ M and N $\cdots$ M distances in protein clusters, in those cases when the NH $\cdots\pi$  interaction prevails over stacking, they amount to 3.2–3.8 and  $< 4.3$  Å, respectively. If stacking dominates, the NH $\cdots$ M values noticeably increase, falling within the range of 3.8–5.0 Å.<sup>11</sup>

Now, let us clarify the question of where in the polypeptide chain amino acid residues can be located to form an NH $\cdots\pi$  bond between them, and in what terms it is usually expressed. It is known that the polypeptide chain is usually read from the *N*-terminal amino acid residue (see Fig. 1). Accordingly, the NH-donor moiety is denoted by the symbol *i* (sometimes *n*), and the following amino acid residues by the symbols (*i* + 1), (*i* + 2), etc. If the NH $\cdots\pi$  bond is formed with the moiety following the NH-donor and bearing the aromatic moiety, then this interaction is characterized as *i* → (*i* + 1). In the case when the aromatic residue precedes the NH-donor, the interaction is designated as *i* → (*i* – 1). The most common interactions in proteins are of the type *i* → (*i* – 2), followed by *i* → (*i* + 3) with a large margin. However, there are also many inter-

**Table 1.** Gas-phase interaction energies calculated by the 3-21G IMPT method between the benzene ring of phenylalanine and carboxamide, guanidinium, and imidazolium groups in some proteins.<sup>17</sup>

Protein code <sup>a</sup>	Interacting groups	Interaction energy, kcal mol <sup>-1</sup> (see <sup>b</sup> )	Predominant type of interaction
7rsa	Asn 44 – Phe 46	3.58	NH $\cdots\pi$
6xia	Asn 91 – Phe 93	3.61	Stacking
2gbp	Asn 256 – Phe 16	3.70	Stacking
lova	Gln A223 – Phe A198	6.26	NH $\cdots\pi$
3fgf	Arg 107 – Phe 95	5.61	Stacking
2fb4	Arg H19 – Phe H80	6.55	Stacking
5tmn	Arg E260 – Phe E178	6.67	Stacking
1snc	Arg 81 – Phe 76	7.03	NH $\cdots\pi$
2cyp	Arg 127 – Phe 276	7.74	Stacking
6xia	Arg 176 – Phe 241	8.48	Stacking
5tmn	Arg E101 – Phe E40	8.53	NH $\cdots\pi$
4ptp	Arg 65A – Phe 82	8.68	Stacking
2hms	Arg A110 – Phe A107	8.72	Stacking
2fb4	Arg H72 – Phe H29	9.80	NH $\cdots\pi$
2fb4	Arg H98 – Phe H27	10.07	NH $\cdots\pi$
2cdv	His 35 – Phe 76	7.12	Stacking
2tsc	His A57 – Phe A 244	7.24	Stacking
4bp2	His 48 – Phe 5	7.74	Stacking
2hmz	His A77 – Phe A 55	8.48	Stacking
5cpa	His 120 – Phe 116	11.09	NH $\cdots\pi$
1mbc	His 36 – Phe 106	11.71	Stacking
2cts	His 235 – Phe 397	12.84	NH $\cdots\pi$

<sup>a</sup> Code taken from Protein Data Bank (PDB). <sup>b</sup> Hereinafter the interaction (binding) energy is considered to be positive regardless of the conventions accepted in the original publications.

actions between highly distant amino acid residues (see, *e.g.*, Table 1). As a rule, this occurs in globular proteins in which the amino acid helix strand folds, most often due to the formation of sufficiently strong disulfide bonds between cysteine residues removed in the amino acid sequence ( $E_{S-S} = 55 \text{ kcal mol}^{-1}$ ). The resulting folded form, which is referred to as the tertiary proteins structure, provides closeness of the initially distant NH-donor and NH-acceptor ( $\pi$ -donor) and the formation of  $\text{NH}\cdots\pi$  bond between them.

$\text{XH}\cdots\pi$  bonds are often called soft ones. This means both their relatively low energy and a pronounced tendency to change geometry under the influence of various factors. The softness of  $\text{XH}\cdots\pi$  bonds allows them to participate in the fine tuning of protein conformations, which is necessary for the implementation of the corresponding biological functions.

Along with intramolecular, intermolecular  $\text{XH}\cdots\pi$  interactions are also very important. Most often, they manifest themselves when receptors of membrane proteins recognize signalling and exogenous molecules, for example, hormones, neurotransmitters, oligopeptides, drugs, *etc.*<sup>13, 14, 18</sup> In addition, they are responsible for the formation of quaternary protein structures, which include nucleoprotein complexes and complex proteins like hemoglobin, consisting of several interconnected polypeptide strands.

The above, along with the imposition of other non-covalent forces on the  $\text{XH}\cdots\pi$  interactions, makes their study directly on living tissues very difficult. Therefore, soon after the discovery of  $\text{XH}\cdots\pi$  interactions in proteins, studies were launched on their modelling on simpler synthetic objects. This review summarizes the information accumulated since then on this issue. We focused mainly on  $\text{NH}\cdots\pi$  interactions, given their high prevalence and, in part, our current research interests.<sup>19, 20</sup>

## 2. Research methods

The choice of research methods for model  $\text{NH}\cdots\pi$  clusters is primarily determined by their stability. Thus, in the case of simple and especially intermolecular models with the participation of benzene rings and neutral amino groups, the dissociation energy of  $\text{NH}\cdots\pi$  bonds does not exceed  $1-3 \text{ kcal mol}^{-1}$ . This greatly impedes XRD and solution studies. Therefore, most of the information concerning such models was obtained based on quantumchemical calculations, as well as gas-phase spectral measurements under conditions of a supersonic jet, which make it possible to strongly cool the sample.

The most commonly used laser spectroscopic method in the gas phase is the so-called double resonance IR/UV spectroscopy, based on a double optical excitation of jet-cooled neutral molecules, coupled to a fluorescence or mass-spectrometric detection. UV spectroscopy enables spectroscopists to selectively detect conformations or tautomers. IR/UV spectroscopy provides single-conformation IR spectra, which are then assigned by comparison with quantum chemistry calculations.

Individual components and variations of this method are also called laser-induced fluorescence excitation (LIF), dispersed fluorescence (DF), mass-resolved one-colour resonance enhanced two-photon ionization (RE2PI). Furthermore, various types of IR spectroscopy are often used, including combined IR/UV spectroscopy. A detailed

description of all this techniques can be found in the experimental part of some relevant works.<sup>8, 21</sup>

To simplify the experimental procedures and improve the reliability of the data, researchers seek to increase the stability of  $\text{NH}\cdots\pi$  complexes. This is especially facilitated by the creation of preorganized models and the use of positively charged proton donors, *e.g.*, ammonium salts. The advantage of preorganized structures is the proximity and optimal fixation of the NH-donor and NH-acceptor relative to each other. The resulting stabilization of  $\text{NH}\cdots\pi$  clusters makes it possible to carry out their comprehensive studies both in solid form and in solution.

One of the main features of the majority of biologically significant molecules is their high flexibility and, as a consequence, the existence in the form of an equilibrium mixture of many conformers. The latter usually have a crumpled or folded shape, although in some cases unfolded conformations may also be more advantageous. Following this circumstance, we will further consider the existing models of  $\text{NH}\cdots\pi$  clusters based on this principle.

## 3. Unfolded models

### 3.1. $\text{NH}\cdots\pi$ complexes of benzene with ammonia, amines and ammonium ions

Although the benzene molecule is often regarded as non-polar because of its symmetry consistent with zero dipole moment, this is not strictly the case. The point is that carbon atoms in benzene, being  $\text{sp}^2$  hybridized, have a slightly higher electronegativity than hydrogen atoms. As a result, the hydrogen edge of the ring acquires a partial positive charge, while the carbon rim with its  $\pi$ -electron sextet is negative (Fig. 6a). Such polarization makes benzene one of the strongest organic quadrupoles (Fig. 6b), the  $\pi$ -system of which can interact with numerous Lewis acids, including a proton, metal ions or ammonium cations.<sup>22-24</sup> Let us first consider the  $\pi$ -complexes of benzene with ammonia and other simple NH-donors.

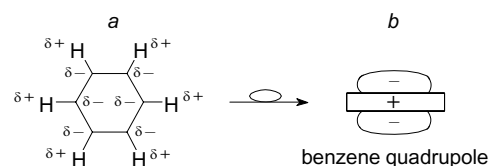


**Figure 6.** Polarization of C–H bonds (a) and schematic representation of quadrupole nature of the benzene ring (b). The figure was created by the authors using data of Ref. 22.

Apparently, the first report on the existence of the  $\text{C}_6\text{H}_6 \cdot \text{NH}_3$  complex, in which ammonia acts as a proton donor for the benzene  $\pi$ -system, appeared in *Nature* in 1993 (Ref. 25) (see also the review<sup>26</sup>). The evidences for this were obtained for supersonic jet conditions and were based on RE2PI method and high-resolution IR spectroscopy. In addition, they were supported by quantum chemical calculations (*ab initio*, MP2/6-31G\*\*). The results indicated that in vapours with a deficiency of ammonia (the latter is necessary to minimize the formation of a stronger HB between  $\text{NH}_3$  molecules), monodentate complex **1** is formed, in which only one N–H bond is oriented to the centroid of the benzene ring (Fig. 7). In this case, the rotational  $\text{C}_3$  axis of the  $\text{NH}_3$  molecule is inclined to the

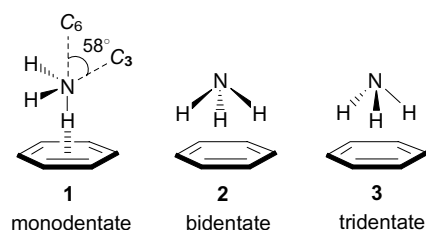


**Figure 7.** Mono-, bi- and tridentate benzene–ammonia complexes. The figure was created by the authors using data of Refs 25, 26.

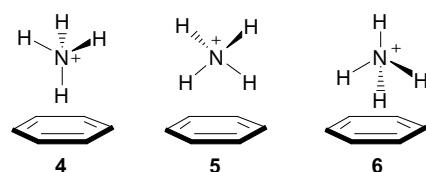
$C_6$  axis of the ring at an angle of  $58^\circ$ . Simultaneously, the  $NH_3$  molecule rapidly rotates around the  $N-H$  bond vector, which makes it possible for two other  $NH$  atoms to be attracted to the carbon edge of the ring. The minimum  $N\cdots M$  distance for the theoretically optimized structure **1** is  $3.6 \text{ \AA}$ .<sup>26</sup> The experimental value of the  $NH\cdots\pi$  bond energy in the  $C_6H_6\cdot NH_3$  complex was estimated as  $1.4 \text{ kcal mol}^{-1}$  (see Ref. 27) ( $1.84 \pm 0.12 \text{ kcal mol}^{-1}$  according to other data<sup>28,29</sup>) while quantumchemical calculations, depending on their level, ranged from  $0.1$  to  $2.4 \text{ kcal mol}^{-1}$ .

It is believed that the  $NH_3$  molecule, known for the ease of pyramidal inversion, when complexed with benzene, does not undergo such inversion. The first ionization potential ( $IP_1$ ) of complex **1** is  $9.07 \pm 0.03 \text{ eV}$ ,<sup>27</sup> which is slightly lower than  $IP_1$  of benzene itself ( $9.21 \text{ eV}$ ). It was suggested that the  $NH\cdots\pi$  bond in complex **1** is predominantly electrostatic<sup>30</sup> with a certain contribution from the dispersion component.<sup>26,30</sup>

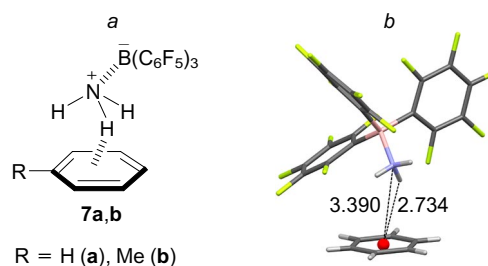
Di- and tridentate structures **2** and **3** were also considered, which, according to theoretical calculations, should be slightly less stable.<sup>25,26</sup> At the same time, the analysis of the  $NH$  stretching vibrations in IR spectra and a number of other measurements testified to the existence of bidentate complex **2**.<sup>31</sup>

As expected, based on the much higher proton-donating ability of the ammonium ion compared to that of ammonia, the  $C_6H_6\cdot NH_4^+$  complex is about an order of magnitude more stable than  $C_6H_6\cdot NH_3$ . Thus, according to MP2 calculations of mono-, bi-, and tridentate complexes **4–6** (Fig. 8), their energy (without BSSE correction) in the gas phase is  $21.7$ ,  $22.4$ , and  $20.0 \text{ kcal mol}^{-1}$ , respectively. At the same time, the  $N\cdots M$  distance decreases from  $3.6 \text{ \AA}$  in  $C_6H_6\cdot NH_3$  down to  $2.9 \text{ \AA}$  in  $C_6H_6\cdot NH_4^+$ .<sup>32</sup>

Of interest are  $NH\cdots\pi$  complexes **7a,b** of benzene and toluene with the Lewis adduct of ammonia with tris(pentafluorophenyl)borane  $NH_3\cdot B(C_6F_5)_3$  (Fig. 9a), which were successfully characterized by XRD and IR spectroscopy.<sup>33</sup> As can be seen from Fig. 9b, the nitrogen atom is located approximately above the centre of the benzene ring, while

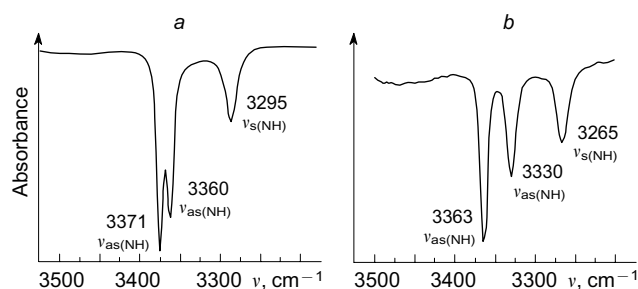


**Figure 8.** Mono-, bi- and tridentate benzene–ammonium ion complexes. The figure was created by the authors using data of Ref. 32.



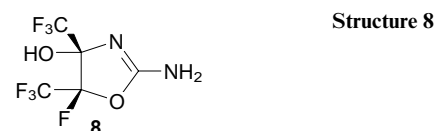
**Figure 9.**  $NH\cdots\pi$  Complexes of tris(pentafluorophenyl)borane–ammonia with benzene and toluene (**7a,b**) (a) and molecular structure of **7a** with selected key distances in  $\text{\AA}$  (b) (CCDC refcode UBUBAW,  $T = 90 \text{ K}$ ). The figure was created by the authors using data of Ref. 33.

the proton participating in the formation of the  $NH\cdots\pi$  bond is slightly deflected from it. The  $N\cdots M$  distances in solid complexes **7a,b** are  $3.28$  and  $3.21 \text{ \AA}$ , while the  $NH\cdots M$  distances are  $2.64$  and  $2.48 \text{ \AA}$ , respectively. These values are intermediate between the analogous distances in the complexes  $C_6H_6\cdot NH_3$  and  $C_6H_6\cdot NH_4^+$  (only theoretically calculated data are available for the latter two). As might be expected, the maxima of symmetric and asymmetric  $NH$  stretching vibrations in the IR spectra of complexes **7a** are shifted towards lower frequencies by  $30 \text{ cm}^{-1}$  (Fig. 10). Although accurate data on the  $NH\cdots\pi$  hydrogen bond energy in complexes **7a,b** are lacking, there are some indications on their insufficient stability. Thus, when dried under reduced pressure, **7a** lost a benzene molecule. Similarly,  $^1H$  NMR spectrum of **7a** in  $CDCl_3$  represents an overlay of the spectra of benzene and the  $(C_6F_5)_3B\cdot NH_3$  complex, which indicates the displacement of the benzene molecule by deuteriochloroform.



**Figure 10.** Region of stretching vibrations of  $N-H$  bonds in IR spectra (nujol) of  $(C_6F_5)_3B\cdot NH_3$  (a) and complex **7a** (b). The figure was created by the authors using data of Ref. 33.

There are few examples of  $NH\cdots\pi$  complexes between benzene and amines. One of them concerns the 2-amino-4,5-dihydrooxazole derivative **8**, which was isolated as a solvate with a benzene molecule.<sup>34</sup> XRD study revealed the presence of a distinct and moderately short ( $2.66 \text{ \AA}$ )  $NH\cdots\pi$  bond between one of the hydrogen atoms of the  $NH_2$  group and the benzene ring centroid in the crystal lattice of **8**



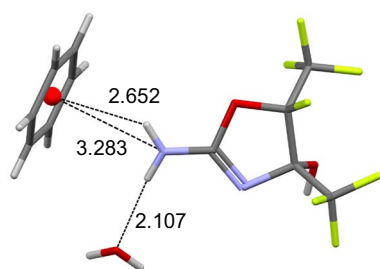


**Figure 11.**  $\text{NH}\cdots\pi$  and  $\text{NH}\cdots\text{O}$  interactions in benzene solvate hemihydrate of amine **8** (NAJPIZ, 100 K). The figure was created by the authors using data of Ref. 34.

(Fig. 11). The  $\text{N}\cdots\text{M}$  distance is 3.28 Å, while the second amine proton forms a 2.11 Å long  $\text{NH}\cdots\text{O}$  bond with the solvate water molecule. Notably, that although the  $\text{OH}\cdots\pi$  interaction is usually stronger than  $\text{NH}\cdots\pi$ , the 4-OH group in **8** does not participate in it, what can be explained by its spatial shielding. Other complexes of this kind between 2-aminobenzothiazole and phenylacetic acid have been also documented.<sup>35</sup> A specific cluster of benzene with dimethylammonium cation is described in Section 4.1 (structure **86**).

### 3.2. $\text{NH}\cdots\pi$ complexes of simple benzene derivatives

The complexity of the study of  $\text{NH}\cdots\pi$  complexes of benzene derivatives, in addition to their instability, lower symmetry, and mutual influence of the benzene ring and the substituent, lies in the possibility of the formation of HBs not only with the ring  $\pi$ -system, but also with a substituent (especially when it contains lone electron pairs). In the first case, we will consider such a cluster as a  $\pi$ -complex, and in the second, as a  $\sigma$ -complex. In this regard, we'll discuss a comparative study of the interaction in the gas phase of ammonia with benzene, toluene, chlorobenzene, fluorobenzene and 1,4-difluorobenzene.<sup>31</sup> For this, the two-photon resonance ionization (R2PI), microwave and predissociation IR spectroscopy in the region of stretching vibrations of  $\text{N}-\text{H}$  bonds were employed. The experimental results were compared with *ab initio* calculations (MP2 theory level). Both approaches were in good agreement with each other and showed the formation of the complexes depicted in Fig. 12.

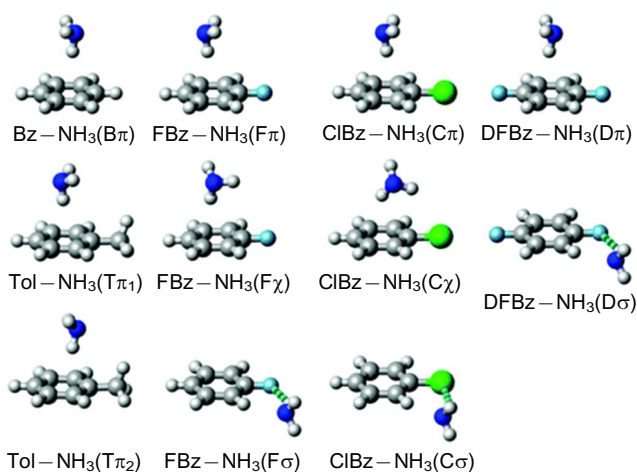


**Figure 12.** Theoretically optimized structures of  $\sigma$ -,  $\pi$ - and  $\pi,\sigma$ -complexes of ammonia with benzene and its fluoro-, chloro-, difluoro- and methyl derivatives. Reproduced from Ref. 31 with permission of the American Chemical Society.

In agreement with the data of the aforementioned study,<sup>25</sup> it was found that benzene forms only a monodentate  $\pi$ -complex in the gas phase. In the case of toluene, the monodentate  $\pi$ -complex, existing in the form of two rotational conformers, was also identified. In one of them, all three  $\text{N}-\text{H}$  bonds are directed towards the methyl group, while in the other they point to the opposite direction. In the case of fluoro- and chlorobenzenes, the data were interpreted in favour of the formation of three complexes. The  $\sigma$ -structure with  $\text{NH}\cdots\text{F}(\text{Cl})$  hydrogen bond was attributed to one of them, to the second, the structure of the  $\pi$ -complex was assigned, while the third one was determined as a  $\sigma,\pi$ -cluster of mixed type. For 1,4-difluorobenzene, two monodentate complexes with  $\text{NH}\cdots\pi$  and  $\text{NH}\cdots\text{F}$  bonds were detected. However, later, based on the rotational spectra, an unambiguous conclusion was made that the only stable 1,4-difluorobenzene- $\text{NH}_3$   $\sigma$ -complex can exist.<sup>36,37</sup>

The average value of the calculated binding energies for the considered  $\pi$ -complexes was estimated at 3–3.5 kcal mol<sup>-1</sup> without taking zero-point energy (ZPE) into account and about 2.5 kcal mol<sup>-1</sup> with ZPE. The smallest (3.39 Å)  $\text{NH}\cdots\text{M}$  distance for the  $\pi$ -complexes and the largest stability were recorded for the toluene- $\text{NH}_3$  complex. It was also noted that the structure of ammonia  $\pi$ -complexes of benzene compounds is largely determined by dispersion forces. In another study of this kind, based on the data of resonance-enhanced multiphoton ionization spectroscopy (REMPI) and quantumchemical calculations (RICC2 method), Gosling *et al.*<sup>38</sup> concluded that fluorobenzene forms only  $\sigma$ -complex with ammonia.

For 4-fluorotoluene-ammonia complex, two-photon ionization spectra featured signals of two forms assigned to the  $\text{NH}\cdots\text{F}$   $\sigma$ -complex **9a** and the  $\pi$ -complex with the  $\text{NH}\cdots\pi$  hydrogen bond **9b** (Fig. 13). In this case, the signals in the low-frequency region of the spectrum were assigned to the  $\pi$ -complex, and in the high-frequency region, to the  $\sigma$ -complex. A quantumchemical calculation gave close values of bond energies in two forms.<sup>38</sup> Similar conclusions based on the study of IR/UV double resonance spectra were also reached by Cocket *et al.*<sup>40</sup> with the difference that the assignment of signals in the high-frequency and low-frequency regions attributed to  $\text{N}-\text{H}$  bonds was inverse.

From the set of experimental and calculated data, anisole-ammonia complex was assigned structure **10**, in which the ammonia molecule is bound to anisole by three hydrogen bonds of  $\text{NH}\cdots\text{O}$ ,  $\text{N}\cdots\text{HC}$  and  $\text{NH}\cdots\pi$  types (see Fig. 13).<sup>39</sup> In a study,<sup>41</sup> the length of the  $\text{NH}\cdots\pi$  bond in the anisole- $\text{NH}_3$  complex was estimated at 3.02 Å, and its dissociation energy at 3.82 kcal mol<sup>-1</sup>, which looks quite realistic.

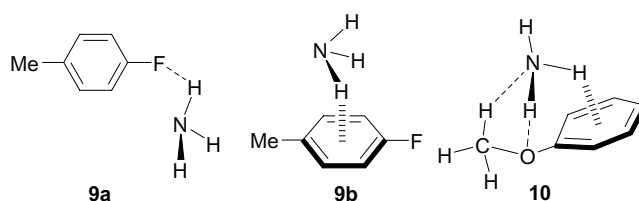


**Figure 13.** Structures suggested for complexes 4-fluorotoluene- $\text{NH}_3$  (**9a,b**) and anisole- $\text{NH}_3$  (**10**). The figure was created by the authors using data of Refs 38, 39.

The interaction of phenylacetylene with ammonia, methylamine, water and methanol as proton donors has been studied.<sup>42,43</sup> Due to more extended  $\pi$ -system and a lower ionization potential than that of benzene (8.82 eV vs 9.24 eV), phenylacetylene should exhibit a greater tendency to form  $\text{NH}\cdots\pi$  complexes. Fortunately, such complexes are quite informative because of the presence of easily detectable  $\text{C}\equiv\text{C}$  and  $\text{C}_{\text{sp}}-\text{H}$  bonds. On the other hand, methylamine, like ammonia, has a fairly high basicity and very low NH-acidity, which is why, when forming hydrogen bonds, they tend to behave more like proton acceptors than proton donors. As research methods, the double IR/UV spectroscopy and a wide range of quantumchemical methods (mainly *ab initio* with the MP2 level of theory) were employed.

As can be seen from Fig. 14, the IR spectrum of phenylacetylene contains three bands of stretching vibrations of the  $\text{C}_{\text{sp}}-\text{H}$  bond, namely, two intense ones at 3325 and 3343  $\text{cm}^{-1}$  and one of low intensity at 3334  $\text{cm}^{-1}$ , located strictly between the first two ( $\pm 9 \text{ cm}^{-1}$ ). The latter is attributed to the vibrations of the unperturbed C–H bond, while the other two are considered as a consequence of the so-called Fermi resonance, reflecting the resonance of the  $\nu_{\text{C}-\text{H}}$  vibrations with two out-of-plane vibrations of the  $\text{C}\equiv\text{C}$  bond. It is known that the Fermi resonance disappears when the  $\text{C}\equiv\text{C}$  triple bond enters into any interactions, for example, of the  $\pi$ -type.

Experimental and theoretical data clearly indicate that, upon the interaction of phenylacetylene with ammonia, only structure **11** with the  $\text{C}_{\text{sp}}\text{H}\cdots\text{N}$  hydrogen bond is realized, in which ammonia behaves as a proton acceptor.<sup>42</sup> This is evidenced by a strong displacement (by 103  $\text{cm}^{-1}$ ) of the  $\nu(\text{C}_{\text{sp}}-\text{H})$  bond to the low-frequency region. The stabilization of this complex and the absence of  $\text{NH}\cdots\pi$  interaction is not surprising, since the acidity of the CH bond ( $\text{p}K_{\text{a}}$  23.2) in phenylacetylene is 10 orders of magnitude higher than the NH-acidity of ammonia ( $\text{p}K_{\text{a}}$  33). It is assumed that electrostatic forces dominate here.<sup>43</sup>

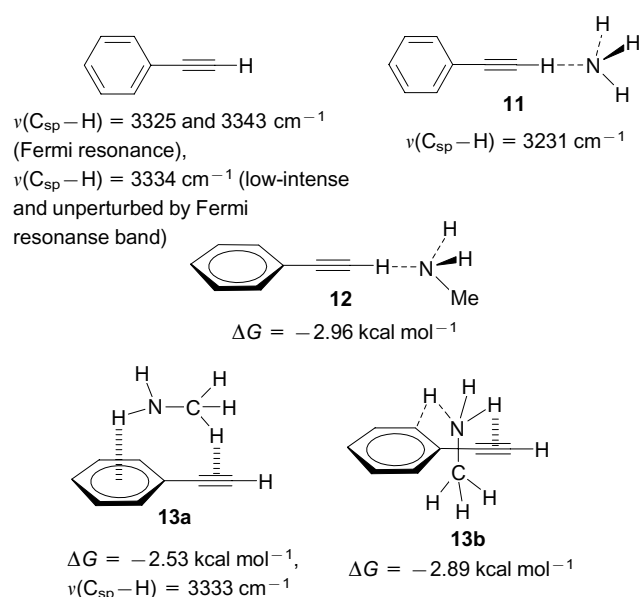


**Figure 14.** Phenylacetylene and its complexes with  $\text{NH}_3$  and  $\text{MeNH}_2$ . The figure was created by the authors using data of Refs 42, 43.

Surprisingly, the phenylacetylene–methylamine complex, according to its IR spectrum, has a completely different structure, although the basicity of  $\text{MeNH}_2$  ( $\text{p}K_{\text{a}}$  10.6) is almost 1.5 orders of magnitude higher than that of  $\text{NH}_3$  ( $\text{p}K_{\text{a}}$  9.2). Indeed, the  $\nu(\text{C}_{\text{sp}}-\text{H})$  band in this complex, just like in phenylacetylene itself, lies at 3333  $\text{cm}^{-1}$ , simultaneously losing the triplet structure characteristic of the Fermi resonance. Based on quantumchemical calculations of the  $\text{PhC}\equiv\text{CH}\cdot\text{MeNH}_2$  complex, three optimized structures **12** and **13a,b** were revealed, which correspond to potential energy minima (see Fig. 14).<sup>43</sup> Structure **12** fits a global minimum, while structures **13a** and **13b** are local ones. Based on the spectral data, preference was given to structure **13a**, in which methylamine forms two  $\pi$ -bonds, acting as a CH-donor with respect to the  $\text{C}\equiv\text{C}$  bond and as an NH-donor with respect to the benzene ring. The abnormal behaviour of methylamine in comparison with ammonia was explained by a more extensive bond system in the former, which highlights not electrostatic, but dispersion interactions with the participation of both components of the complex.

It was also suggested<sup>43</sup> that complex **13a** is the primary kinetic product of the reaction, while structure **13b** is a thermodynamic product into which **13a** transforms over time. To the naturally arising question of why complex **13b** is thermodynamic and not **12**, it was noted that, firstly, the energy difference between both types of clusters is very small and, secondly, the corresponding  $\Delta G$  values substantially depend on the chosen calculation method. Under these circumstances, it cannot be ruled out that complex **13a** may also be more stable, as evidenced by the IR spectroscopic data.

An IR/UV study of the interaction of phenylacetylene with triethylamine was also reported.<sup>42</sup> Despite the even greater basicity of  $\text{Et}_3\text{N}$  ( $\text{p}K_{\text{a}}$  10.9) as compared to  $\text{NH}_3$ , it, like methylamine, does not form  $\sigma$ -cluster of the  $\text{PhC}\equiv\text{C}-\text{H}\cdots\text{N}(\text{Et})_3$  type. In contrast to methylamine, the IR spectrum of the complex with  $\text{Et}_3\text{N}$  retains the Fermi resonance for the  $\nu(\text{C}_{\text{sp}}-\text{H})$  band. Taken together, these data indicate that the interaction of triethylamine with phenylacetylene does not affect the  $\text{C}\equiv\text{C}$  bond and has dispersion nature touching on mostly the benzene ring  $\pi$ -system.

### 3.3. $\text{NH}\cdots\pi$ complexes of condensed arenes

There are few reports on this topic. The 1-naphthol– $\text{NH}_3$  complex was studied by rotational spectroscopy and two-photon resonance ionization, which was supplemented by quantumchemical calculations.<sup>44</sup> Using the *ab initio* method (MP2 level of theory), the stability of two 1-naphthol– $\text{NH}_3$  isomeric structures with a composition of 1:2 was compared, one of which (**14a**) contains only the conventional  $\text{OH}\cdots\text{N}$  and  $\text{NH}\cdots\text{N}$  intermolecular HBs, and the other (**14b**) also contains an  $\text{NH}\cdots\pi$  bond (Fig. 15). Although both forms have similar energies, the rotational spectroscopic data are more consistent with structure **14b**. The latter differs by the smallest distance (2.568 Å) between NH proton and the centroid of the nearest benzene ring.

An anthracene–ammonia complex was examined using fluorescence spectra and a number of other methods.<sup>45</sup> According to the data obtained, the ammonia molecule was proposed to be located above the central benzene ring with a distance  $\text{N}\cdots\text{M}$  of 3.6 Å (Fig. 16), which is typical of HBs in other ammonia complexes of arenes. Based on the calculation results, it was suggested that the internal rota-

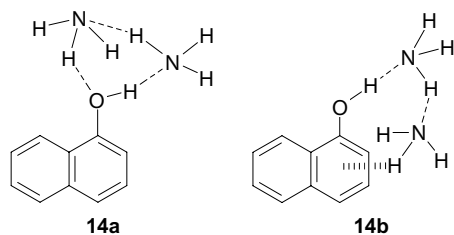


**Figure 15.** Proposed structures of isomeric 1:2 1-naphthol–NH<sub>3</sub> complexes. The figure was created by the authors using data of Ref. 44.

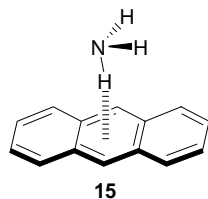


**Figure 16.** Supposed structure of anthracene–NH<sub>3</sub> complex. The figure was created by the authors using data of Ref. 45.

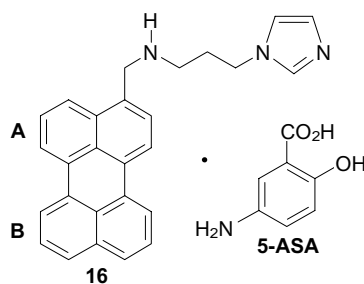


**Figure 17.** Fluorescent reagent **16** for the determination of 5-aminosalicylic acid (**5-ASA**). The figure was created by the authors using data of Ref. 46.

tion of the NH<sub>3</sub> molecule in complex **15** relative to the centre of mass of ammonia and anthracene is hindered due to the anisotropy of the  $\pi$ -system.

Pandith *et al.*<sup>46</sup> created a highly sensitive fluorescent sensor based on imidazole-containing perylene **16** for determining the drug 5-aminosalicylic acid (**5-ASA**). The action of the sensor is based on the formation of a stable 1:1 complex with **5-ASA**, in which, in addition to stacking and H-bonding between the imidazole ring and the carboxyl group, the components are connected also by NH $\cdots\pi$  bonds (3.55 Å) between the NH<sub>2</sub> group of **5-ASA** and the **B** fragment of the perylene system (Fig. 17).

### 3.4. NH $\cdots\pi$ complexes of arenes with (thio)carboxamides

The importance of such complexes is determined by the fact that they are especially often found in proteins<sup>11,16</sup> and some other natural compounds, for example, vitamin B<sub>12</sub> (see Section 7.3). Apparently, the Nikolic's group pioneered in considering the issue of modelling the corresponding NH $\cdots\pi$  interactions using benzene and its alkyl derivatives as  $\pi$ -donors and *N*-alkylcarboxamides as proton donors.<sup>47–50</sup> The frequencies of stretching vibrations  $\nu_{\text{NH}}$  in *N*-methyl-, *N*-ethyl-, *N*-butyl- and *N*-cyclohexyl derivatives of formamide, acetamide and propionamide were measured, using a 10–100 molar excess of arene as a solvent (Table 2). It was noted that, in comparison with solutions of carboxamides in CCl<sub>4</sub> ( $\nu_{\text{NH}} = 3455 \text{ cm}^{-1}$ ) in arene media, this band noticeably shifts to the low-frequency region. This observation was attributed to the formation of an NH $\cdots\pi$  hydrogen bond between the NH proton and the benzene

**Table 2.** Shifts of  $\nu_{\text{NH}}$  value in the IR spectra of non-associated carboxamides in arene media and the stability constants of arene–amide  $\pi$ -complexes (selected data).

Carboxamide	$\pi$ -Donor	$\Delta\nu_{\text{NH}}$ , cm <sup>-1</sup>	Stability constant, dm <sup>3</sup> mol <sup>-1</sup>	Ref.
<i>N</i> -Cyclohexyl- formamide	Benzene	–23	0.190	47
	Toluene	–28	0.257	47
	Ethylbenzene	–30	0.274	47
	<i>n</i> -Butylbenzene	–32	0.283	47
<i>N</i> - <i>tert</i> -Butyl- formamide	Benzene	–23	0.26	48
	Toluene	–29	0.31	48
	Ethylbenzene	–30	0.33	48
	<i>n</i> -Butylbenzene	–31	0.35	48
	<i>p</i> -Xylene	–32	0.36	48
	Mesitylene	–38	0.43	48
	Durene	–42	0.50	48
<i>N</i> -Ethylacet- amide	Benzene	–19	0.29	49
	Toluene	–24	0.37	49
<i>N</i> -Methyl- propionamide	Benzene	–19	0.23	49
	Toluene	–24	0.28	49
	Ethylbenzene	–26	0.32	49
	<i>n</i> -Propylbenzene	–28	0.35	49
	<i>p</i> -Xylene	–31	0.38	49
<i>N</i> - <i>n</i> -Butyl- propionamide	Benzene	–20	0.20	50
	Toluene	–25	0.25	50
	Ethylbenzene	–26	0.30	50
	<i>n</i> -Propylbenzene	–27	0.32	50
<i>N</i> - <i>tert</i> -Butyl- propionamide	Benzene	–18	0.16	50
	Toluene	–23	0.20	50
	Ethylbenzene	–25	0.20	50
	<i>n</i> -Propylbenzene	–26	0.23	50

ring. This was also supported by the fact that the displacement values,  $\Delta\nu_{\text{NH}}$ , (as well as the integral intensity of the band and the stability constants of the complexes) increased upon the introduction of alkyl substituents into the aromatic ring (see Table 2).

Cheng *et al.*<sup>51</sup> significantly contributed to these studies by estimating geometric and energetic parameters of arene–carboxamide complexes. As a model, a benzene–*N*-methylformamide complex was used, for which quantum-chemical calculations were performed using the MP2 method. It was found that the N $\cdots$ M distance, depending on parameters of the calculation, is in the range 3.2–3.6 Å, while the HB energy for the optimized structure is 4.37 kcal mol<sup>-1</sup> in average. This is almost twice as much as for the C<sub>6</sub>H<sub>6</sub>·NH<sub>3</sub> complex, which can be due to the increased NH-acidity of carboxamides ( $\text{p}K_{\text{a}} \approx 14–16$ ) in comparison with ammonia and alkylamines ( $\text{p}K_{\text{a}} \approx 33–35$ ).<sup>52</sup>

In compounds in which the arene and amide components are part of one molecule, the situation is more complicated, and, in the solid form, the amide hydrogen bonds NH $\cdots$ O=C usually prevail over NH $\cdots\pi$  ones. Examples are acetamidonaphthalenes **17**<sup>53</sup> and **18**.<sup>54</sup> Thus, when considering the XRD structure of each individual molecule

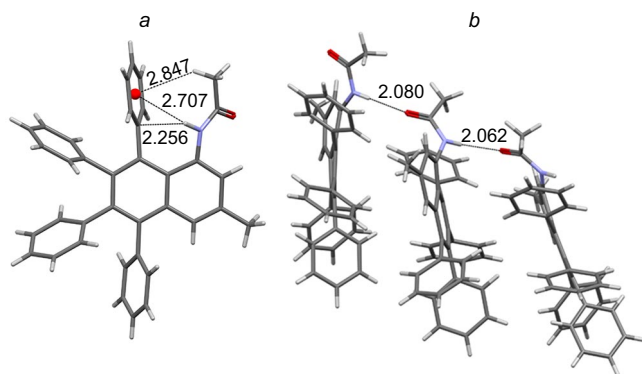
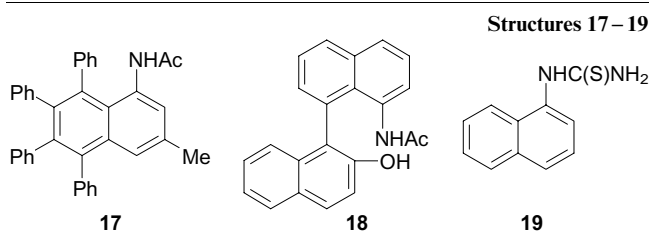


**Figure 18.** Molecular structure of one of three independent molecules of **17** (FAGTAK, 283–303 K) (a) and a fragment of crystal packing of **17** (b). The figure was created by the authors using data of Ref. 53.

**17** (Fig. 18 a), one might get the impression that  $\text{NH}\cdots\pi$  and  $\text{CH}\cdots\pi$  interactions between the acetamido group and the phenyl ring at position 8 dominate. This is supported by the very short distance (2.26 Å) between the NH proton and the  $C_i$  atom of the phenyl substituent. At the same time, attention should be drawn to the poor orientation of the N–H vector to the face of the 8-Ph group: the dihedral angle between this plane and the H–N–C=O plane of the amide group is only  $32.1^\circ$ . The reason for this becomes clear when considering the crystal lattice of amide **17** (Fig. 18 b). It consists of chains in which the naphthalene rings of neighbouring molecules are located approximately parallel to each other, and the C=O and N–H bonds are directed towards each other, forming amide hydrogen bonds  $\text{N–H}\cdots\text{O}=\text{C}$ . The length of these bonds (2.06–2.08 Å) is much shorter than those of  $\text{N–H}\cdots\text{M}$  and  $\text{N–H}\cdots\text{C}_i$  bonds (see Fig. 18 a). In fact, carbonyl oxygen in solid amide **17** forms bifurcated HBs such as a relatively weaker intramolecular  $\text{NH}\cdots\pi$  and a stronger intermolecular  $\text{NH}\cdots\text{O}=\text{C}$  bonds.



In binaphthyl amide **18**, two naphthalene systems are nearly orthogonal, thus making it possible for the amide NH-group to enter  $\text{NH}\cdots\pi$  interaction with the benzene ring of another naphthalene moiety, which is activated by the OH group (Fig. 19). In this case, the  $\text{NH}\cdots\text{M}$  distance (2.78 Å) is slightly less than the sum of the van der Waals (VDW) radii of hydrogen atom (1.2 Å) and the half-width of the benzene ring ( $\sim 1.7$  Å) (2.513 Å). The NH-proton is even closer to the  $C_i$  atom of the same benzene ring, *i.e.*, the  $\text{NH}\cdots\pi$  interaction in **18** is quite efficient.

Probably, in compound **18** there is also a relatively weak interaction of the NH-proton with the oxygen atom of the OH group, to which, along with electrostatic, dispersion forces make some contribution. Neighbouring carbonyl and hydroxyl groups are involved in the formation of the crystal

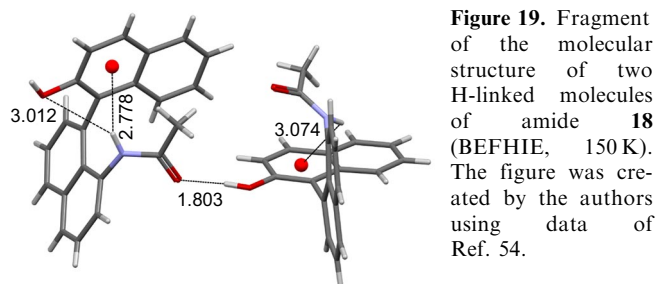


**Figure 19.** Fragment of the molecular structure of two H-linked molecules of amide **18** (BEFHIE, 150 K). The figure was created by the authors using data of Ref. 54.

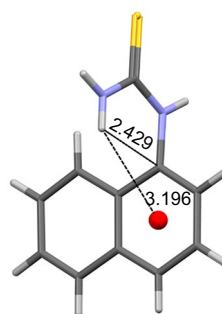


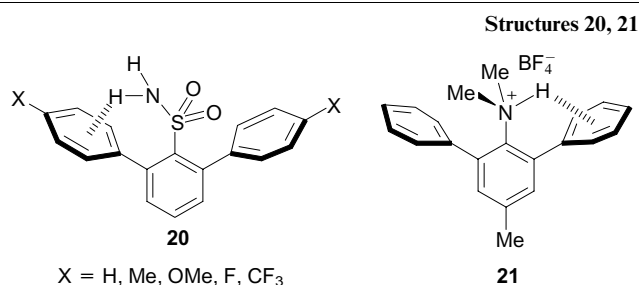
**Figure 20.** Molecular structure of 1-(1-naphthyl)-2-thiourea **19** (MOJDAS, 100 K). The figure was created by the authors using data of Ref. 55.

lattice of **18**: the length of  $\text{C}=\text{O}\cdots\text{HO}$  hydrogen bonds is only 1.80 Å (see Fig. 19). For additional information on the involvement of carboxamide groups in  $\text{NH}\cdots\pi$  interactions see Sections 3.8, 4, 5, 7.2, 8 and reviews.<sup>11, 16</sup>

The data of the XRD study of 1-(1-naphthyl)-2-thiourea **19** revealed the presence of  $\text{NH}\cdots\pi$  interactions between the  $\text{NH}_2$  group and the  $\pi$ -system of the benzene ring linked to the thioamide function (Fig. 20).<sup>55</sup> To provide this interaction, the thioamide group rotates relative to the plane of the aromatic system at angle of  $79.6^\circ$ .

### 3.5. $\text{NH}\cdots\pi$ complexes with sulfonamides

Recently, a simulation of  $\text{NH}\cdots\pi$  interactions with the participation of an aromatic sulfonamide group has been carried out.<sup>56</sup> As objects of study, 2,6-diarylbenzenesulfonamides **20** were taken, containing a number of donor and acceptor substituents in the *para*-positions of the flanking phenyl groups. XRD measurements of difluoride **20** ( $\text{X} = \text{F}$ ) established the formation of an  $\text{NH}\cdots\pi$  bond with one of the benzene rings with an  $\text{NH}\cdots\text{M}$  distance of 2.68 Å and an  $\text{NHM}$  angle of  $134.2^\circ$ . Along with the fairly clear direction of the NH-bond vector towards the centroid of the *ortho*-phenyl group, there are two other characteristic features of the  $\text{NH}\cdots\pi$  binding. One of them is a larger angle of rotation around the  $\text{C}_{\text{Ar}}-\text{C}_{\text{Ar}}$  bond of the phenyl ring facing the NH-proton. For difluoride **20**, it is  $63.9^\circ$  vs  $57.5^\circ$  for another phenyl group. Even more revealing is the sharp flattening of the  $\text{NH}_2$  group in **20** ( $\Sigma\text{N} = 347.5^\circ$ ) in comparison with unsubstituted (parent)



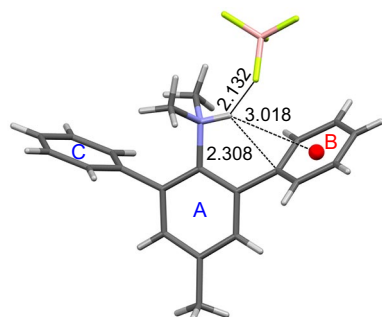


**Figure 21.** Molecular structure of salt **21**. Selected parameters:  $\varphi_{AB} = 58.7^\circ$ ;  $\varphi_{AC} = 84.9^\circ$ ;  $\Sigma\text{CNC} = 338.7^\circ$ ;  $\text{NH}\cdots\text{FBF}_3^- = 2.13 \text{ \AA}$  (YUWVOF, 100 K). The figure was created by the authors using data of Ref. 59.

benzenesulfonamide ( $\Sigma\text{N} = 334.7^\circ$ ). Obviously, this is due to an increase in the *s*-component of the valence orbitals of the more planar nitrogen atom, which enhances NH-acidity and, consequently, the  $\text{NH}\cdots\pi$  interaction. An increase in the proton acceptor properties of the flanking phenyl nuclei, when electron-donor substituents are placed into them, leads to the same result.

Based on the XRD studies of hydrazinylsulfonamides<sup>57</sup> and hydrazincarbodithioic acid esters,  $\text{NH}\cdots\pi$  interactions in their crystal lattices were also revealed.<sup>58</sup>

Strategy of using the flanking phenyl groups to model  $\text{NH}\cdots\pi$  interactions turn out to be quite successful in the case of the dimethylammonium group. Thus, in the protonated form of *N,N*-dimethyl-2,6-diphenyl-*p*-toluidine **21**, despite the imperfect orthogonality of the 2-Ph group and the central benzene ring and strong bifurcation of  $\text{NH}$ -hydrogen with the participation of the counterion (XRD data, Fig. 21), the  $\text{NH}\cdots\text{C}_i$  distance is just about 2.31 Å, while the shortest (Me)CH $\cdots\text{C}_i$  distances characterizing  $\text{CH}\cdots\pi$  interactions on the left side of the molecule are at the level of 2.60 Å.<sup>59</sup> However, looking ahead, it should be said that the placement of dimethylammonium and phenyl groups in the *peri*-positions is more effective comprising the next progressive step in modelling  $\text{NH}\cdots\pi$  interactions (see Section 3.8).

### 3.6. $\text{NH}\cdots\pi$ complexes of arenes with NH-heterocycles

Considering the great importance of nitrogen heterocycles in biochemical systems, for example, histidine and tryptophan in proteins, purines and pyrimidines in nucleic acids and ATP, pyridines, pyridinium and imidazolium salts in enzymes, pyrrole in heme and chlorophyll,<sup>60</sup> they have become very attractive objects for modelling  $\text{NH}\cdots\pi$  interactions as both proton donors and proton acceptors. In this regard, it is logical to start this Section with pyrrole and pyrrole-based systems.

XRD analysis of unsubstituted pyrrole showed that T-oriented dimers **22** are formed in its crystals, in which one molecule acts as an NH-donor and the other as a proton acceptor (Fig. 22).<sup>61</sup> In this case, the NH-proton is oriented not to the ring centroid, but to  $\text{C}_\beta$  atoms, on which, as is known,<sup>63</sup> the largest negative  $\pi$ -charge is concentrated. In the case of 1-(2-hydroxyphenethyl-2)pyrrole dimer **23**, the OH groups are bonded to  $\text{C}_\alpha$  atoms,<sup>64</sup> which is apparently due to the greater stability of the ten-membered ring architecture in comparison with that which would arise at the  $\text{OH}\cdots\pi$  binding at pyrrole  $\text{C}_\beta$  positions. The  $\text{NH}\cdots\text{C}_\beta$  and  $\text{OH}\cdots\text{C}_\alpha$  distances in dimers **22** and **23** are 2.57 and 2.52 Å, respectively.

Self-association of pyrrole was also registered in solution.<sup>65</sup> Thus, according to quantumchemical calculations [B3LYP/6-31++G(d,p)] and IR spectra, pyrrole in  $\text{CCl}_4$

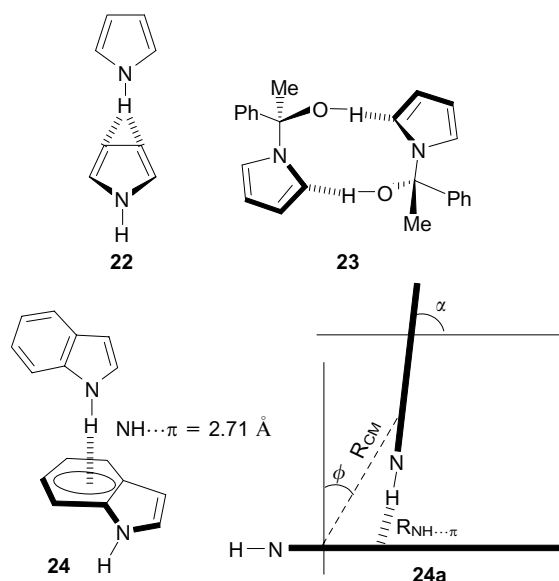


**Figure 22.** Schematic representation of structures of pyrrole and indole dimers. Definition of intermolecular parameters, defining the mutual orientation of the units within the T-shaped indole dimer (**24a**). The figure was created by the authors using data of Refs 61, 62.

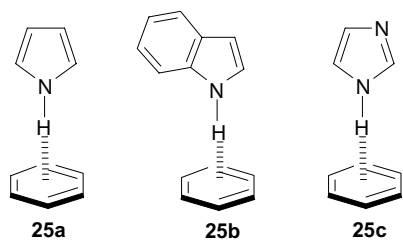
forms  $\text{NH}\cdots\pi$  dimers with the T-configuration. In them, the centres of mass of monomer units are separated from each other by 4.52 Å, the interplanar angle is  $73.0^\circ$ , and the  $\text{NH}\cdots\pi$  distance is 2.48 Å, which is in good agreement with XRD data. In the Fourier-IR spectrum of pyrrole in a dilute  $\text{CCl}_4$  solution, the  $\nu_{\text{NH}}$  band has the form of a sharp peak at  $3495 \text{ cm}^{-1}$ . In more concentrated solutions, a broadened band appears with a centre at  $3408 \text{ cm}^{-1}$ , assigned to the  $\text{NH}\cdots\pi$  bond in the dimer. Thus, the red shift value,  $\Delta\nu_{\text{NH}}$ , is  $-87 \text{ cm}^{-1}$  (see also Ref. 66) which almost coincides with the calculated data ( $-84 \text{ cm}^{-1}$ ).

Based on theoretical calculations and IR spectra, indole, similarly to pyrrole, forms T-dimer **23** (Fig. 22).<sup>62</sup> However, structure **23**, optimized using the B3LYP/6-31++G(d,p) method, indicates that the formation of  $\text{NH}\cdots\pi$  bond occurs at the benzene rather than at the pyrrole ring. The interplanar angle  $\alpha$  (see Fig. 22, structure **24a**) is almost right ( $89.4^\circ$ ). The distance between the centres of mass of two molecules,  $R_{\text{CM}}$ , and the length of the  $\text{NH}\cdots\pi$  bond are 6.21 and 2.71 Å, respectively, while the angle  $\varphi$  between the straight line connecting the centres of mass and the normal is  $51.5^\circ$ . Noteworthy is the somewhat longer  $\text{NH}\cdots\pi$  bond length in indole dimer **23** compared to pyrrole dimer **21**, which indicates its lower stability. The calculated  $\text{NH}\cdots\pi$  bond energy for dimer **23** is only  $2.15 \text{ kcal mol}^{-1}$ . Returning to the orientation of the  $\text{NH}\cdots\pi$  bond vector in the indole dimer to the benzene ring, it is interesting to note that in the case of tryptophan residues in protein structures this orientation is approximately equally distributed between the benzene and pyrrole rings.<sup>11</sup>

Using quantumchemical calculations (DFT-D density functional, SCS-MP2 and SCS-CC2 level of theory), as well as IR/UV double resonance spectroscopy under the supersonic-jet-cooled conditions the complexes of pyrrole with benzene and benzene- $\text{d}_6$  were examined.<sup>67</sup> The results of the study indicate their T-shaped structure **25a**, in which the pyrrole ring is slightly inclined (by  $\pm 13^\circ$ ) to the normal drawn to the plane of the benzene ring. The distance  $\text{N}\cdots\text{M}$

to the centroid of the benzene ring is 3.13 Å, and the red shift of the  $\nu_{\text{NH}}$  band relative to free pyrrole ( $\nu_{\text{NH}} = 3531 \text{ cm}^{-1}$ ) is  $-59 \text{ cm}^{-1}$ , which indicates a weaker  $\text{NH}\cdots\pi$  interaction than in dimer **22** of pyrrole itself ( $-87 \text{ cm}^{-1}$ ). Similar study of indole–benzene dimer using IR/UV double resonance spectroscopy revealed that in gas phase it also exists in T-form **25b** with  $\text{NH}\cdots\pi$  hydrogen bond.<sup>68</sup> This is supported by the red shift ( $\nu_{\text{NH}} = 3479 \text{ cm}^{-1}$ ) of the indole N–H stretching frequency ( $\nu_{\text{NH}} = 3525 \text{ cm}^{-1}$ ).

Structures 25a–c



The vibration frequencies of benzene C–H bonds in the IR spectrum of complexes **25a,b** practically do not change compared to those of benzene itself, which excludes  $\text{CH}\cdots\pi$  interactions and confirms the acceptor action of the benzene ring with respect to the pyrrole NH-group. In the UV spectrum of **25a**, a red shift of the long-wavelength band of benzene by  $58 \text{ cm}^{-1}$  relative to pure benzene was recorded. This was attributed to the violation of the symmetry of the  $\pi$ -electron system of benzene due to somewhat distorted geometry of the  $\text{NH}\cdots\pi$  hydrogen bond.

Crystallographic studies of proteins showed that  $\pi$ -interactions involving such an important amino acid as histidine are very common in them.<sup>11</sup> It is estimated that  $\sim 80\%$  of the contacts between the imidazole ring of histidine and the aromatic rings of phenylalanine, tyrosine, and tryptophan are  $\text{CH}\cdots\pi$  and only are  $\sim 20\%$   $\text{NH}\cdots\pi$  interactions. In both cases, the imidazole ring behaves as a proton donor. Trachsel *et al.*<sup>69</sup> simulated these interactions by studying the IR and UV spectra of a deeply cooled imidazole–benzene complex. DFT calculations of the ground and excited states using dispersion corrections and correlation methods SCS–MP2 and SCS–CC2 showed that complex **25c** has a  $C_s$ -symmetric T-shaped structure with an  $\text{NH}\cdots\pi$  bond vector directed to the benzene ring. Also, the NH-bond is inclined by  $12^\circ$  to the benzene  $C_6$  symmetry axis. IR spectra did not contradict this geometry. In particular, the  $\nu_{\text{NH}}$  band in the IR spectrum of complex **25c** is shifted by  $-73 \text{ cm}^{-1}$  towards lower frequencies relative to spectrum of pure imidazole ( $\nu_{\text{NH}} = 3518 \text{ cm}^{-1}$ ). The dissociation energy of the  $\text{NH}\cdots\pi$  bond for the ground state of **25c** in the gas phase was estimated as moderately strong ( $5.43 \text{ kcal mol}^{-1}$ ). The authors did not find experimental evidence for the existence of a  $\text{CH}\cdots\pi$  hydrogen bond in the ground state of **25c**, which is not entirely consistent with the predominance of this geometry in proteins. In this regard, it was suggested that  $\text{CH}\cdots\pi$  contacts in protein structures arise not so much as a result of energetically more favourable binding, but as a result of crystalline packing and folding of the polypeptide chain.

Other attractive pyrrole-based objects for studying  $\text{NH}\cdots\pi$  interactions are 9*H*-pyrido[3,4-*b*]indoles **26a,b**, also known as  $\beta$ -carbolines.<sup>70–72</sup> They possess a rather extended  $\pi$ -system, which includes *N*-heteroatoms of the pyrrole and

pyridine types. This makes them both potential NH- and  $\pi$ -donors, as well as proton acceptors, which expands the possibility of their binding to biochemical receptors through various types of non-covalent interactions. Perhaps for this reason, a number of medicines have been created on their basis, and some of their representatives are found in nature and are considered as a type of indole alkaloids.

Moreover, the behaviour of  $\beta$ -carbolines **26a,b** towards benzene, naphthalene, phenanthrene and some azaarenes was also examined (Table 3).<sup>72</sup> Using FTIR spectroscopy and quantumchemical calculations (AM1/MOPAC) it was shown that the  $\nu_{\text{NH}}$  stretching vibration band of **26a** in  $\text{CCl}_4$  decreases its intensity and, at the same time, a new band appears in the lower-frequency region, the intensity of which increases as the number of  $\pi$ -electrons in the arene grows. These changes were attributed to the formation of T-shaped  $\text{NH}\cdots\pi$  clusters with a composition of 1 : 1, which, according to the results of theoretical calculations, corresponded to minima in the potential energy curves.

Analysis of the change in the intensity of the low-frequency band made it possible to calculate the association constants of the complexes (see Table 3), which increase with the expansion of the arene  $\pi$ -system, and, consequently, a decrease in its first ionization potential (growth of  $\pi$ -donor ability). In this context, however, it is not clear why the  $\Delta\nu_{\text{NH}}$  values themselves in the indicated complexes practically do not change in the series benzene–naphthalene–phenanthrene. Moving from **26a** to its 1-methyl derivative (harmine) **26b**, the association constants and  $\Delta\nu_{\text{NH}}$  values are noticeably decreased, which can be explained by steric reasons (especially in the case of naphthalene and phenanthrene) that hinders realization of the optimal geometry for the complex.

When arenes are replaced by azaheterocycles such as pyridine, quinoline, and phenanthridine, the structure of the resulting complexes changes dramatically. This is evidenced by a strong increase in their stability constants, as well as the value of  $\Delta\nu_{\text{NH}}$  (more than an order of magnitude! See Table 3). It is obvious that in these cases the nature of the bond between the components of the complex changes from  $\text{NH}\cdots\pi$  mainly to  $\text{NH}\cdots\text{N}$ .

Tsuzuki *et al.*<sup>73</sup> carried out a detailed quantumchemical study (*ab initio* methods, 6-31G\* and 6-311G\*\*, MP2 level

**Table 3.** Association constants of complexes of  $\beta$ -carbolines **26a,b** with arenes and azaarenes, values of the shifts of the stretching vibration bands of the N–H bond in FTIR spectra.<sup>72</sup>

Proton acceptor	$\beta$ -Carboline <b>26a</b>		1-Methyl- $\beta$ -carboline <b>26b</b>	
	association constant ( $K_a$ ), $\text{M}^{-1}$	shift ( $\Delta\nu_{\text{NH}}$ ), $\text{cm}^{-1}$	association constant ( $K_a$ ), $\text{M}^{-1}$	shift ( $\Delta\nu_{\text{NH}}$ ), $\text{cm}^{-1}$
Benzene	$0.16 \pm 0.06$	39	$0.145 \pm 0.006$	30
Naphthalene	$0.42 \pm 0.06$	36	$0.20 \pm 0.01$	29
Phenanthrene	$0.65 \pm 0.04$	37	$0.23 \pm 0.01$	28
Pyridine	$1.86 \pm 0.03$	320	$2.5 \pm 0.2$	320
Quinoline	$1.86 \pm 0.09$	303	$1.86 \pm 0.09$	322
Phenanthridine	$2.04 \pm 0.09$	314	$1.86 \pm 0.09$	318

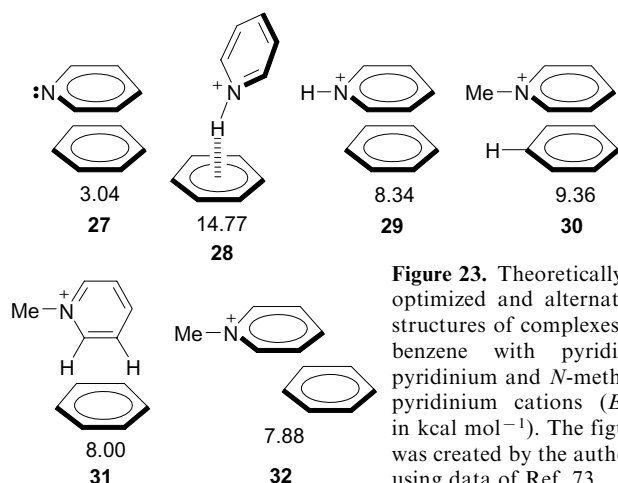


**Figure 23.** Theoretically optimized and alternative structures of complexes of benzene with pyridine, pyridinium and *N*-methylpyridinium cations ( $E_{\text{int}}$  in kcal mol<sup>-1</sup>). The figure was created by the authors using data of Ref. 73.

of theory) of benzene complexes with pyridine, pyridinium and *N*-methylpyridinium cations. Their attention was focused on the geometry of the complexes and the interaction energy ( $E_{\text{int}}$ ) of their components. It was shown that in the weakest benzene–pyridine complex **27** both rings are located in face-to-face manner, which is typical of  $\pi$ , $\pi$ -stacking (Fig. 23); the value of  $E_{\text{int}}$  in this case was equal to 3.04 kcal mol<sup>-1</sup>.

It is believed that the interaction of the rings in **27** is predominantly dispersive. A similar stacking is realized in benzene–*N*-methylpyridinium complex **30**, in which the interaction energy is almost three times higher than in **27**. The strongest interaction (14.77 kcal mol<sup>-1</sup>), related to the NH $\cdots$  $\pi$  type, takes place in the benzene–pyridinium complex **28**. The interaction in the alternative structure **29** with displaced  $\pi$ -stacking is almost half of that of **28**. In the benzene–*N*-methylpyridinium pair, the lowest energy has a structure with  $\pi$ , $\pi$ -stacking **30**, while forms **31** with CH $\cdots$  $\pi$  bonds and **32** with displaced  $\pi$ , $\pi$ -stacking are less stable. Based on the large difference in the stability of benzene–pyridine **27** and benzene–pyridinium complexes **28** and **29**, it was concluded that in the latter two species the attraction is determined not so much by dispersion as in **27**, as by electrostatic and induction forces.

The amide group plays an important role in structural biology not only in an open-chain form, as in polypeptides and proteins, but also in a cyclic form, for example, in nucleobases (guanine, uracil, thymine, cytosine). To simulate NH $\cdots$  $\pi$  interactions with the participation of such compounds, the investigation of complexes of 2- and 4-pyridones (**2PY** and **4PY**) with benzene<sup>74</sup> and various fluorobenzenes was performed.<sup>75–78</sup> The latter are denoted below as **1FB**, **2FB**, **3FB**, **4FB**, **5FB** and **6FB** depending on the number of fluorine atoms.

Along with quantumchemical calculations (MP2 and SCS-MP2), double resonance IR/UV spectroscopy of strongly cooled dimers was used. As shown by the results of theoretical calculations, for the **2PY**·C<sub>6</sub>H<sub>6</sub> complex, the T-shaped structure **33** with NH $\cdots$  $\pi$  hydrogen bond is the most stable (Fig. 24). In it, the pyridone ring is slightly inclined (by 12°) to the benzene ring, which, as in other similar cases (*cf.* Fig. 5), reflects a compromise between the perfectly orthogonal T-form and the plane-parallel form with  $\pi$ , $\pi$ -stacking. The energy of the NH $\cdots$  $\pi$  bond in **33** is estimated at 6.02 kcal mol<sup>-1</sup>, which is similar to that of the O–H $\cdots$ O hydrogen bond in the water dimer. Frequencies

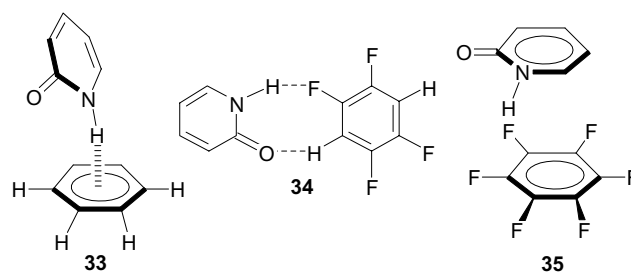


**Figure 24.** Structural motives in complexes of 2-pyridone with benzene and fluorobenzenes. The figure was created by the authors using data of Refs 75–78.

of stretching vibrations of N–H and C=O bonds in **2PY**·C<sub>6</sub>H<sub>6</sub> complex relative to the spectrum of pure 2-pyridone are reduced by 56 and 10 cm<sup>-1</sup>, respectively, which also indicates a rather strong NH $\cdots$  $\pi$  interaction and a relatively weak participation of the C=O group in it. At the same time, the stretching vibrations of the C–H benzene bonds are almost unchanged ( $\sim 2$  cm<sup>-1</sup>) compared to benzene itself, suggesting that they are not involved in the binding with 2-pyridone.

For complexes of 2-pyridone with fluorobenzenes, the picture is much more complicated.<sup>75,77,78</sup> Complexes **2PY**·*n***FB**, where  $n = 1–4$ , are formed by two HBs, namely, C–H $\cdots$ O=C and NH $\cdots$ F–C (structure **34**). In this case, with an increase in the number of fluorine atoms, the C–H $\cdots$ O=C bond becomes stronger than NH $\cdots$ F–C (for **2PY**·**4FB**, by 4.11 kcal mol<sup>-1</sup>).

Unlike fluorobenzenes having at least one C–H bond, hexafluorobenzene is stabilized mainly due to  $\pi$ , $\pi$ -stacking (structure **35**) with an interaction energy of 5.81 kcal mol<sup>-1</sup>. In structure **35**, a certain contribution of NH $\cdots$ F bonding is also allowed ( $E_{\text{int}} = 2.32$  kcal mol<sup>-1</sup>), which, in addition to the calculated data, is evidenced by the slight inclination of the plane of the pyridone molecule to the C<sub>6</sub>F<sub>6</sub> plane, thus promoting the approach of the NH-group to one of the fluorine atoms. Table 4 summarizes the data on the interaction energies in all six **2PY**·*n***FB** dimers. As can be seen, a significant contribution of the  $\pi$ , $\pi$ -stacking component commensurate with the H-bonding also occurs in the complexes of 1,2,4,5-tetrafluoro- and pentafluorobenzenes. The specificity of hexafluorobenzene in this

**Table 4.** Calculated interaction energies, ( $E_{\text{int}}$ , kcal mol<sup>-1</sup>)<sup>a</sup> in complexes of 2-pyridone with fluorobenzenes.<sup>78</sup>

Complex	Type of binding		Resulting character of binding
	H-bonding	$\pi$ , $\pi$ -stacking	
<b>2PY</b> · <b>1FB</b>	6.47	–	Exclusively H-bonding
<b>2PY</b> · <b>2FB</b>	6.68	–	Exclusively H-bonding
<b>2PY</b> · <b>3FB</b>	6.36	–	Exclusively H-bonding
<b>2PY</b> · <b>4FB</b>	6.66	6.66	Equality of two types of binding
<b>2PY</b> · <b>5FB</b>	6.74	6.13	Small prevalence of H-bonding
<b>2PY</b> · <b>6FB</b>	2.32	5.81	Strong prevalence of $\pi$ , $\pi$ -stacking

<sup>a</sup> Along with the bond energies, the bond dissociation energies were also calculated. Their values, which are  $\sim 10\%$  lower in magnitude, do not influence the conclusions regarding the main trends.

series is explained as follows. The  $C_6F_6$  molecule is also a quadrupole, but the direction of the quadrupole moment in it is opposite to that of benzene. Since fluorine is more electronegative than carbon, the edge of the ring in  $C_6F_6$  is negatively charged, while a positive electrostatic potential forms over the ring itself. This circumstance prevents the formation of the  $NH\cdots\pi$  bond, while the stacking with  $\pi$ -donors becomes much more preferable.

### 3.7. $NH\cdots\pi$ self-association of aniline and NH-heterocycles

Aniline is of interest as a model containing two proton-donor N–H bonds and two proton-acceptor centres (nitrogen atom and the ring  $\pi$ -system). Such structure suggests the possibility of self-association of aniline to form dimeric clusters of the head-to-head **36** or head-to-tail **37** types (Fig. 25). Yeh *et al.*<sup>79</sup> calculated the energies of both forms in the gas phase using the methods of molecular mechanics (MM) and molecular dynamics (MD). In MD simulation, the head-to-head shape **36** with two parallel phenyl rings turned out to be more stable. On the contrary, the MM method gave preference to the head-to-tail conformation,<sup>44</sup> in which each  $NH_2$  group of one molecule forms an  $NH\cdots\pi$  bond with the benzene ring of the other with antiparallel orientation of the phenyl groups.

Apart the calculations, the resonance two-photon spectroscopy R2PI has been used, according to which structure **36** prevails.<sup>79</sup> However, in the same 1996, studying aniline dimers by infrared and laser mass spectroscopy, Sugawara *et al.*<sup>80</sup> came to a little different conclusion. They completely ruled out the head-to-head structure **36** in favour of **37**. Considering the inconsistency of these conclusions, Yamamoto *et al.*<sup>81</sup> later repeated these experiments and performed *ab initio* calculations with the MP2/cc-pVDZ level of theory. Based on the results obtained, they concluded that both structures, **36** and **37**, correspond to potential energy minima ( $E_{int} = 3.36$  and  $4.54$  kcal mol<sup>-1</sup>), but structure **37** with two  $NH\cdots\pi$  bonds is  $1.18$  kcal mol<sup>-1</sup> more stable.

XRD analysis of aniline at 100 K also showed that  $NH\cdots\pi$  and  $NH\cdots N$  hydrogen bonds are the strongest in the crystal lattice, being realized inside the herringbone stacks that form layers.<sup>82</sup> The energy of interaction of molecular pairs from adjacent layers due to H-bonds of two types are estimated at  $2.2$ – $3.8$  kcal mol<sup>-1</sup>, and according to the so-called PIXSEL calculations,  $NH\cdots\pi$  interactions make greater contribution. In addition,  $CH\cdots\pi$  contacts are also involved in the formation of the crystal lattice, due to which the total interaction energy of molecular pairs can reach  $5$  kcal mol<sup>-1</sup>. As can be seen from Fig. 26, the distance between the NH-proton and the centroid ( $\sim 2.62$  Å) and the nitrogen atom in the neighbour molecule ( $2.36$  Å) is noticeably less than the sum of the

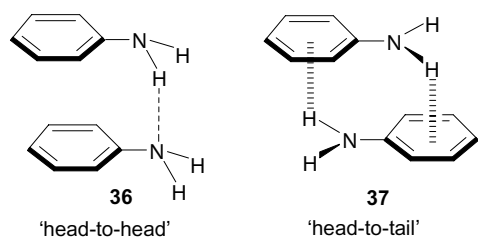


**Figure 25.** Conformations of aniline dimer calculated for the gas phase. The figure was created by the authors using data of Ref. 79.

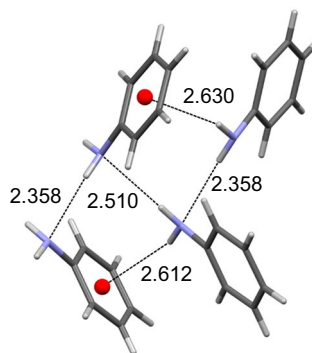


**Figure 26.** Fragment of aniline crystal structure (BAZGOY01, 100 K). The figure was created by the authors using data of Ref. 82.

VDW radii of the hydrogen atom ( $1.2$  Å) and the half-width of the benzene ring ( $1.7$  Å).

In Section 3.6, we have already mentioned the self-association of pyrrole and indole. Recall that pyrrole in the solid state gives T-type  $NH\cdots\pi$  dimers **22**, in which the NH-proton of one molecule is directed to the  $C_\beta$  atoms of the other. It is noteworthy, however, that along with the  $NH\cdots C3(4)$  distances ( $2.57$  Å), the  $NH\cdots M$  distance ( $2.60$  Å) is also rather short (Fig. 27a). Surprisingly, there are still no reliable XRD studies on unsubstituted indole (see, *e.g.*, Ref. 85). Nevertheless, some indirect data, for example, obtained for a co-crystal of *N,N'*-di-*n*-butyl-3,6-bis(phenylethynyl)pyromellitic di-imide bis(indole) indicate the presence of  $NH\cdots\pi$  interactions between the NH group of one indole molecule and the benzene ring of another one (Fig. 28).<sup>86</sup> According to quantumchemical calculations and IR spectra,<sup>66</sup> self-association of indole also proceeds *via* the  $NH\cdots\pi$  binding with participation of the benzene ring (see Fig. 22, structure **24**).

Information on the self-association of multinuclear analogues of pyrrole and indole is no less interesting. XRD studies of carbazole<sup>83</sup> showed that its crystallization resulted in the formation of T-type  $NH\cdots\pi$  poly-associates similar to pyrrole (Fig. 27b). Indeed, the N–H bond in carbazole is symmetrically oriented to the  $\beta$ -carbon atoms of another molecule with  $NH\cdots C_\beta$  distances of  $2.59$  Å (for pyrrole,  $2.57$  Å). In this case, similar to pyrrole, the molecules are antiparallel to each other, and the interplanar angle is  $56.3^\circ$ , which is noticeably less than in the pyrrole dimer ( $70.1^\circ$ ). The latter indicates the presence of other non-covalent interactions in carbazole crystals due to its more extended  $\pi$ -system, such as  $CH\cdots\pi$  or  $\pi,\pi$ -stacking; notably, the  $N\cdots M$  distance is  $3.372$  Å, which almost coincides with the sum of the VDW radii of the N atom and the half-width of the aromatic ring.

The dependence of the geometry of  $NH\cdots\pi$  aggregates on the extension of the  $\pi$ -system is also traced in 3,6-di(4-alkoxyphenyl)carbazoles.<sup>84</sup> Thus, in dimers with two *p*-anisyl and 4-propoxyphenyl groups, the interplanar angle decreases to  $47.7^\circ$  and  $41.5^\circ$ , respectively (Fig. 27c,d). It is also noteworthy that in Fig. 27d the proton donor group behaves specifically with its N–H vector directed to the benzene, not pyrrole, ring of the carbazole system as in Fig. 27a–c. Apparently, this is due to an increase in steric factors when replacing methoxy with bulkier propoxy groups, which also affects the crystal packing. This explanation is supported by a noticeable increase in the banana-like curvature of the molecules upon transition to the propoxy-substituted compound (Fig. 27d).

A series of indolocarbazoles **38**–**41** with semiconducting properties was synthesized.<sup>87</sup> XRD studies and DFT calcu-

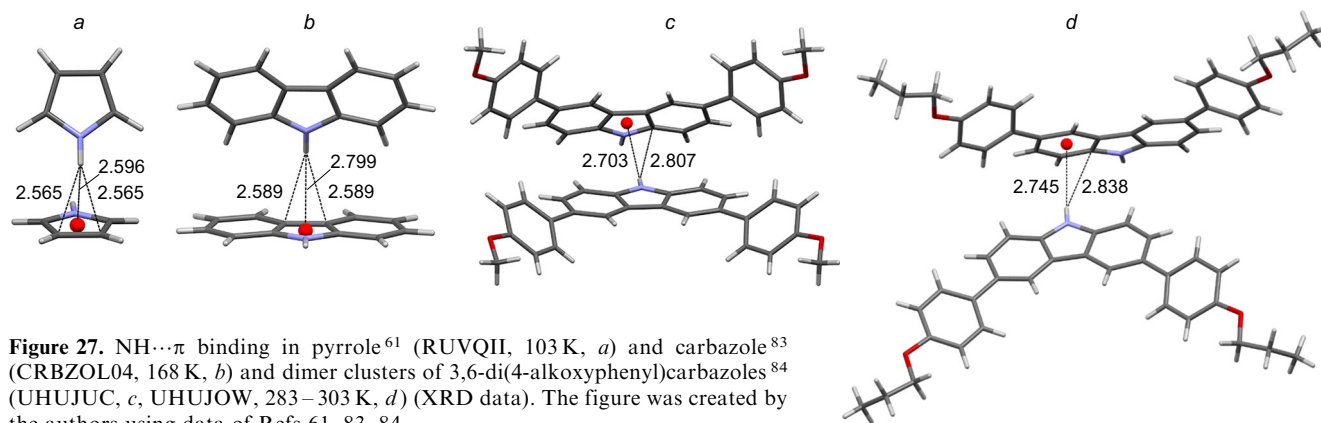


**Figure 27.** NH $\cdots\pi$  binding in pyrrole<sup>61</sup> (RUVQII, 103 K, *a*) and carbazole<sup>83</sup> (CRBZOL04, 168 K, *b*) and dimer clusters of 3,6-di(4-alkoxyphenyl)carbazoles<sup>84</sup> (UHUJUC, *c*, UHUJOW, 283–303 K, *d*) (XRD data). The figure was created by the authors using data of Refs 61, 83, 84.

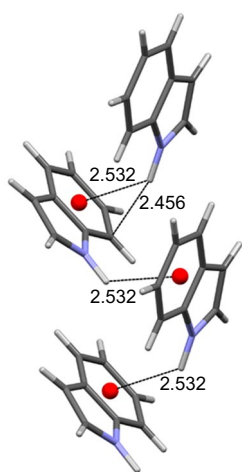
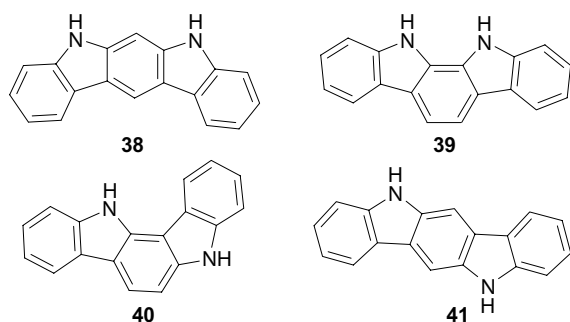


**Figure 28.** Self-association of indole in a co-crystal of *N,N'*-di-*n*-butyl-3,6-bis(phenylethynyl)pyromellitic diimide bis(indole) (NOCTUV, 123 K). The figure was created by the authors using data of Ref. 86.

lations disclosed the presence of NH $\cdots\pi$  dimer clusters in them, which enhance their conductivity. The energy of NH $\cdots\pi$  interactions is estimated at about 2.4 kcal mol<sup>-1</sup>, which is comparable to the energy of CH $\cdots\pi$  interactions also observed in these dimers (2.2 kcal mol<sup>-1</sup>). Accordingly, it was found that dimers of compounds **38** and **39** with the *syn*-oriented N–H bonds are more stable and thus encouraging for their examination as semi-conductors.

Analysis of the XRD data for the salt formed by 2-aminothiazolium cation with (2,4-dichlorophenoxy)-acetate anion showed self-association of two cations with participation of NH<sub>2</sub> group of one unit and thiazolium ring centroid of the other one in its crystal lattice.<sup>88</sup>

**Structures 38–41**



### 3.8. *peri*-Disubstituted naphthalenes as NH $\cdots\pi$ models

It is known that due to the ‘proximity effect’ of *peri*-substituents, 1,8-disubstituted naphthalenes are often used to study strong short hydrogen bonds,<sup>89,90</sup> to simulate transition states,<sup>91</sup> to stabilize atropisomers,<sup>92,93</sup> to conduct various cyclizations,<sup>62</sup> to synthesize elementochelates,<sup>94</sup> *etc.*<sup>95</sup> Taking this into account, we recently proposed 1,8-disubstituted naphthalenes **42–49** (Ref. 19, 20) as models for studying NH $\cdots\pi$  interactions. They have the advantage of synthetic availability and stability, allowing XRD and practically any spectral measurements, providing information for the solid state, solution and the gas phase. Phenyl, 4-methoxyphenyl, 4-hydroxyphenyl, 2-naphthyl and 1-pyrrolyl groups were used as the  $\pi$ -donor components, and positively charged Me<sub>2</sub>NH<sup>+</sup> and NH-pyridinium along with neutral NH<sub>2</sub> and NHAc groups served as proton donors. In model salts **42–47**, low-nucleophilic tetrafluoroborate was the counterion (Fig. 29).

Two above-mentioned examples of neutral 1,8-disubstituted naphthalene **17** and **18** should be pointed out, in

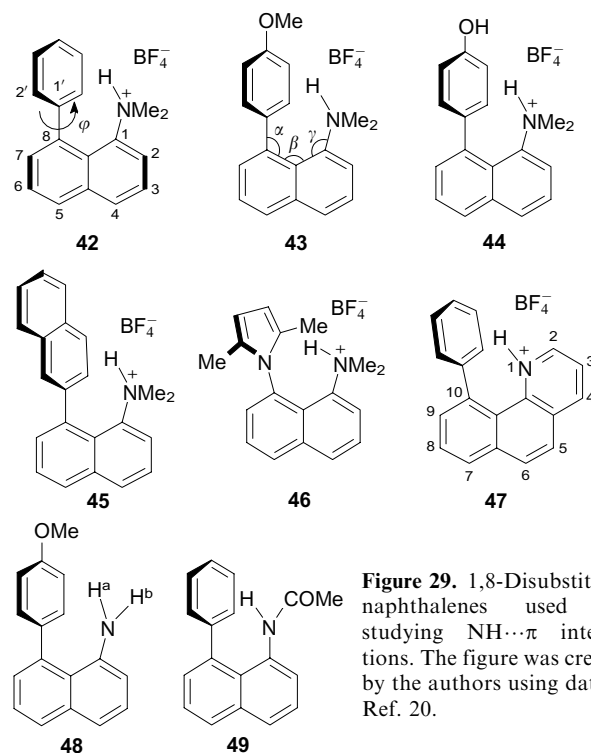


**Figure 29.** 1,8-Disubstituted naphthalenes used for studying NH $\cdots\pi$  interactions. The figure was created by the authors using data of Ref. 20.

which the acetamido group acted as a proton donor. However, these sterically congested compounds were not specially taken as models of NH $\cdots\pi$  interactions and the latter were considerably masked by other types of hydrogen bonds.

Some important parameters that shed light on the nature of NH $\cdots\pi$  interactions in compounds **42–49** are summarized in Table 5. The first thing that attracts attention is the rather strict orientation of the NH bond vector in compounds **42–46** to the plane of the phenyl group in the position 8 [compare the values of the dihedral angles  $\angle$ HNC(1)C(2), which are close to 180°]. Simultaneously, the 8-phenyl group turns around the C(8)–C(1') bond almost perpendicular to the naphthalene ring ( $\varphi = 79–88^\circ$ ).

Due to the specific arrangement of *peri*-substituents in salts **42–46**, the NH-proton is much closer to the C<sub>i</sub> atom of the phenyl group (2.05–2.08 Å) than to the centroid (NH $\cdots$ M = 2.39–2.50 Å). The only exception, which should be discussed in more detail, is salt **46** with a 2,5-dimethyl-1-pyrrolyl substituent. In this compound, the distances of the NH proton from the ring centroid and the pyrrole N-atom are exactly the same (2.07 Å), and the first of them (NH $\cdots$ M) is the shortest among all currently known models with NH $\cdots\pi$  interaction.

Taking into account the short length of the NH $\cdots$ N bond in **46**, the question arises whether this circumstance can be interpreted as the direct participation of the lone electron pair of the pyrrole nitrogen atom in the formation of HB. We tend to give a definitely negative answer to it, since the sum of the bond angles at the pyrrole N-atom at **46** is 359°, *i.e.*, the heteroatom retains the planarity inherent in the sp<sup>2</sup>-state and, in fact, is fully involved in the 6 $\pi$ -electron aromatic system. It seems reasonable to classify such a hydrogen bond as NH $\cdots$ N( $\pi$ ).<sup>19</sup>

Meanwhile, pyrrole-containing systems have also been described in which the N-heteroatom is markedly pyramidal under similar circumstances, although its participation in cyclic conjugation is not in doubt. It is logical to denote such bonds as NH $\cdots$ N(*n*, $\pi$ ).<sup>19</sup> They are realized, for example, in the protic salts of 1-methyl-9-dimethylamino-benzo[g]indole **50–52**. The participation of not only the

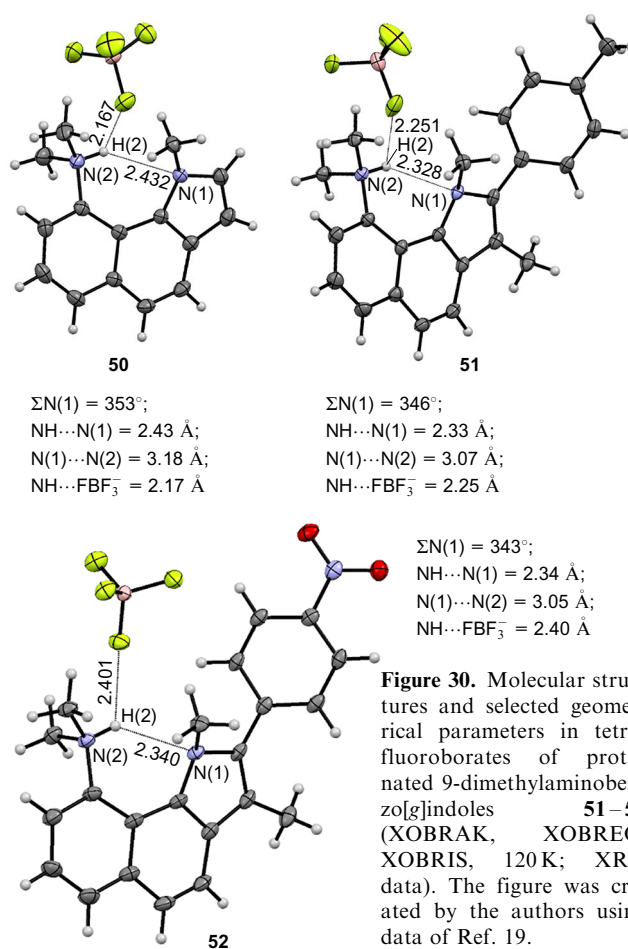


**Figure 30.** Molecular structures and selected geometrical parameters in tetrafluoroborates of protonated 9-dimethylamino-benzo[g]indoles **51–53** (XOBRAK, XOBREO, XOBRIK, 120 K; XRD data). The figure was created by the authors using data of Ref. 19.

ring  $\pi$ -system, but also the electron pair of the heteroatom in hydrogen bonding, in addition to the loss of planarity by the latter (Fig. 30, parameter  $\Sigma$ N1), is evidenced by a noticeable deviation of the N(1)–Me group from the mean plane of the molecule.

**Table 5.** Selected bond lengths, distances (Å) and angles (deg) in compounds **42–49** [all XRD measurements were conducted at 120 K except for salt **45** (100 K)].<sup>20</sup>

Parameter	Compound							
	<b>42</b>	<b>43</b>	<b>44</b> <sup>a</sup>	<b>45</b>	<b>46</b>	<b>47</b>	<b>48</b>	<b>49</b>
$\varphi$ <sup>b</sup>	83.8 (84.1)	78.7 (76.4)	86.1 (84.3)	73.5 (70.3)	88.1 (86.9)	62.8 (57.4)	76.1 (74.3)	48.5 (45.1)
$\angle$ HNC(1)C(2)	178(2)	171(2)	178(4)	177(2)	174(2)	177(2) <sup>c</sup>	145(6) <sup>d</sup> 167(4) <sup>e</sup>	60(4)
NH $\cdots$ M <sup>f</sup>	2.39(2)	2.41(2)	2.45(3)	2.56(4)	2.07(2)	2.84(2)	2.70(4) <sup>d</sup>	3.66(2)
$\angle$ NHM <sup>f</sup>	173(2)	165(2)	172(3)	167(3)	171(2)	153(2)	144(5) <sup>d</sup> 126(4) <sup>e</sup>	75(2)
NH $\cdots$ C(1')	2.06(2)	2.06(2)	2.05(3)	2.08(4)	2.07(2)	2.29(2)	2.30(4)	2.84(2)
$\angle$ NHC(1) <sup>g</sup>	146(2)	148(2)	151(4)	147(3)	144.1(11)	118.1(12)	125(4)	118.2(11)
NH $\cdots$ F(BF <sub>3</sub> <sup>-</sup> )	3.67(2)	3.55(2)	3.30(3) <sup>h</sup>	3.14(4)	4.21(2)	2.19(2)	–	–

<sup>a</sup> Average values for four independent cations. <sup>b</sup> Rotation angle of the aryl (pyrrolyl) substituent relative to the average naphthalene ring plane. Estimation of the same parameter *via* torsion angle C(7)C(8)C(1')C(2') is given in parentheses. <sup>c</sup> Torsion angle HNC(1a)C(4a) (atom numbering corresponds to the IUPAC rules). <sup>d</sup> For the H<sup>a</sup> atom of the NH<sub>2</sub> group (see Fig. 29). <sup>e</sup> For the H<sup>b</sup> atom of the NH<sub>2</sub> group. <sup>f</sup> M is centroid of the phenyl (pyrrolyl) substituent; in the case of **45**, M refers to the lower benzene ring. <sup>g</sup> NHC(2) and NHN for compounds **45** and **46**, respectively. <sup>h</sup> Average value for two of four independent molecules; two others form dimer pairs because of NH $\cdots$ OH binding, in which the BF<sub>4</sub><sup>-</sup> counterions are located outside the cations at the NH $\cdots$ F(BF<sub>3</sub><sup>-</sup>) distances of 4.37(3) and 4.95(3) Å.

The degree of pyramidalization of the N1 atom and, therefore, the  $\text{NH}\cdots\text{N}(n,\pi)$  HB energy in salts **50–52** is noticeably influenced by the substituent at position 2 of the pyrrole ring. The HB is more stable in benzo[*g*]indoles **51**, **52** bearing 2-aryl groups. Apparently, 2-aryl substituents sterically facilitate the deviation of the N(1)–Me group from the heterocyclic ring plane, which moves it further away from the NH-proton. This, in turn, weakens the bifurcation of the latter with the  $\text{BF}_4^-$  anion [see Fig. 30, compare the tendency for the parameters  $\text{NH}\cdots\text{N}(1)$ ,  $\text{N}(1)\cdots\text{N}(2)$  and  $\text{NH}\cdots\text{F}(\text{BF}_4^-)$ ]. Thus, the distance from the NH-proton to the nearest fluorine atom of the  $\text{BF}_4^-$  anion decreases in the series **52** (2.40 Å) > **51** (2.25 Å) > **50** (2.17 Å). Among salts **42–47**, the HB bifurcation is especially pronounced in benzo[*h*]quinolinium salt **47** (2.19 Å). As a result, the  $\text{NH}\cdots\pi$  interaction is sharply weakened, as evidenced by a decrease in the values of  $\varphi$  and NHM angles and an increase in the  $\text{NH}\cdots\text{M}$  and  $\text{NH}\cdots\text{C}(1')$  distances (see Table 5).

The influence of the counterion on  $\text{NH}\cdots\pi$  interactions in salts **42–47** and **50–52** does not allow adequate assessment of their energy ( $E_{\text{HB}}$ ), due to its strong and uneven underestimation.<sup>19</sup> To exclude this complication, theoretical calculations of the  $E_{\text{HB}}$  values were carried out for ‘naked’ cations **42–44**, **46** and **50–52** in the gas phase and in a solution of MeCN (Table 6). As expected, they arranged the first group of cations both for the gas phase and the solution in the series **46** > **43** > **44** > **42**, which closely coincides with a decrease in the proton-acceptor ability of the  $\pi$ -donor substituent at position 8. In benzo[*g*]indole cations **50–52**, the  $E_{\text{HB}}$  values turned out to be on average 3 kcal mol<sup>-1</sup> lower than in **42–44**, **46**, apparently due to the less favourable arrangement of the pyrrole ring relative to the  $\text{Me}_2\text{NH}^+$  group.

Let us now turn to neutral models **48** and **49** with  $\text{NH}_2$  and  $\text{NHAc}$  groups as proton donors. The first thing that attracts attention in the structure of amine **48** (Fig. 31) is the strong pyramidalization of the nitrogen atom ( $\Sigma\text{N} = 338.3^\circ$ ), which sharply distinguishes it from the completely flat  $\text{NH}_2$  group in 1-aminonaphthalene, which is coplanar with the ring, and benzene complex of 2-amino-

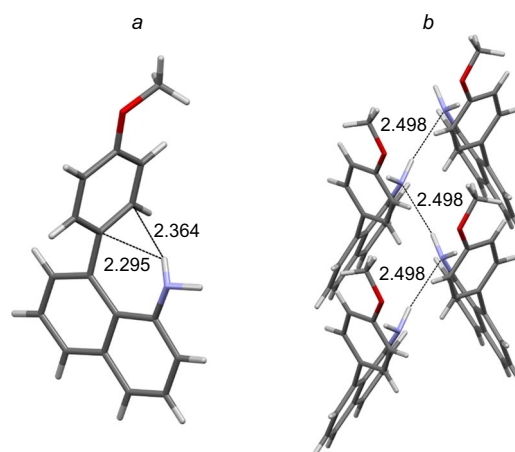


**Figure 31.** Molecular structure (a) and fragment of the crystal lattice (b) of amine **48** (JUXFEQ, 120 K). The figure was created by the authors using data of Ref. 20.

oxazoline **8** ( $\Sigma\text{N} = 360.0^\circ$ ).<sup>34</sup> The second feature of the  $\text{NH}_2$  group in **48** is the striking difference in the lengths of the internal (0.85 Å) and external (1.07 Å) N–H bonds. While the length of N–H bond directed to the  $\pi$ -system of the benzene ring is close to the common values for aniline  $\text{NH}_2$  groups (0.84–0.90 Å), the external N–H bond is strongly stretched (1.07 Å). It is known that the proton-donor X–H bonds involved in HB formation are usually elongated. Stretching of the external N–H bond in amine **48** suggests that it is also involved in strong conventional H-bonding. This is confirmed by considering the crystal lattice of **48**. As can be seen from Fig. 31 b, the external N–H bonds in each crystallographic unit of **48** are linked by rather short HB with the amine nitrogen of the neighbouring molecule ( $\text{NH}\cdots\text{N} = 2.5$  Å).

In contrast to  $\text{NH}\cdots\text{N}$  hydrogen bonds, the stretching of N–H bonds in the case of noticeably weaker  $\text{NH}\cdots\pi$  interactions cannot be so significant. Indeed, the internal N–H bond (0.84 Å) in the benzene complex of 2-amino-oxazoline **8** is only 0.01 Å longer than the external one (0.83 Å).<sup>34</sup> In amine **48**, the internal N–H bond has approximately the same length (0.85 Å) as in **8**. It is possible that the slight increase in length in **48** is caused by differences in the hybridization of two nitrogen atoms or by the orientation of the NH-vector at **48** not to the centroid or the ring C(1') atom, but to the middle of the C(1')–C(2') bond. In any case, however, there is little doubt that a weak  $\text{NH}\cdots\pi$  bond exists in amine **48**, as evidenced, for example, by a significant facing of the *p*-anisyl group towards the N–H vector.

Considering the increased NH-acidity of carboxamides in comparison with that of arylamines,<sup>52</sup> one could expect that  $\text{NH}\cdots\pi$  binding in compound **49** would be very noticeable. However, XRD measurements showed that the crystal lattice of **49** is formed exclusively by intermolecular amide bonds  $\text{NH}\cdots\text{O}=\text{C}$  (Fig. 32 b).<sup>20</sup> This distinguishes compound **49** from its more complex naphthalene analogues **17** and **18**, in which  $\text{NH}\cdots\pi$  interactions are superimposed with other types of non-covalent bonds.

One of the significant advantages of *peri*-disubstituted naphthalene is an opportunity to systematically study  $\text{NH}\cdots\pi$  interactions in its solutions using <sup>1</sup>H NMR spectra. Here one can draw an analogy with the classic example of the  $\text{CH}\cdots\pi$  hydrogen bond between chloroform and ben-

**Table 6.** Calculated energies of  $\text{NH}\cdots\pi$  hydrogen bonds in ‘naked’ cations **42–44**, **46** (Ref. 20) and **50–52** (Ref. 19) [B3LYP/6-311++G(d,p)].<sup>a</sup>

Cation	Medium	$E_{\text{HB}}$ , kcal mol <sup>-1</sup>	Cation	Medium	$E_{\text{HB}}$ , kcal mol <sup>-1</sup>
<b>42</b>	Gas phase	13.69	<b>46</b>	MeCN	12.07
		13.77 ZPE			12.29 ZPE
<b>42</b>	MeCN	11.73	<b>50</b>	Gas phase	10.5
		11.83 ZPE			10.7 ZPE
<b>43</b>	Gas phase	14.10	<b>50</b>	MeCN	8.8
		14.28 ZPE			8.8 ZPE
<b>43</b>	MeCN	12.03	<b>51</b>	Gas phase	11.2
		12.28 ZPE			11.4 ZPE
<b>44</b>	Gas phase	13.93	<b>51</b>	MeCN	9.4
		14.10 ZPE			9.7 ZPE
<b>44</b>	MeCN	11.95	<b>52</b>	Gas phase	10.9
		12.19 ZPE			11.1 ZPE
<b>46</b>	Gas phase	14.98	<b>52</b>	MeCN	9.2
		15.34 ZPE			9.8 ZPE

<sup>a</sup> Calculations using the dispersion Grimme correction did not lead to significant changes in the  $E_{\text{HB}}$  values.<sup>19</sup>

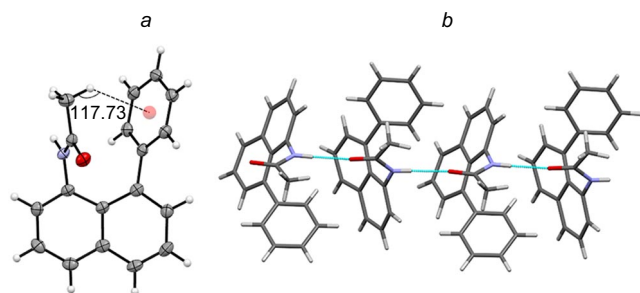


**Figure 32.** Molecular structure (a) and a chain of H-bonded associates along the *c* axis (b) in the crystal lattice of amide **49** (JUXDUE, 120 K). The figure was created by the authors using data of Ref. 20.

zene (Fig. 33), which manifests itself in a noticeable shielding ( $\Delta\delta_{\text{CH}} = -1.56$  ppm) of the  $\text{CHCl}_3$  proton.<sup>96</sup> The existence of complex **53** in the solid state both inside and outside the supramolecular container was also confirmed using the XRD method,<sup>97–99</sup> it is noteworthy that the  $\text{CH}\cdots\pi$  distance in this case strongly depends on the external environment, varying from 2.103 to 2.826 Å. It is natural to believe that such an effect can also be useful for evaluating the  $\text{NH}\cdots\pi$  interaction (see, *e.g.*, Ref. 100). The corresponding values of chemical shifts,  $\delta_{\text{NH}}$ , and paramagnetic displacement,  $\Delta\delta_{\text{NH}}$ , for some *peri*-disubstituted naphthalenes relative to the reference compounds, are represented in Table 7. As the reference compounds bearing no aromatic substituent in the adjacent *peri*-position, 1-aminonaphthalene **57**, 1-acetamidonaphthalene **60**, and dimethyl(naphth-1-yl)ammonium **54** and benzo[*h*]quinolinium tetrafluoroborates **56** were chosen.

It follows from Table 7 that the largest paramagnetic shifts,  $\Delta\delta_{\text{NH}}$  (–3.27 and –3.07 ppm), are observed for salts **46** and **55** containing 1-pyrrolyl groups as proton acceptors, while for their aryl analogues **42–45**  $\Delta\delta_{\text{NH}}$  values are 2.5–3 times less (–0.90...–1.38 ppm), and for neutral amines **48**, **58** and **59** they are only –0.32...–0.35 ppm. It was then shown that in the case of salts **42–46** and **55**, which do not have pronounced bifurcate interactions of the NH-proton with the  $\text{BF}_4^-$  anion, there is a satisfactory linear correlation between the  $\Delta\delta_{\text{NH}}$  values and the  $\text{NH}\cdots\text{M}$  distances.<sup>20</sup>

Apparently, two factors mainly determine the magnitude of the paramagnetic shift of the NH proton signal in the NMR spectra of compounds **A–D**. Both act in opposite directions, with the result that  $\Delta\delta_{\text{NH}}$  reflects their compromise. The first factor is the magnetic anisotropy of the aromatic ring and the presence of a ring current, the paramagnetic component of which causes shielding of the NH proton. The second factor is the deshielding of the proton involved in the formation of a hydrogen bond. The first

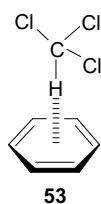


**Figure 33.** Chemical shifts of the chloroform CH-proton in cyclohexane and benzene solutions. The figure was created by the authors using data of Ref. 96.

$\delta_{\text{CH}} = 7.27$  ppm (cyclohexane),  
 $5.71$  ppm (benzene)

**Table 7.** Changes in the chemical shifts of NH-protons in compounds **A–D** induced by the paramagnetic component of the ring current of neighbouring aryl and pyrrolyl groups.<sup>20</sup>

Type of compound	R	No	Solvent	$\delta_{\text{NH}}$ , ppm	$\Delta\delta_{\text{NH}}$ , ppm
<b>A</b>	H	<b>54</b>	$\text{CD}_3\text{CN}$	9.47	–
<b>A</b>	Ph	<b>42</b>	$\text{CD}_3\text{CN}$	8.09	–1.38
<b>A</b>	4-MeOC <sub>6</sub> H <sub>4</sub>	<b>43</b>	$\text{CD}_3\text{CN}$	8.45	–1.02
<b>A</b>	4-HOC <sub>6</sub> H <sub>4</sub>	<b>44</b>	$\text{CD}_3\text{CN}$	8.57	–0.90
<b>A</b>	Naphth-2-yl	<b>45</b>	$\text{CD}_3\text{CN}$	8.30	–1.17
<b>A</b>	2,5-dimethyl-pyrrol-1-yl	<b>46</b>	$\text{CD}_3\text{CN}$	6.20	–3.27
<b>A</b>	Pyrrol-1-yl	<b>55</b>	$\text{CD}_3\text{CN}$	6.40	–3.07
<b>B</b>	H	<b>56</b>	$\text{CD}_3\text{CN}$	13.92	–
<b>B</b>	Ph	<b>47</b>	$\text{CD}_3\text{CN}$	12.35	–1.57
<b>C</b>	H	<b>57</b>	$\text{CDCl}_3$	4.04	–
<b>C</b>	Ph	<b>58</b>	$\text{CDCl}_3$	3.72	–0.32
<b>C</b>	4-MeOC <sub>6</sub> H <sub>4</sub>	<b>48</b>	$\text{CDCl}_3$	3.69	–0.35
<b>C</b>	Naphth-2-yl	<b>59</b>	$\text{CDCl}_3$	3.70	–0.34
<b>D</b>	H	<b>60</b>	$\text{CDCl}_3$	7.96	–
<b>D</b>	Ph	<b>51</b>	$\text{CDCl}_3$	7.03	–0.93
<b>D</b>	4-MeOC <sub>6</sub> H <sub>4</sub>	<b>61</b>	$\text{CDCl}_3$	7.19	–0.77
<b>D</b>	Naphth-2-yl	<b>62</b>	$\text{CDCl}_3$	6.97	–0.99

factor dominates especially clearly in the case of group **A** compounds.

As for amine **48**, all data indicate that, in contrast to the solid state, there is no intramolecular  $\text{NH}\cdots\pi$  binding in solution. Indeed, in the <sup>1</sup>H NMR spectrum of **48** in  $\text{CDCl}_3$ , NH<sub>2</sub> protons appear as a two-proton singlet at  $\delta$  3.69 ppm. Their equivalence is retained even at –90 °C, indicating fast rotation of the amino group in the NMR time scale. Some paramagnetic shift ( $\Delta\delta_{\text{NH}} = -0.35$  ppm) of the NH<sub>2</sub>-signal relative to that in 1-aminonaphthalene **57**, as in the spectra of amines **58** and **59**, most likely reflects the alternate short-term stay of each NH-proton in the paramagnetic region of the ring current of the neighbouring aromatic rings.

The absence of stable  $\text{NH}\cdots\pi$  HB in **48** is also confirmed by IR spectra. Thus, the bands of symmetric and antisymmetric stretching vibrations of the NH<sub>2</sub> group in the solution of **48** in  $\text{CCl}_4$  ( $\nu_{\text{s}} = 3401$   $\text{cm}^{-1}$ ,  $\nu_{\text{as}} = 3495$   $\text{cm}^{-1}$ ) in comparison with amine **57** ( $\nu_{\text{s}} = 3395$   $\text{cm}^{-1}$ ;  $\nu_{\text{as}} = 3476$   $\text{cm}^{-1}$ ) undergo a blue shift, rather than a red shift as usual during the formation of the HB, including  $\text{NH}\cdots\pi$  bond.<sup>67</sup>

The situation for solutions of carboxamides **49**, **61** and **62** looks ambiguous. Their <sup>1</sup>H NMR spectra in  $\text{CDCl}_3$  demonstrate a moderate paramagnetic shift of the NH signal ( $\Delta\delta_{\text{NH}} = -0.77$ ...–0.99 ppm) relative to that in spectrum of 1-acetamidonaphthalene **60** (see Table 7). At the same time, in the IR spectra of **49** and **61**, the  $\nu_{\text{NH}}$  band is strongly shifted to the high-frequency region (Table 8). The IR spectral data, which indicate the absence of  $\text{NH}\cdots\pi$  interactions in amides **49** and **61** in solution, seem to be more reliable. The blue shift of the  $\nu_{\text{NH}}$  band, along with an

**Table 8.** IR spectra of 1-acetamido-8-arylnaphthalenes (regions of NH and C=O groups, 0.1 M solutions in CCl<sub>4</sub>).

Compound	$\nu_{\text{NH}}$ , cm <sup>-1</sup>	$\nu_{\text{CO}}$ , cm <sup>-1</sup>	$\Delta\nu_{\text{NH}}$ , cm <sup>-1</sup>	$\Delta\nu_{\text{CO}}$ , cm <sup>-1</sup>
<b>49</b>	3426	1701	157	50
<b>61</b>	3437	1704	169	53
<b>62</b>	3269	1651	—	—

increase in the  $\nu_{\text{CO}}$  frequency and a paratropic shift of the NH-signal in the <sup>1</sup>H NMR spectrum, can be interpreted as a result of the destruction of carboxamide associates.

#### 4. Folded and caged models

The main disadvantage of unfolded and predominantly intermolecular models is that they are poorly preorganized for effective NH... $\pi$  interaction. This circumstance (in thermodynamic terms, the entropy factor) seriously reduces the stability of the complexes. As a result, their research requires special methods and conditions (see Section 2), which quite often leads to contradictory conclusions. The only exceptions are *peri*-disubstituted naphthalenes (see the previous Section), in which the NH... $\pi$  binding is provided by the ‘proximity effect’ of the proton-donor and proton-acceptor units.

Since the NH... $\pi$  interactions in proteins and other biomolecules are commonly realized within folded and sufficiently preorganized structures, their similar intramolecular models seem to be very attractive. Over the past quarter century, several approaches have been proposed to make progress in this direction. Most of them use motifs of supramolecular chemistry, when the model is based on the derivatives of cyclophanes, cryptands, podands, calixarenes, chelated metal complexes, *etc.* In their molecules, both interacting components are either part of a single structural unit, or they are initially separated, but one of them, under suitable conditions, is encapsulated inside the cavity of the other.

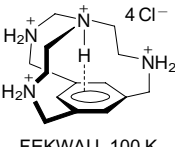
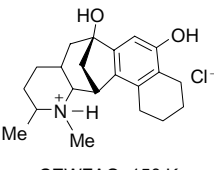
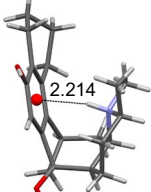
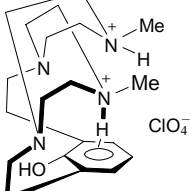
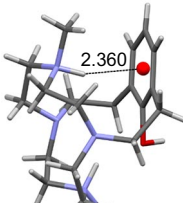
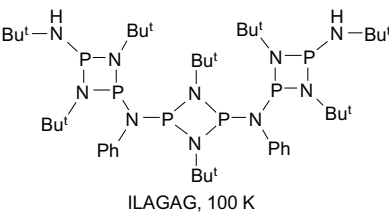
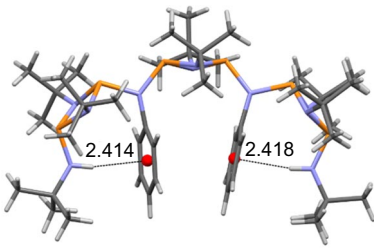
The preorganized effect can be also achieved largely in ammonium salts if the  $\pi$ -donating arene or heteroarene is a part of a relatively complex anion. In this case, the very electrostatic attraction of counterions becomes a preorganizing factor. Typical examples of such models are summarized in Table 9. It is convenient to divide them into three general types:

(I) One-component systems based on a neutral molecule, cation or salt.

(II) Two-component systems in which an NH-donor guest is encapsulated into host framework.

(III) Two-component systems in which arene or heteroarene guest molecule (*e.g.*, benzene, pyrrole, imidazole, *etc.*) is encapsulated into an NH-containing cavity.

**Table 9.** Pre-organized structures of frame and folded type with NH... $\pi$  bond.

Compound (type of structure)	Chemical structure, CCDC refcode and temperature of XRD measurements	XRD structure	Distances NH...M (N...M), Å	Ref.
<b>65 (I)</b>	 FEKWU, 100 K		2.15 (2.97)	101
<b>66 (I)</b>	 CEWFAO, 150 K		2.21 (3.04)	102
<b>67 (I)</b>	 HOXGEG, 283–303 K		2.36 (3.36)	103
<b>68 (I)</b>	 ILAGAG, 100 K		2.41 (3.28), 2.42 (3.29)	104

**Table 9** (continued).

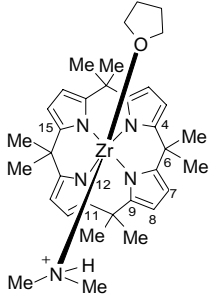
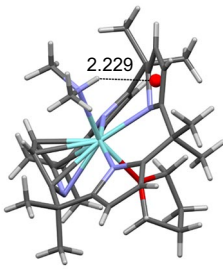
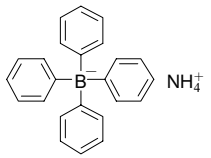
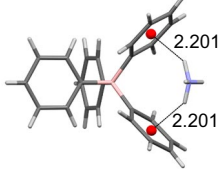
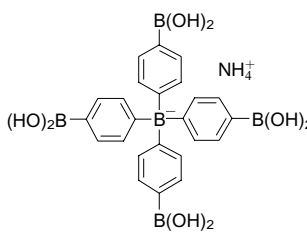
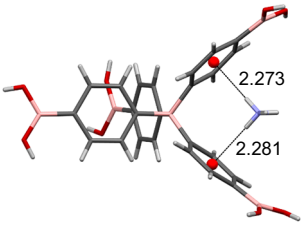
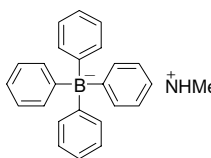
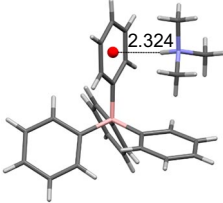
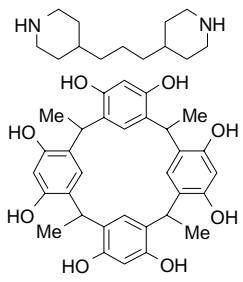
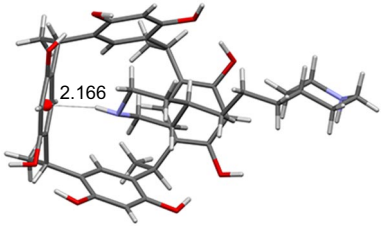
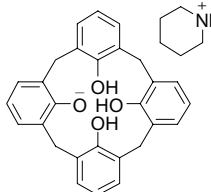
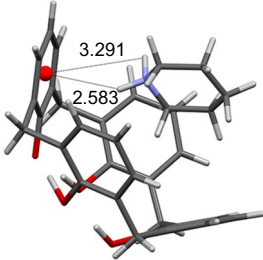
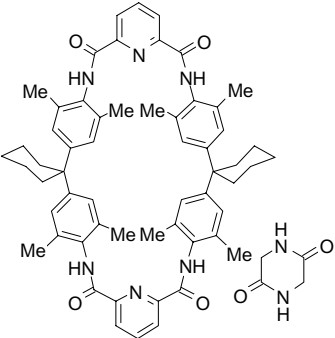
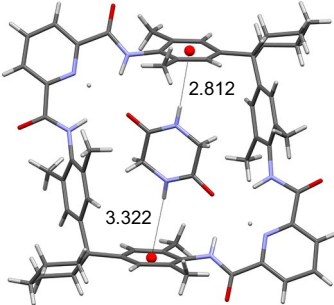
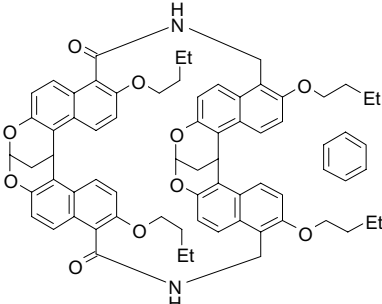
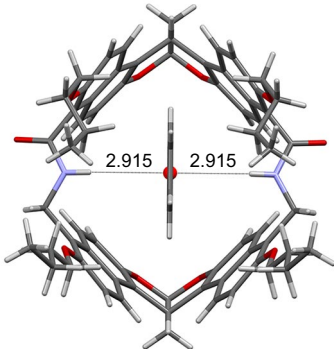
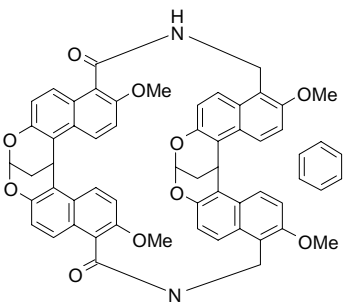
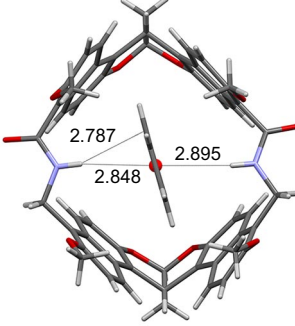
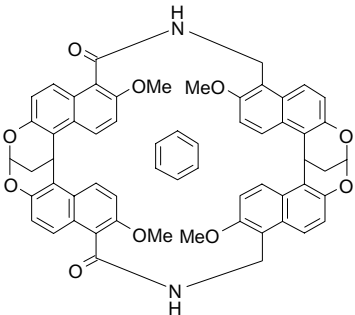
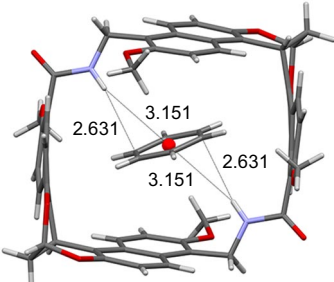
Compound (type of structure)	Chemical structure, CCDC refcode and temperature of XRD measurements	XRD structure	Distances NH...M (N...M), Å	Ref.
69 (I)	 YOGJUA, 100 K		2.23 (2.91)	105
70 (I)	 AMPHEB, 120 K		2.20 (3.04) <sup>a</sup>	106
71 (I)	 YIJXEX, 100 K		2.27 (3.12)	107
72 (I)	 RIPVEU, 150 K		2.32 (3.20)	108
73 (II)	 JARCUB, 90 K		2.17 (3.08)	109
74 <sup>b</sup> (II)	 NUNJUB, 283–303 K		2.58 (3.34)	110

Table 9 (continued).

Compound (type of structure)	Chemical structure, CCDC reocode and temperature of XRD measurements	XRD structure	Distances NH...M (N...M), Å	Ref.
75 (II)	 <p>RACKAH, 283–303 K</p>		2.81 (3.58), 3.32 (3.85)	103
76 (III)	 <p>TIHDAS, 150 K</p>		2.92 (3.77)	14
77 (III)	 <p>IJOQQQ, 100 K</p>		2.85 (3.72), 2.90 (3.74)	15
78 (III)	 <p>IJOREH, 100 K</p>		3.15 (4.01)	15

**Table 9** (continued).

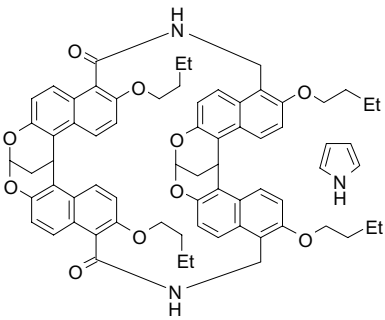
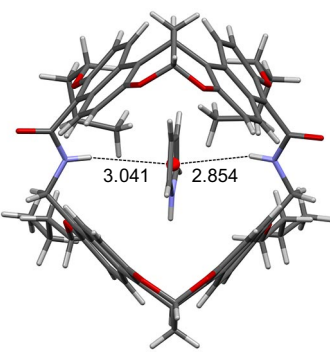
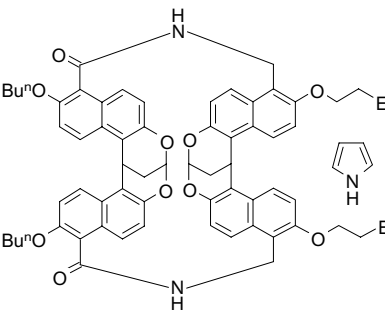
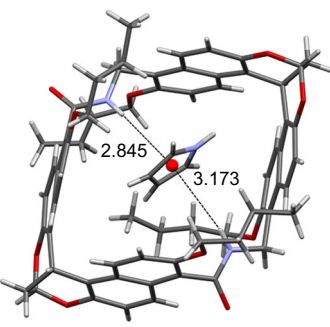
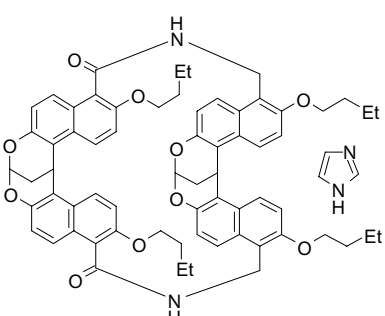
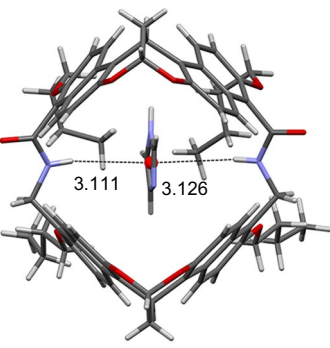
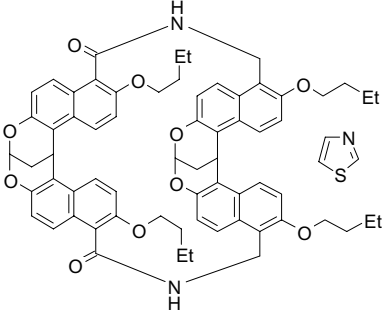
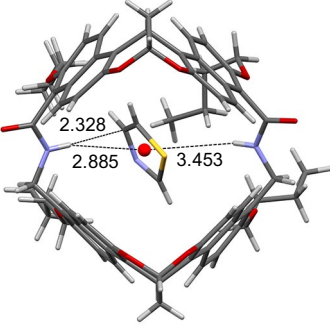
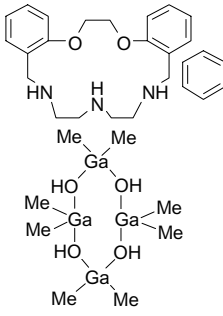
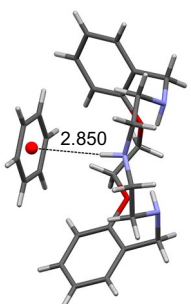
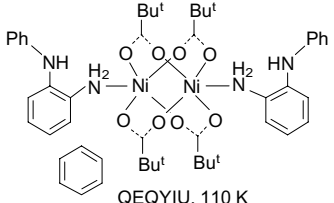
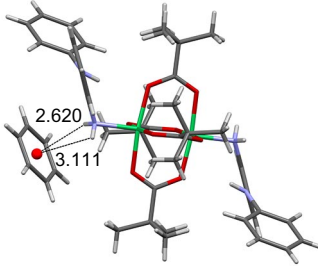
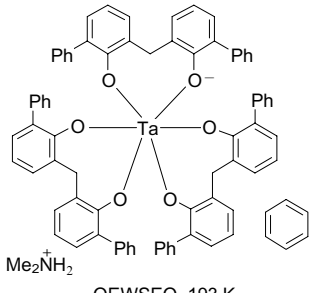
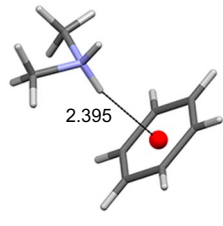
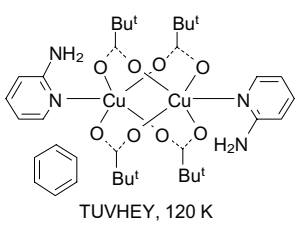
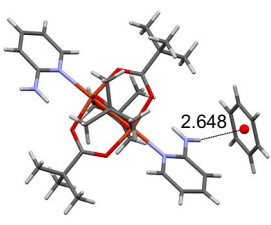
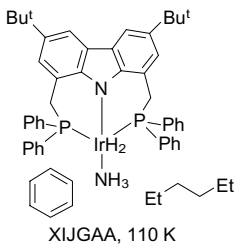
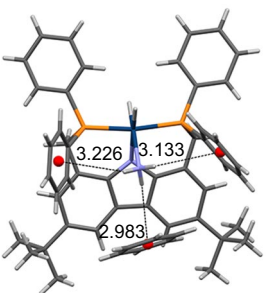
Compound (type of structure)	Chemical structure, CCDC reocode and temperature of XRD measurements	XRD structure	Distances NH...M (N...M), Å	Ref.
79 (III)	 <p>TIHFIC, 150 K</p>		2.85 (3.65), 3.04 (3.88)	14
80 (III)	 <p>TIHFOI, 150 K</p>		2.85 (3.71), 3.17 (4.04)	14
81 (III)	 <p>TIHDUM, 150 K</p>		3.11 (3.83), 3.13 (3.95)	14
82 (III)	 <p>TIHFUO, 160 K</p>		2.89 (3.69), 3.45 (4.23)	14

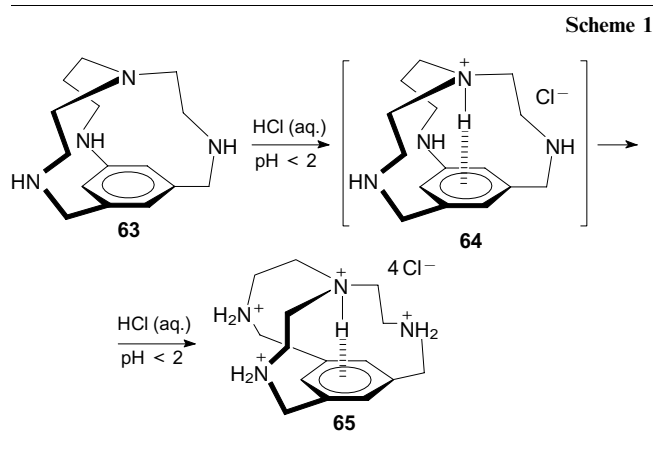
Table 9 (continued).

Compound (type of structure)	Chemical structure, CCDC refcode and temperature of XRD measurements	XRD structure	Distances NH...M (N...M), Å	Ref.
83 <sup>c</sup> (III)	 <p>PUJXIB, 283–303 K</p>		2.85 (3.75)	111
84 (III)	 <p>QEYIU, 110 K</p>		2.62 (NH <sub>2</sub> ...C <sub>6</sub> H <sub>6</sub> ) (3.20)	112
85 <sup>c</sup> (III)	 <p>QWSEQ, 193 K</p>		2.40 (3.26)	113
86 <sup>d</sup> (III)	 <p>TUVHEY, 120 K</p>		2.65 (3.49), 2.88 (3.65), 3.04 (3.77)	114
87 <sup>e</sup> (III)	 <p>XIJGAA, 110 K</p>		2.98 (3.54)	115

<sup>a</sup> The neutron diffraction study of this salt gives for the NH...M and N...M distances of 2.067 and 3.023 Å, respectively;<sup>116</sup> <sup>b</sup> there are two independent cation–anion pairs in crystals; NH...π interaction is observed in only one of them; <sup>c</sup> In XRD structure the complex is omitted for clarity; <sup>d</sup> three independent molecules; the structure with the minimum distance NH...M is shown; <sup>e</sup> NH...M distances (for phenyl groups bound to P atoms) are 3.13 and 3.23 Å.

### 4.1. One-component NH $\cdots\pi$ systems

A typical representative of the first group of models is compact tetraazacyclophane **63** (Scheme 1), in the inner space of which no other Lewis acid except for a proton can be placed.<sup>101</sup> The  $pK_a$  values of this tetraacid base determined by potentiometric titration in an aqueous solution are:  $pK_a^1 = 10.24$ ;  $pK_a^2 = 8.5$ ;  $pK_a^3 = 7.5$ ;  $pK_a^4 = 2.6$ . The first of these values characterizes the thermodynamic basicity of the bridging tertiary N-atom. Indeed, as shown by DFT calculations, monoprotonation of **63** in the gas phase, leading to the formation of cation **64**, is 14 kcal mol<sup>-1</sup> more favourable than that of the next secondary N-atom. This is explained by the formation of the NH $\cdots\pi$  bond between the encapsulated NH-proton and the benzene ring, which can be considered as the internal solvation of monocation **64**. In similar calculations for a solvating (aqueous) medium, the mentioned difference in monoprotonation energies decreases to 7 kcal mol<sup>-1</sup> due to the possibility of external solvation of the NH<sub>2</sub><sup>+</sup> groups. Nevertheless, monocation **64** again remains the most stable species under these conditions. At the same time, kinetic basicity, *i.e.*, the rate of attachment of a proton to secondary nitrogen atoms in **63**, due to their lower steric shielding, is probably higher. This assumption allows understanding why the authors of the discussed work failed to obtain monocation **64** in an individual state, because of which they had to deal only with tetracation **65** (as tetrachloride).



XRD measurements showed that the internal N–H vector in **65** is almost perfectly directed to the benzene ring centroid (NHM angle is 179°) with NH $\cdots$ M and N $\cdots$ M distances of 2.15 and 2.97 Å, respectively. Both latter values lie very close to the lower bounds of these distances measured for a wide range of compounds with NH $\cdots\pi$  interactions. Unfortunately, in the <sup>1</sup>H NMR spectrum of salt **65**, it was not possible to register the signal of the internal NH-proton due to its fast exchange (in the NMR time scale) with the protons of the NH<sub>2</sub><sup>+</sup> groups.

Compounds **66**–**69** belong to other members of the models of the first group (see Table 9). It is easy to see that they are not as perfectly preorganized as tetracation **65**, which manifests itself in somewhat larger NH $\cdots$ M and N $\cdots$ M distances. Worth noting is cyclobis(phosphazene) **68**, in which there are two identical NH $\cdots\pi$  interactions, strongly symmetrizing this complex structure. Changing the bulkiness of substituents present in the four-membered rings allows modulating the geometric characteristics of

the entire system. Compound **69** is of interest, since the pyrrole system is involved as a  $\pi$ -donor in the formation of NH $\cdots\pi$  hydrogen bond instead of the more traditional benzene ring (*cf.* compounds **46** and **55**).

Despite the non-framework architecture of ammonium tetraphenylborate salts **70** and **71**, the NH $\cdots\pi$  interaction in them is very effective. Apparently, this is a consequence of both the strong electrostatic attraction of the cation and anion, and the polydentate nature of both counterions. Indeed, NH $\cdots\pi$  bonding in these salts involves four benzene rings and all N–H bonds of the NH<sub>4</sub><sup>+</sup> cation (Fig. 34). Due to this, chains are formed in the crystal lattice, including completely identical NH $\cdots\pi$  bonds with lengths of 2.20 and 2.27 Å for **70** and **71**, respectively. The N $\cdots$ M distances (3.04 and 3.12 Å) are also quite short, which is lower than the sum (3.3 Å) of the VDW radii of the nitrogen atom and the half-thickness of the benzene ring. Against this background, the NH $\cdots\pi$  interaction of the tetraphenylborate anion with the monodentate cation of trimethylammonium in salt **72** looks expectedly weaker (see Table 9). It is noteworthy, however, that in **72** there is also a weak CH $\cdots\pi$  interaction between one of the Me groups of the proton donor and the nearest benzene ring of the tetraphenylborate anion (Fig. 35).

### 4.2. Two-component NH $\cdots\pi$ host–guest systems

#### 4.2.1. NH-Donor as a guest

The Table 9 shows data for three models of type II (compounds **73**–**75**).<sup>103, 109, 110</sup> The  $\pi$ -donor component in them is a calixarene or a macrocyclic framework structure, and the proton donor is a neutral diamine, 1,4-di(piperidin-4-yl)propane, piperidinium cation and glycine-based dike-

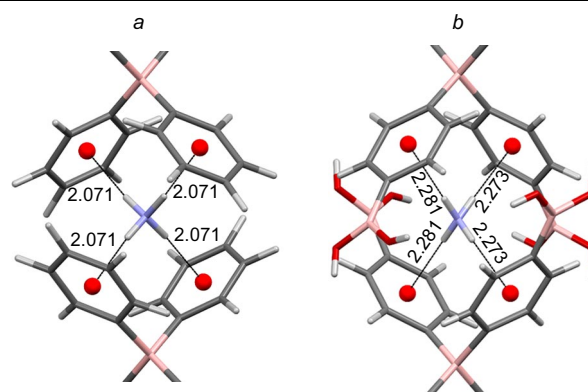


**Figure 34.** Fragments of the crystal lattice of ammonium tetraphenylborates **70** (a) and **71** (b). The figure was created by the authors using data of Refs 106, 107.

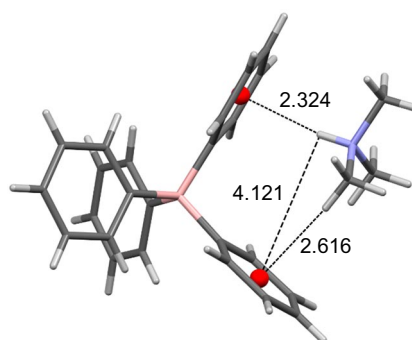


**Figure 35.** NH $\cdots\pi$  and CH $\cdots\pi$  contacts in salt **72**. The figure was created by the authors using data of Ref. 108.

topiperazine, respectively. Despite the significantly higher NH acidity of the piperidinium cation in **74**, judging by the  $\text{NH}\cdots\text{M}$  and  $\text{N}\cdots\text{M}$  parameters, the efficiency of the  $\text{NH}\cdots\pi$  interaction is noticeably higher in model **73** with neutral amino groups. A reasonable explanation for this may be the rod-like form of 1,4-di(piperidin-4-yl)propane, which allows its deeper penetration into calixarene cavity. XRD patterns are consistent with such explanation. In the case of model **75**, the internal cavity of the macrocyclic receptor is somewhat large for the guest molecule, as evidenced by the increased  $\text{NH}\cdots\pi$  distance (2.81 Å), and for the second NH group it reaches 3.32 Å.

#### 4.2.2. Benzene and other aromatics as guests

In  $\text{NH}\cdots\pi$  clusters of the group III (see Table 9), the guest molecule is benzene (**76–78** and **83–87**)<sup>14, 15, 112–115</sup> or five-membered heterocycle such as pyrrole, imidazole, and thiazole (**79–82**),<sup>14</sup> while the proton donors in the host molecule more often are part of carboxamide (**76–82**) and, less often, amino groups of the alkyl (**83**) or aniline type (**84, 86**); in one case (**87**), the proton donor is an ammonia molecule coordinated with an iridium atom. Representatives of the  $\text{NH}\cdots\pi$  models of group III are distinguished by even longer  $\text{NH}\cdots\text{M}$  and  $\text{N}\cdots\text{M}$  distances, which are in the ranges of 2.7–3.0 and 3.2–4.2 Å, respectively. Apparently, the main reason for this is the entropy factor caused by the disorder and strong anisotropy of the free benzene or heteroarene molecule, which requires additional energy consumption for its proper fixation. Interestingly, imidazole and thiazole in structures **81** and **82** form  $\text{NH}\cdots\pi$  rather than  $\text{NH}\cdots\sigma$  clusters. At the same time, in the case of thiazole, attention is drawn to a very short contact (2.33 Å) between the NH proton and the C(4) atom of the heterocyclic ring.

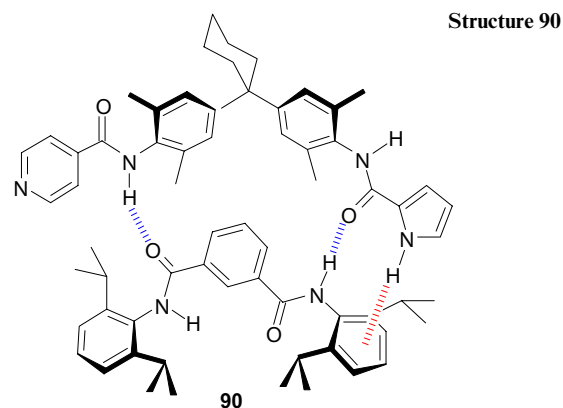
In addition to the structures represented in Table 9, cluster  $\text{C}_6\text{H}_6\cdot[\text{HNMe}_2]^+$  (**85**) should be mentioned. It was rather unexpectedly isolated in the reaction of 2,2'-methylene-bis(6-phenylphenol) **88** with pentakis(dimethylamino) tantalum **89** (Scheme 2). The cluster is a salt in which the tantalum-containing chelate exists in the form of an anion, and dimethylamine, which is eliminated during the reaction, is in the form of a dimethylammonium cation. The sample that was subjected to XRD analysis contained crystallization benzene (2.3  $\text{C}_6\text{H}_6$  molecules per one metal complex species). Surprisingly, despite the electrostatic attraction of the anion and the cation and the disorder of the  $\text{Me}_2\text{NH}^+$  cation in the crystal, the latter donates the NH proton not to the benzene rings of the macrocyclic ligand, but to one of the  $\text{C}_6\text{H}_6$  solvate molecules. The resulting complex **85** is the simplest example of benzene  $\text{NH}\cdots\pi$  clusters known to date, for which an XRD study was carried out (see Fig. 9). Interestingly, the  $\text{NH}\cdots\pi$  distance in this cluster is rather short and amounts to 2.40 Å.

Concluding this Section, it should be emphasized that caged and folded models, along with their preorganization and a certain simulation of biological structures, have their drawbacks. They lie mainly in a tedious preparation of most

of them, as well as in the difficulty of creating a space without too large voids and at the same time not being too cramped for the chosen molecular guest.

#### 4.3. Zip-complexes

In the so-called zip complexes, two usually horseshoe-shaped components, formed by a certain number of covalently linked functional groups, are linked to each other through multiple non-covalent bonds. Thus, Adams *et al.*<sup>117</sup> synthesized complex **90**, in two parts of which (on the left and in the centre), adhesion is provided by  $\text{NH}\cdots\text{O}=\text{C}$  hydrogen bonds, while on the right due to  $\text{NH}\cdots\pi$  interaction between the pyrrolic NH group and the benzene ring. Comparing the stability constant of this complex in chloroform solution with that of a related complex devoid a pyrrole group, the  $\text{NH}\cdots\pi$  bond energy in **90** was estimated to be  $1.1 \pm 0.1 \text{ kcal mol}^{-1}$ . It is noteworthy that, as expected, the resonance of pyrrole hydrogen NH in the <sup>1</sup>H NMR spectrum of **90** was paramagnetically shifted (–1.5 ppm). At the same time, the resonances of the NH amide protons were shifted to a low field (+1.4...2.1 ppm).



## 5. Folded/unfolded models

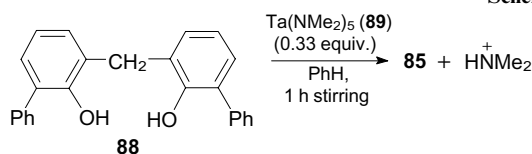
The models of this group directly simulate the high flexibility of proteins and some other biologically important compounds and their ability to change easily their conformation from folded to unfolded and *vice versa*.

### 5.1. Short peptide and diketopiperazine models

In the context of the above material, the idea of modelling  $\text{XH}\cdots\pi$  interactions using short peptides seems pretty obvious. Studies of this kind started around the turn of the century. To exclude the formation of zwitterionic structures, modified analogue of classical di-, tri-, and (much less often) tetrapeptides containing protective groups such as  $\text{NHCOCH}_3$  and  $\text{CONH}_2$  at their termini are usually tested. The main goal of such simulations consisted in clarification of local backbone/chain and intra-backbone (normally amide one) interactions and their influence on conformational mobility and the character of protein folding.

A great majority of such experiments were conducted in the gas phase using double IR/UV resonant laser spectroscopy at a temperature close to zero degrees Kelvin (supersonic jet expansion). Quite narrow stretching vibration peaks at 3370–3450 were commonly assigned to  $\text{NH}\cdots\pi$  bonds. Their number and  $\nu_{\text{NH}}$  frequencies indicated the number and possible nature of the conformers. Additional

Scheme 2



information was provided by UV spectroscopy, since the change in the position of absorption bands of the chromophore (phenyl or indole residue) testified to its involvement in the  $\text{XH}\cdots\pi$  interaction. The final conclusion about structure of each conformational isomer was obtained on the basis of the high-level theoretical calculations. Both the methods of these investigations and the corresponding results have been recently generalized in three excellent reviews.<sup>8, 118, 119</sup> Given this circumstance, below we only briefly highlight the most general trends and results. Some of them are presented in Table 10.

One of the main problems in modelling non-covalent protein interactions using amino acids and peptides is the high flexibility of the latter, making it rather difficult to conduct fairly accurate measurements. A typical example is the study in which the conformational activity of tripeptide glycyl-phenylalanyl-alanine was examined.<sup>127</sup> The authors' approach consisted in evaluation of surface free energy of various Gly-Phe-Ala conformers. Theoretical calculations (molecular dynamics, meta-dynamics and high-level *ab initio*) combined with the measurement of IR and two-photon resonance ionization spectra (R2PI), revealed 16 conformations for the gas phase, which differed in the shape of the peptide backbone. The differences in the corresponding potential energy minima did not exceed  $3 \text{ kcal mol}^{-1}$ . Conformation **91** with an  $\text{NH}\cdots\pi$  bond of the  $i \rightarrow (i-1)$  type turned out to be the most stable (Fig. 36).

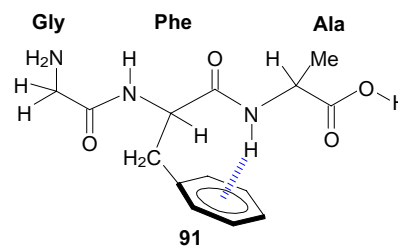


**Figure 36.**  $\text{NH}\cdots\pi$  interaction of type  $i \rightarrow (i-1)$  for the most stable conformation of tripeptide Gly-Phe-Ala (gas-phase calculation). The figure was created by the authors using data of Ref. 127.

Paradoxically as it may seem at first glance, a significant number of cases have been reported where the complication of the peptide structure leads to a decrease in the number of conformers. This is due to an increase in the rigidity of their molecular structure, which limits the number of degrees of freedom. Thus, while seven different conformers were identified for tyrosine in the gas phase (see also similar data for phenylalanine<sup>128</sup>), judging by the number of  $\nu_{\text{NH}}$  peaks in the IR spectrum, for di- and tripeptides, Tyr-Gly and Tyr-Gly-Gly, their number was reduced to four and three, respectively.<sup>122</sup>

As mentioned in the Introduction, the formation of the amide HBs is a key factor which stabilizes both the protein  $\alpha$ -helix and  $\beta$ -sheet. This is also manifested in oligopeptide

**Table 10.** Selected survey of peptides with aromatic side chains used for modelling  $\text{NH}\cdots\pi$  and other non-covalent interaction in proteins.

Peptide	Type	Short results	Ref.
Ac-Phe-Pro-NH <sub>2</sub> Ac-Pro-Phe-NH <sub>2</sub>	Capped model tripeptides	Only a limited number of minimum energy structures have been described. All of them are stabilized by $\text{NH}\cdots\text{O}=\text{C}$ HBs along backbone. No reliable information concerning $\text{NH}\cdots\pi$ interactions is provided	120
Ac-Phe-NH <sub>2</sub>	Capped model dipeptide	The most stable conformer is stabilized by a weak but significant $\text{NH}\cdots\pi$ interaction of the most common type $\text{Ar}(i) \rightarrow \text{NH}(i+1)$	121
Tyr Tyr-Gly Tyr-Gly-Gly	Amino acid, dipeptide, tripeptide	As the peptides get larger, fewer stable conformers are observed. The structural trends similar to those in phenylalanine-glycine-glycine and tryptophan-glycine-glycine were found. The effect of dispersive forces in Phe-Gly-Gly for stabilizing a folded structure is replaced by that of hydrogen bonding in Trp-Gly-Gly. No reliable information concerning their stabilization with $\text{NH}\cdots\pi$ interaction is provided	122
Ac-Leu-Val- Tyr(Me)-NHMe	Capped model tetrapeptide	Two stable conformations of this peptide were observed and by means of force field, <i>ab initio</i> , and DFT calculations their structures were determined as having folded arrangements with two different binding motifs: (a) a combined g-turn/b-turn structure and (b) a triple g-turn structure. The dominated type of HB is $\text{NH}\cdots\text{O}-\text{C}$ interaction along backbone. No $\text{NH}\cdots\pi$ interaction was registered	123
Ac-Trp-NH <sub>2</sub> Ac-Trp-NHMe	Capped model dipeptide	Using a large combination of sophisticated spectral methods, the conformational isomerization dynamics of two tryptophan-containing dipeptides has been studied. For this, single conformations of the molecules studied were selectively excited in well-defined NH stretch fundamentals. It was assumed that the rate-limiting steps of such isomerizations (about $10 \text{ kcal mol}^{-1}$ ) are mainly determined by energy of rotation around amide $\text{C}(\text{O})\text{N}$ bonds. A possible influence on this process of $\text{NH}\cdots\pi$ interactions was not mentioned.	124
Ac-Phe-NHMe Ac-Phe-NH <sub>2</sub> Ac-Gly-Phe-NH <sub>2</sub> Ac-Phe-Phe-NH <sub>2</sub>	Capped model di- and tripeptides	It has been shown that IR spectroscopy in the $3410-3460 \text{ cm}^{-1}$ frequency range provides a convincing diagnostic of the formation of $\text{NH}\cdots\pi$ bonds, in good agreement with theoretical indicators, in particular the partial electron transfer to the $\sigma^*\text{NH}$ orbital and the NCI critical electron density. It also provides a strength scale, ranking the IR spectroscopic features in this range according to the backbone conformation and the orientation of the aromatic side chain	125
Ac-Phe-Phe-NH <sub>2</sub> Ac-Trp-Tyr-NH <sub>2</sub> Ac-Phe-Phe-Phe-NH <sub>2</sub>	Capped model tri- and tetrapeptides	Different types of aromatic-aromatic arrangements have been found, illustrating the important significance of hydrophobic interactions between aromatic rings as well as the backbone NH amide groups/aromatic side groups interactions	126

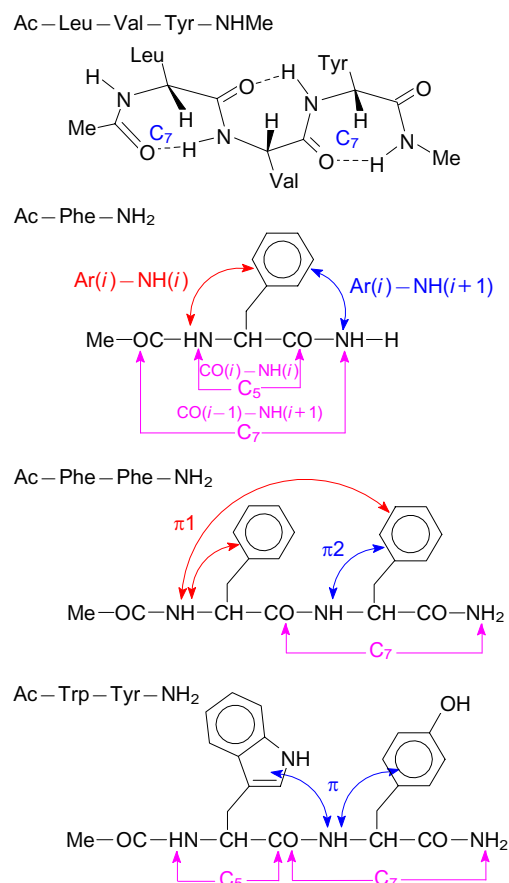


**Figure 37.** Selected examples of amide  $\text{NH}\cdots\text{O}=\text{C}$  and  $\text{NH}\cdots\pi$  hydrogen bonds in some peptide models. The figure was created by the authors using data of Refs 121, 123, 126.

models (Fig. 37). Formally, during the formation of  $\text{NH}\cdots\text{O}=\text{C}$  bonds in the protein chain, rings of various sizes are closed, which, for example, for a five- and six-membered ring is denoted by the symbols C(5) and C(7), respectively. In some short peptides, even if they contain residues of aromatic amino acids,  $\text{NH}\cdots\pi$  bonds are not detected at all. This depends on the nature of neighbouring amino acid residues and, to a large extent, on the character of specific chain turns (the classification of the latter is given in reviews<sup>8,118</sup>).

With the help of peptide models, it was found that the coexistence of several aromatic amino acids in them can lead to the formation of sandwich-like hydrogen bonds. In such cases one proton enters into  $\text{NH}\cdots\pi$  interaction with two aromatic residues at once, for example, indole and *p*-hydroxyphenyl as in a tripeptide  $\text{Ac-Trp-Tyr-NH}$  (see Fig. 37). It is believed that in real proteins, such stabilization of domains with a high content of aromatic rings can improve their hydrophobicity.<sup>118,126</sup> Interestingly, in the IR

spectra of models with sandwich hydrogen bonds, the bands of the  $\nu_{\text{NH}}$  stretching vibrations are in the region of  $3370\text{--}3380\text{ cm}^{-1}$ , *i.e.*, they undergo a greater red shift compared to monodentate  $\text{NH}\cdots\pi$  ( $3415\text{--}3450\text{ cm}^{-1}$ ) and especially free  $\text{N-H}$  bonds in simple amides ( $\sim 3495\text{ cm}^{-1}$ ). For comparison, the  $\nu_{\text{NH}}$  values of  $\text{NH}\cdots\text{O}=\text{C}$  bonds lie within  $3300\text{--}3350\text{ cm}^{-1}$ , depending on the degree of their stretching.

The possibility of structuring peptide chains through  $\text{NH}\cdots\pi$  interactions in solution was also studied.<sup>129,130</sup> For this, a series of oligomeric pseudopeptides with the inclusion of  $\alpha$ -amino acids containing aromatic ring was synthesized. One of the model compounds of this kind **92**, in which some of the  $\text{N-H}$  amide bonds are protected by a phthalimide group, is shown in Fig. 38. Using  $^1\text{H}$  NMR and FTIR spectroscopy,  $\text{NH}\cdots\pi$  interaction of type  $i \rightarrow (i+2)$  between the amide  $\text{N-H}$  bond and phenylalanine residue, very rare for proteins, was found in **92**. One evidence of this was the paramagnetic shift of the  $\text{NH}$  proton signal ( $\Delta\delta = -0.8\text{ ppm}$ ).

More recently, a series of dipeptides and tripeptides of type **X** capable of assuming a stable folded conformation have been reported (Fig. 39a).<sup>131</sup> The central fragment in them is an unnatural amino acid based on  $\beta$ -proline **Y**, abbreviated as **Abh** (7-azabicyclo[2.2.1]heptane-2-carboxylic acid). By means of amide bonds, phenylalanine is attached to it as an *N*-terminal component, and glycine, alanine, leucine, *etc.*, as a *C*-terminal one (Fig. 39b). The rigidity of the whole structure is provided by the proline component, which allows the benzene ring of phenylalanine and the  $\text{NH}$  group of the *C*-terminal amino acids to be close to each other, entering into  $\text{NH}\cdots\pi$  interaction. Due to this, the latter can be registered using the NMR method both in weakly polar ( $\text{CDCl}_3$ ) and polar ( $\text{DMSO-d}_6$ ) solvents up to a temperature of  $100\text{ }^\circ\text{C}$ . As one can see, this is the  $i \rightarrow (i+2)$  type of interaction. Notably, that  $\delta$  values of the amide proton  $\text{NH}$  in the NMR spectra of these compounds manifest a rather strong paramagnetic shift lying close to 6 ppm (*cf.* Table 7).

An attractive way to reduce the flexibility of a polypeptide chain, leading to a reduction in the number of its conformational isomers, is the modelling of the  $\text{NH}\cdots\pi$  interactions using diketopiperazines (DKP) — products of dehydration of  $\alpha$ -amino acids. The DKPs based on tryptophan, tyrosine, and phenylalanyl have been examined.<sup>21,132–134</sup> Let us consider, as an example, linear phenylalanyl-phenylalanine (**93, 94**) and its DKP structures (**95, 96**), two diastereomers of which are shown in Fig. 40.

As can be seen from Fig. 41, in the solid form, DKP is asymmetric, with one benzyl group hanging over the piperazine ring, and the other turned outward from it.<sup>135</sup> According to quantumchemical calculations [B3LYP-D3/6-311 + g(d,p)], such a structure is also the most stable in the gas phase. Its stabilization is provided by a combination of  $\text{CH}\cdots\pi$  and  $\text{NH}\cdots\pi$  interactions. The former with the  $\text{CH}\cdots\pi$  distance of  $2.69\text{ \AA}$  is manifested between the  $\text{CH}_2$

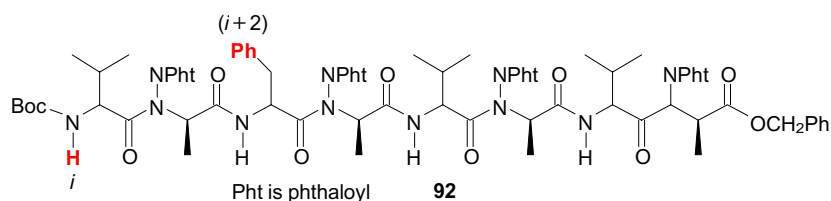


**Figure 38.** An example of a model pseudopeptide illustrating the possibility of structuring such compounds through  $\text{NH}\cdots\pi$  interactions. The figure was created by the authors using data of Ref. 129.

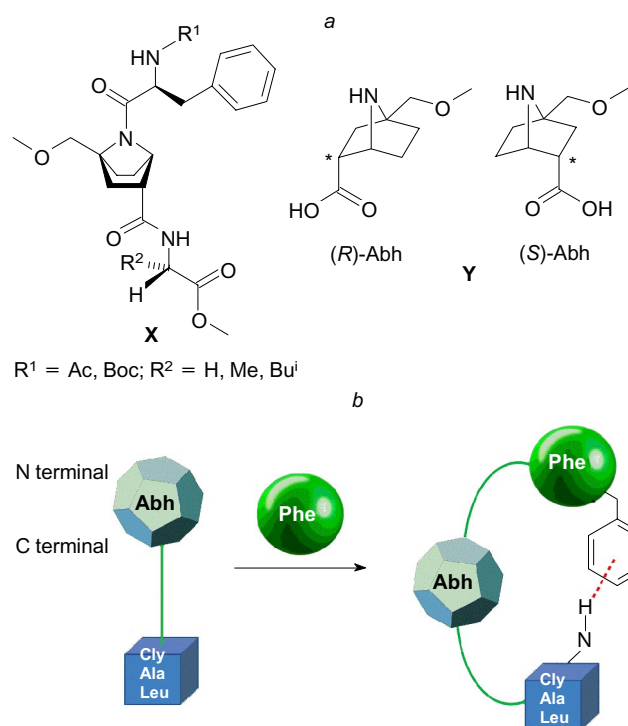


**Figure 39.** Schematic representation of the rigid proline-containing tripeptides as model for study  $\text{NH}\cdots\pi$  interactions in solution. The figure was created by the authors using data of Ref. 131.

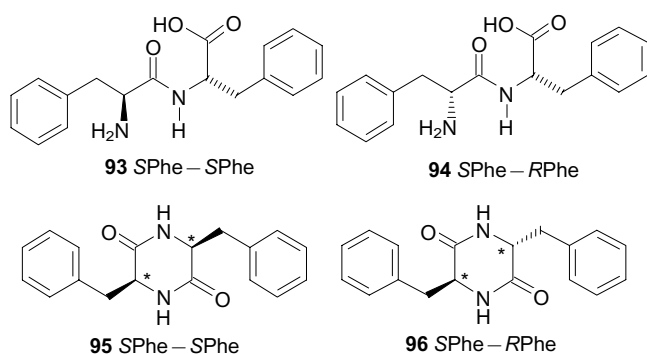


**Figure 40.** Linear (93, 94) and diketopiperazine (95, 96) structures of phenylalanyl-phenylalanine diastereomers. The figure was created by the authors using data of Ref. 132.

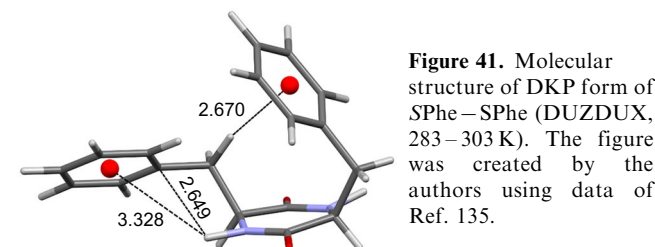


**Figure 41.** Molecular structure of DKP form of SPhe-SPhe (DUZDUX, 283–303 K). The figure was created by the authors using data of Ref. 135.

group of the outer benzyl group and the centroid of the inner benzene ring. The formation of the  $\text{NH}\cdots\pi$  bond proceeds with the participation of the amide proton and the benzene ring of the unfolded benzyl. The shortest

(2.65 Å) distance is  $\text{NH}\cdots\text{C}_i$ , while the distance to the centroid is much greater (3.23 Å).

Apparently, the DKP structure of this type is retained in solution, as evidenced by the paramagnetic shift of the signal of  $\text{CH}_2$  protons in the  $\text{DMSO-d}_6$  solution.<sup>136</sup> Unfortunately, in this polar solvent, due to the fast exchange of the NH protons in the NMR time scale, it is difficult to determine the exact position of their resonances, while the use of non-polar media was hampered by the low solubility of polar DKPs.

The influence of the chirality of cyclodipeptides and their protonated forms on the conformation and the relative contribution of  $\text{NH}\cdots\pi$  and  $\text{CH}\cdots\pi$  interactions was also studied. Only a negligible dependence of the DKP structure on chirality was noted.<sup>24, 132–134</sup> In addition, whereas in the case of neutral DKPs, their structure is almost equally formed due to  $\text{NH}\cdots\pi$  and  $\text{CH}\cdots\pi$  interactions, when passing to cations in which the proton is attached to the oxygen atom, the  $\text{OH}\cdots\pi$  bonds come to the fore.

## 5.2. Modelling neurotransmitters

Neurotransmitters (NTs) are relatively simple biological molecules that in living organisms provide communication between individual organs and tissues, on the one hand, and receptors of the autonomic or central nervous system, on the other hand. Such interactions serve as a signal to trigger certain biochemical processes.<sup>137</sup> Many of the hundreds of known NTs contain a 2-aminoethyl group attached to aromatic or heteroaromatic rings. Some of them, namely adrenaline, norepinephrine, dopamine, tyramine, serotonin and histamine, are shown in Fig. 42 *b, c*.

In the structure of neurotransmitters, three main points attract attention: 1) the presence of a rather basic ( $\text{pK}_a = 9.8–10.2$ ) primary amino group, 2)  $\pi$ -donor character of aryl and hetaryl substituents, provided by the presence of hydroxy groups or a pyrrole nitrogen atom in them, and 3) the presence of a  $\text{CH}_2\text{CH}_2$  bridge, which makes the distance between the  $\text{NH}_2$  group and the aromatic ring

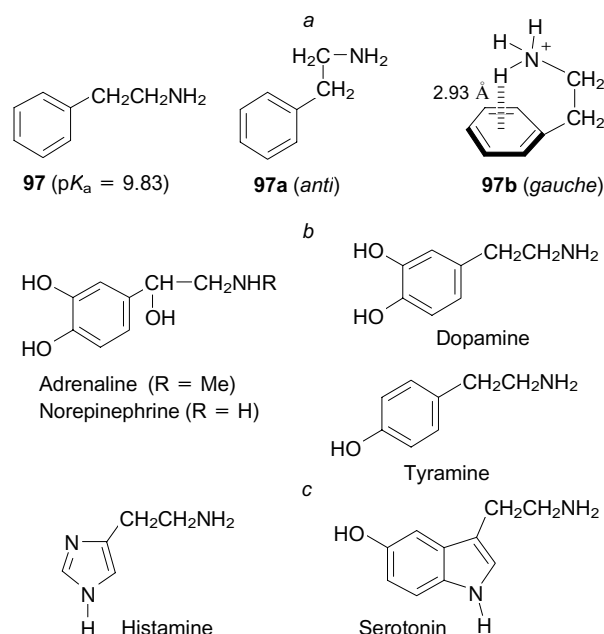


**Figure 42.** Examples of neurotransmitters (*b, c*) and related model compound 2-phenylethylamine (*a*).

approximately the same for all NTs. Taken together, all this leads to two consequences that seem to be especially important for understanding the biological activity of NTs and the diversity of their corresponding cell receptors. Firstly, the aliphatic amino group, even under conditions of low blood alkalinity (pH  $\sim$ 7.4), should exist in tissues predominantly in the protonated form with a tail  $\text{NH}_3^+$  group. Secondly, NTs are capable of taking both the expanded *anti*-form (**97a**) and the folded *gauche*-form (**97b**), which is stabilized by the intramolecular  $\text{N}\cdots\pi$  interaction. Most of the studies attempting to shed light on these issues were performed using 2-phenylethylamine **97** as a model (Fig. 42a). The conformational advantages of the *gauche*-structure have recently been elucidated in the study of the protonated phenylalkylamines of the general formula  $\text{C}_6\text{H}_5(\text{CH}_2)_n\text{NH}_2$  ( $n = 1-4$ ).<sup>138</sup> The experiments, supported by quantumchemical calculations, were carried out in the gas phase using electrospray ionization with subsequent measurement of the infrared multiple photon dissociation (IRMPD) spectra of the ions formed in this case. It was found that the benzylammonium cation does not form a stable *gauche*-form, whereas in protonated 2-phenylethylamine this form is the most stable, differing the free energy of the *anti*-form by  $5.0 \text{ kcal mol}^{-1}$ . The formation of the *gauche*-form is evidenced by the strong red shift of the  $\nu_{\text{NH}}$  band ( $3143 \text{ cm}^{-1}$ ), which is implicit for the bond that provides  $\text{NH}\cdots\pi$  interaction. For comparison, similar bands of the other two N–H bonds are located at  $3307$  and  $3337 \text{ cm}^{-1}$ . The closest ( $2.39 \text{ \AA}$ ) NH proton in the *gauche*-form is directed to the C(*ipso*) atom of the phenyl ring. For phenylalkylamines with 3–4 methylene units, the number of conformations including folded one, increases significantly, but the latter become too stable to maintain the reversible equilibrium necessary for biological processes. This is evidenced by both the absence of  $\nu_{\text{NH}}$  bands in the region of  $3000-3500 \text{ cm}^{-1}$  and quantum chemical calculations showing, in particular, a reduction in the  $\text{NH}\cdots\text{C}(\textit{ipso})$  distances to  $2.25 \text{ \AA}$  (for 3-phenylpropylamine). In a detailed work,<sup>139</sup> in which numerous references can be found on this topic, very close results were obtained using similar methods for 2-phenylethylamine. It has also been argued that the stabilization of the *gauche*-form of 2-phenylethylamine **97b** is partly due to London dispersion forces.

To some extent, 1-amino- and 2-aminoindanes can be considered analogues of 2-phenylethylamine as a model of neurotransmitters. Quantumchemical and spectral studies of their super-jet cooled samples in the gas phase led to the conclusion that 1-aminoindane under these conditions exists as two conformers,<sup>140</sup> and 2-aminoindane<sup>141</sup> as four conformers, of which **98** and **99** are the most stable, being stabilized by weak intramolecular  $\text{NH}\cdots\pi$  bonds (Fig. 43). Their energies were estimated at  $0.7-1.0 \text{ kcal mol}^{-1}$  and  $1.3-2.0 \text{ kcal mol}^{-1}$  for **98** and **99**, respectively, which is comparable to the  $\text{C}_6\text{H}_6\cdots\text{NH}_3$  complex.

One of the quantumchemical arguments in favour of the  $\text{NH}\cdots\pi$  interaction in **98** was the somewhat longer ( $1.0189 \text{ \AA}$ ) N–H<sup>a</sup> bond involved in the chelation as compared to the N–H<sup>b</sup> bond ( $1.0172 \text{ \AA}$ ) (for the further discussion of the effect of the  $\text{NH}\cdots\pi$  interactions with the participation of  $\text{NH}_2$  groups on NH bond length see Ref. 139 and Section 3.8, Fig. 31).

By the example of protonated 2-(*o*-fluorophenyl)ethylamine, the effect of the *ortho*-substituent in the phenyl ring on the preferred geometry of similar NT analogues was

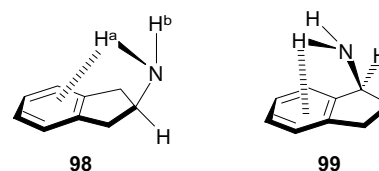


**Figure 43.** Preferred conformations of protonated 1-amino- and 2-aminoindanes. The figure was created by the authors using data of Refs 140, 141.

studied.<sup>142</sup> The study of the range of stretching vibrations of NH bonds revealed three low-energy *gauche*-conformers. The form **100** proved to be the most stable, being stabilized simultaneously by two moderately strong hydrogen bonds:  $\text{NH}^+\cdots\pi$  and  $\text{NH}^+\cdots\text{F}$  (Fig. 44). It was slightly inferior in stability to conformer **101**, stabilized only by the  $\text{NH}^+\cdots\pi$  bond. It was not detected experimentally, but its possible existence in low concentration followed from quantum chemical calculations.

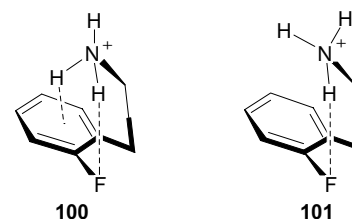


**Figure 44.** The two most stable *gauche*-forms of 2-(*o*-fluorophenyl)ethylamine. The figure was created by the authors using data of Ref. 142.

The situation is less unambiguous for the solid NTs. According to the results of XRD analysis (Table 11), most of them exist in an expanded form even after protonation. This can be explained by the specificity of the crystal packing and the strong influence of the counterion. The important role of the latter factor is confirmed by short distances ( $1.91-2.37 \text{ \AA}$ ) between the anion and the NH proton. In general, the implementation of the folded form with  $\text{NH}^+\cdots\pi$  binding is facilitated by low-nucleophilic anions with a strongly delocalized charge (*e.g.*, picrate) and especially increased  $\pi$ -donor ability of the aromatic ring, as in the case of mescaline and tryptamine.

It is interesting to compare the NT discussed above with acetylcholine **114**, one of the main representatives of such biomolecules (Fig. 45). Among many functions of **114**, the regulation of muscle activity, participation in the parasympathetic nervous system, as well as in the processes associated with learning and memory are especially important. The molecule of **114** contains no groups that could enter into  $\text{NH}\cdots\pi$  interaction, but there is a  $\text{CH}_2\text{CH}_2$  chain, which once again emphasizes its important purpose.

Back in 1990, Dougherty and Stauffer<sup>178</sup> reported the first evidence that the various receptors to which acetylcholine binds contain residues of aromatic amino acids such as phenylalanine, tyrosine, and tryptophan. One such evidence was the high affinity of acetylcholine for the synthetic receptor **115**. The cluster **116** formed between them has a fairly high formation constant ( $K_d = 50 \text{ mM}$ ), which is close to the binding energy of real biological complexes of the

**Table 11.** Conformation of some neurotransmitters and their close analogues according to XRD analysis.

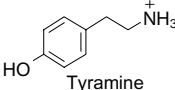
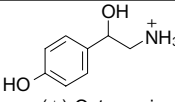
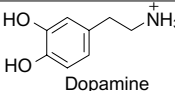
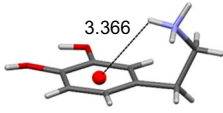
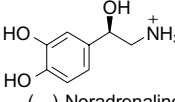
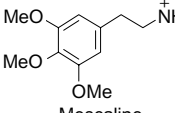
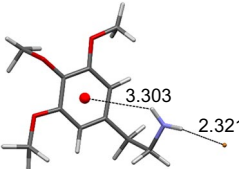
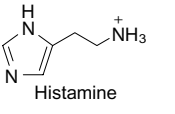
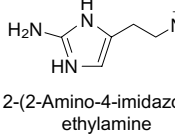
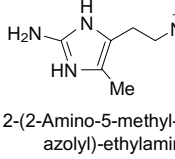
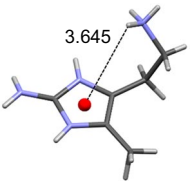
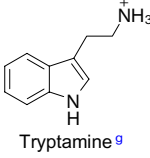
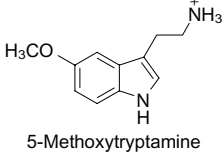
Compound	Neurotransmitter	CCDC refcode ( <i>T</i> , <i>K</i> ) <sup>a</sup>	Anion, X <sup>−</sup>	Conformation	Distances, Å		Ref.
					NH...X <sup>−</sup>	NH...M (N...M)	
97	Phenethylamine Ph(CH <sub>2</sub> ) <sub>2</sub> N <sup>+</sup> H <sub>3</sub>	PEAHCL01	Cl <sup>−</sup>	<i>anti</i>	2.27	—	143
102a	 Tyramine	TYRAMH01 (200) <sup>144</sup> SENJEC (233) <sup>145</sup> TYRAMH <sup>146</sup> TYRAMC <sup>147</sup> TYRAMC11 <sup>148</sup>	<b>B</b> <sup>b</sup>	<i>anti</i>	—	—	144–146
102b			Cl <sup>−</sup>	<i>anti</i>	2.19 <sup>147</sup> 2.29 <sup>148</sup>	—	147, 148
103	 (±)-Octopamine	OCTOPC	Cl <sup>−</sup>	<i>anti</i>	2.09	—	149
104a	 Dopamine	TIRZAX (123) DOPAMN01 MIYLOV	<b>Z</b> <sup>c</sup> Cl <sup>−</sup> 3,5-Dinitrobenzoate	<i>anti</i> <i>anti</i> <i>gauche</i>	— 2.29 1.91 <sup>d</sup>	— — 3.37 (3.940)	150 151 152
							
105a	 (−)-Noradrenaline	NADREN NADRHC	<b>Z</b> Cl <sup>−</sup>	<i>anti</i> <i>anti</i>	— 2.24	— —	153 154
106a	 (−)-Adrenaline	ADRENL ADRTAR	See <sup>c</sup> Tartrate	<i>anti</i> <i>anti</i>	— 1.99	— —	155 156
107	 Mescaline	MESCHB	Br <sup>−</sup>	<i>gauche</i>	2.32	3.30 (3.888)	157
							
108a		HISTAN <sup>158</sup> XOLLIW <sup>159</sup>	<b>B</b>	<i>anti</i>	—	—	158, 159
108b	 Histamine	HISTBR <sup>160</sup> HISTBR01 <sup>161</sup>	Br <sup>−</sup>	<i>anti</i>	2.37 (1.98 <sup>e</sup> ) <sup>160</sup> 2.25 (2.15 <sup>e</sup> ) <sup>161</sup>	—	160, 161
108c		XOLKUH	Cl <sup>−</sup>	<i>anti</i>	2.24 (1.93 <sup>e</sup> )	—	159
108d		XOLLES	2 Cl <sup>−</sup>	<i>anti</i>	2.16	—	159
108e		HISAPH01	2 H <sub>2</sub> PO <sub>4</sub> <sup>−</sup>	<i>anti</i>	2.07	—	162
109	 2-(2-Amino-4-imidazolyl)-ethylamine	DIPDIP10	Dipicrate	<i>gauche</i>	1.96 <sup>f</sup>	3.26 (3.906)	163
							
110	 2-(2-Amino-5-methyl-4-imidazolyl)-ethylamine	DIPDOV10	Dipicrate	<i>gauche</i>	2.28 <sup>f</sup>	3.65 (3.855)	163
							

Table 11 (continued).

Compound	Neurotransmitter	CCDC refcode ( <i>T</i> , <i>K</i> ) <sup>a</sup>	Anion, X <sup>-</sup>	Conformation	Distances, Å		Ref.
					NH...X <sup>-</sup>	NH...M (N...M)	
<b>111a</b>	 Tryptamine <sup>9</sup>	XUDTOF	<b>B</b>	<i>gauche</i>	—	3.57 (3.878)	164
<b>111b</b>		TRYPTA10	Cl <sup>-</sup>	<i>gauche</i>	2.04	3.47 (3.739)	165
<b>111c</b>		DAMNAH	Benzoate	<i>gauche</i>	1.98 <sup>h</sup>	3.23 <sup>h</sup> (3.787)	166
<b>111d</b>		TRYPIC	Picrate	<i>gauche</i>	1.87	3.46 (3.934)	167
<b>112a</b>	 Serotonin	SERHOX	Oxalate	<i>anti</i>	1.89	—	168
<b>112b</b>		VIKWIX	Adipate	<i>anti</i>	2.33 (1.80 <sup>i</sup> )	—	169
<b>112c</b>		SERPIC <sup>170</sup>	Picrate	<i>gauche</i>	2.114 <sup>f</sup> (Ref. 170)	3.32 (3.934) <sup>170</sup>	170,
		SERPIC01 (90) <sup>171</sup>			2.117 <sup>f</sup> (Ref. 171)	3.37 (3.974) <sup>171</sup>	171
<b>113a</b>	 5-Methoxytryptamine	MXTRYP	<b>B<sup>j</sup></b>	<i>gauche</i>	—	3.09 (3.801)	172
<b>113b</b>		MIAMTA	3-Indole-acetate	<i>gauche</i>	1.82 <sup>d</sup>	3.46 (3.905)	173

<sup>a</sup> *T* = 283–300 K, unless otherwise noted. <sup>b</sup> Base. <sup>c</sup> Zwitterion with proton transfer from 3-OH to NH<sub>2</sub>(NH). <sup>d</sup> NH...O<sub>2</sub>C. <sup>e</sup> NH...N (imidazole). <sup>f</sup> NH...O<sub>2</sub>N. <sup>g</sup> The CCDC has data about other tryptamine salts existing in *gauche*-conformations: 4-chlorobenzoate,<sup>174</sup> 2-thiopheneacetate,<sup>175</sup> 3-indoleacetate,<sup>175</sup> adenine-9-yl-acetate.<sup>176</sup> <sup>h</sup> Two independent cation–anion pairs; the smallest distances are shown. <sup>i</sup> NH...O (serotonin). <sup>j</sup> *gauche*-Conformation is also confirmed by rotationally resolved fluorescence spectroscopy and resonant ionization spectroscopy.<sup>177</sup>

host–guest type. Compound **115** forms similar strong complexes with other ammonium salts. Accordingly, the forces promoting the incorporation of the ammonium cation into the cavity were characterized as a ‘cation-π’ interaction.<sup>23</sup> Although living tissues contain many ions and molecules

with lone electron pairs, their interaction with acetylcholine seems to play a secondary role due to the hydrophobicity of the inner cavity of the receptor.

Dougherty’s work initiated many other studies along this line, including those related to NH...π interaction. In

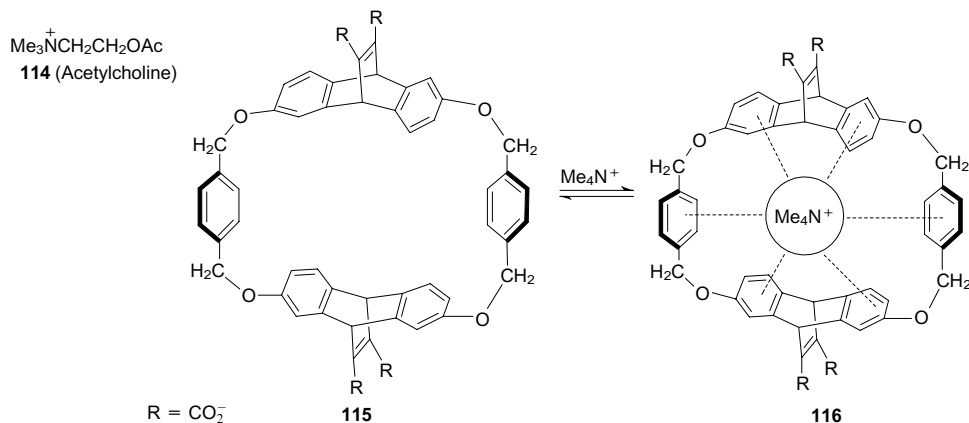
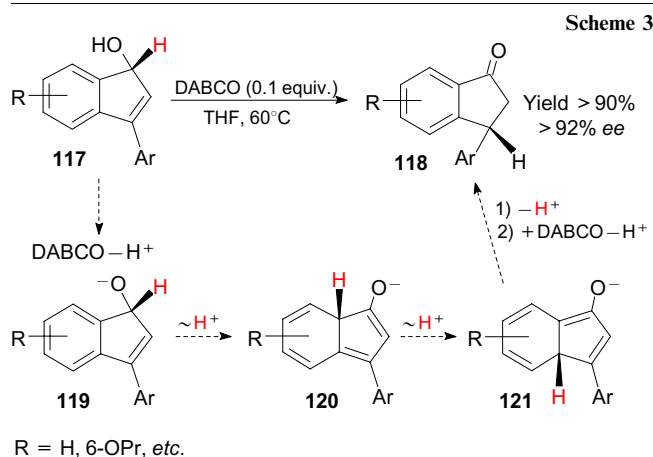


**Figure 45.** Synthetic receptor **115** which efficiently encapsulates acetylcholine **114**. The figure was created by the authors using data of Ref. 178.

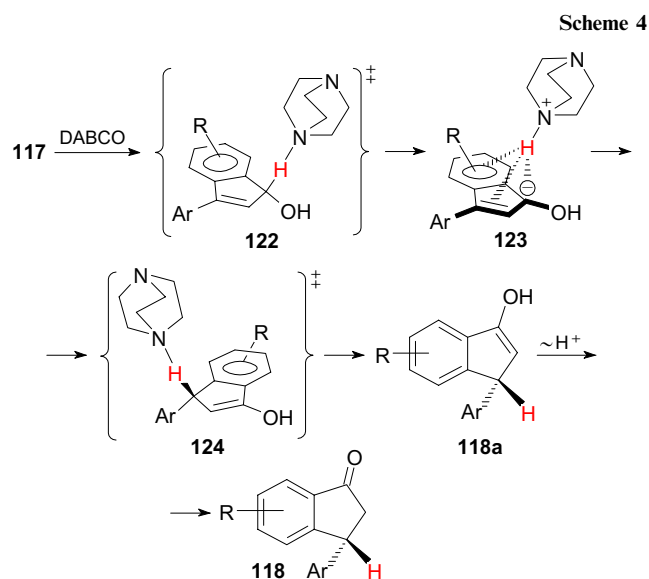
particular, Shishido *et al.*<sup>179</sup> using pre-dissociative IR spectroscopy and mass spectrometry, tried to model molecular recognition of aromatic nuclei by acetylcholine in the gas phase. For this purpose, they simulated the formation of clusters of the trimethylammonium cation with different amounts (1–4 mol. equiv.) of benzene. Using natural bond orbital (NBO) calculations, it was shown that the positive charge in the  $[\text{HNMe}_3]^+$  cation is almost completely dispersed over the methyl groups, as a result of which the interaction of this cation with benzene proceeds exclusively due to  $\text{C}\cdots\pi$ , but not  $\text{NH}\cdots\pi$  binding. Based on this, it was found more accurate to classify the forces responsible for molecular recognition of acetylcholine receptors as ‘activated  $\text{CH}\cdots\pi$  interaction’. The review focused on cation- $\pi$  and anion- $\pi$  interactions has been published by Frontera *et al.*<sup>180</sup>

## 6. Reactions driven by $\text{NH}\cdots\pi$ interactions

One of the yet rare examples of such reactions is the base-catalyzed (preferably with DABCO) isomerization of 3-aryllindenols **117** into 3-aryllindanonones **118** (Scheme 3).<sup>181</sup> Being a variation of the well-known allyl rearrangement, this transformation is remarkable for its high enantioselectivity, which was used for the total synthesis of the muscarinic receptor antagonist (*R*)-tolterodine.<sup>182</sup> Formally, the process represents a concerted suprafacial 1,3-hydrogen shift forbidden by the orbital symmetry rules.

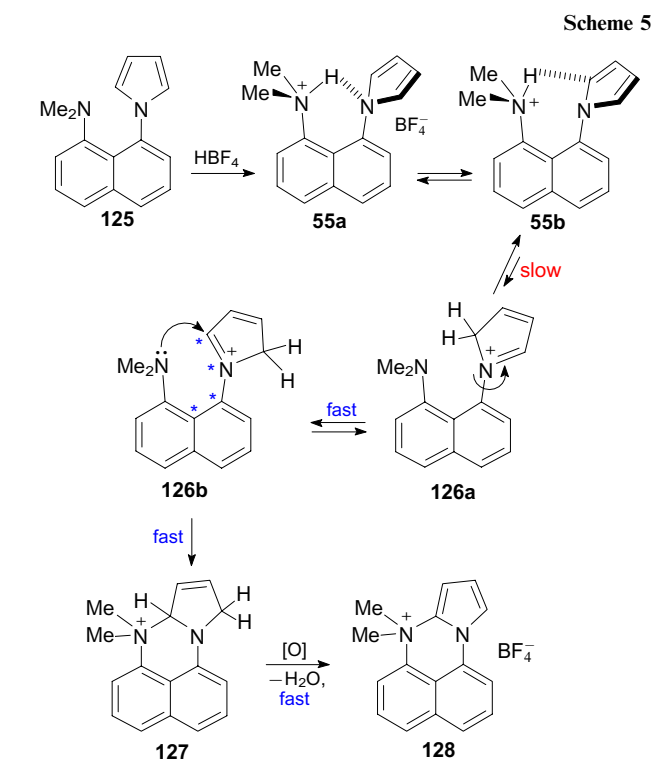


Initially, a stepwise proton transfer mechanism was proposed for it, shown in Scheme 3 and including intermediates **119**–**121**. However, it did not explain two observations: why both enantiomers cannot be obtained at each stage, and how the high activation energy ( $> 30 \text{ kcal mol}^{-1}$ ) is compatible with high stereoselectivity. These issues were clarified in 2018 by Ascough *et al.*<sup>183</sup> Based on theoretical calculations using molecular dynamics for condensed matter, a significantly different mechanism has been proposed, including only two stages of proton transfer (Scheme 4). Its principal feature is the deprotonation at the first stage of the C–H bond, which is geminal to the OH group, instead of the elimination of a proton from a seemingly more acidic hydroxyl. The authors proved that the acidity of this CH bond is at least commensurate with that of the secondary OH group. Indeed, the resulting carbanion **123** is simultaneously stabilized by allyl and benzyl resonances, as well as by conjugation with 3-aryl



group. It was subsequently shown by theoretical calculations that the  $\text{DABCO-H}^+$  cation formed upon ionization of the C–H bond can enter into  $\text{NH}\cdots\pi$  interaction with the formed rather extensive anionic  $\pi$ -system (structures **122**  $\rightarrow$  **123**) and move freely above it. As a result of such sliding over the surface of a five-membered ring, the proton is easily transferred to the C(3) atom (**123**  $\rightarrow$  **124**  $\rightarrow$  **118a**), which retains the stereochemical configuration without disturbing the aromaticity of the benzene ring as in the original mechanism (see structures **120** and **121**). Another important thing is that the activation energy of the whole process, which is limited by deprotonation of the C–H bond, decreases by  $15 \text{ kcal mol}^{-1}$  with this mechanism. Note, that tautomerization of **118a** to the final keto form **118** is determined by the Erlenmeyer–Eltekov rule.

The second example of the influence of  $\text{NH}\cdots\pi$  interactions on the reactivity was the first case of nucleophilic substitution of a hydrogen atom in an unactivated pyrrole ring, recently discovered in our laboratory (Scheme 5).<sup>184</sup> It was found that the treatment of 1-dimethylamino-8-(pyrrol-1-yl)naphthalene **125** with an equimolar amount of  $\text{HBF}_4$  in MeCN produces tetrafluoroborate **55**, which is sufficiently stable in solution for 2–3 h. This is confirmed by the complete similarity of  $^1\text{H}$  NMR spectra of **55** and its much more stable analogue **46** (see Table 7). As noted above (see Table 5 and pp. 14–16), XRD measurements of salt **46** confirmed the formation of a pronounced intramolecular  $\text{NH}\cdots\text{N}(\pi)$  hydrogen bond in its cation. The obvious presence of the similar HB in salt **55** makes it easy to explain its further behaviour. The point is that when the proton spectrum of **55** is measured again after 4 h, the clear signs of the presence of the second substance in the NMR tube appear. Its concentration slowly increases and after some time under ambient conditions it becomes the only product, which is a colourless crystalline pyrrolo[1,2-*a*]dihydroperimidinium tetrafluoroborate **128**. Several circumstances are especially surprising in this transformation. First, this is the very fact of nucleophilic substitution of hydrogen in the electron-rich pyrrole ring. Secondly, the participation of such a weak nucleophile as the aniline  $\text{NMe}_2$  group in it. Third, the oxidation of intermediate **127**, which is necessary for aromatization through the abstraction of the hydride ion, proceeds with the participa-



tion of atmospheric oxygen and does not require the addition of strong oxidants such as  $\text{KMnO}_4$ . At last, the high selectivity and smoothness of the process are striking.

Based on quantum chemical calculations and a number of experiments, a putative mechanism was proposed for the reaction (see Scheme 5). There are good reasons to believe that the rate-determining stage is the formation of 2H-pyrrolium cation **126**. Its activation energy is 14.5 and 17.1  $\text{kcal mol}^{-1}$  for the gas phase and solution in acetonitrile, respectively. It is logical to assume that the formation of cation **126** occurs as a result of the slow sliding of the NH proton along the N–C(2) edge: **55a**  $\rightarrow$  **55b**  $\rightarrow$  **126**. In general, the reaction becomes possible due to the proximity of the *peri*-substituents in **125** and the soft acid catalysis, which activates the pyrrole ring to the nucleophile attack.

## 7. Miscellaneous issues

### 7.1. $\text{NH}\cdots\pi$ interaction and recognition of $\alpha$ -amino acids

In an extensive collaborative study, Blasco *et al.*<sup>185</sup> tried to figure out how biological receptors recognize hydrophilic and hydrophobic amino acids. The former were tested with histidine, aspartic and glutamic acids, and the latter with alanine, phenylalanine, tyrosine and tryptophan. Two pyridine-containing azacrown ethers with a pendant 2-aminoethyl (**129**) or 2-(naphth-1-yl)aminoethyl tail (**130**) served as receptor models. Potentiometric and calorimetric measurements in an aqueous medium, as well as high-level theoretical calculations, were used as research methods. It was assumed that the absence or presence of a 1-naphthyl group would provide a hydrophilic–hydrophobic balance when choosing the amino acids of ligand **129** or **130**. It was found that the binding of the selected amino acids by the ligands is provided mainly by salt interactions (especially with the participation of the amino acid carboxylate anion) and hydrogen bonds. As for  $\text{NH}\cdots\pi$  interactions, they appear only with ligand **129** upon protonation or hydration. One of the complexes formed between the tyrosine molecule and

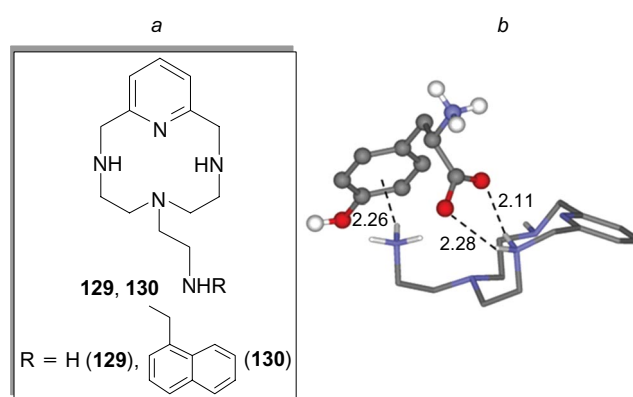


**Figure 46.** Synthetic receptors for the recognition of hydrophilic and hydrophobic amino acids (a); theoretically calculated structure of the adduct of the doubly protonated receptor **129** with the tyrosine molecule lying in the potential minimum (b) Reproduced from Blasco *et al.*<sup>185</sup> with permission of the Royal Society of Chemistry.

the doubly protonated ligand **129** is shown in Fig. 46b. A very short  $\text{NH}\cdots\pi$  bond between the proton of the terminal ammonium group of the ligand and the centroid of the benzene ring of tyrosine deserves attention. To some extent, this interaction can be considered as a model for receptor binding of neurotransmitters carrying the terminal 2-aminoethyl group (see Section 5.2).

### 7.2. $\text{NH}\cdots\pi$ interaction and urea-assisted protein denaturation

Due to multiple non-covalent interactions, proteins commonly exist in a biologically active folded form. However, under the influence of various factors, for example, elevated temperature, mechanical impact or some chemicals, their molecules undergo denaturation, losing their secondary, tertiary and quaternary structure. One of the well-known denaturing agents is urea. The reasons for this have recently been specially studied using a number of experimental and computational methods.<sup>186</sup>

The main object of the study was a small tryptophan-containing protein. It was found that the mechanism of the denaturing action of urea is associated with its high affinity for aromatic nuclei and includes two types of interactions — stacking and the formation of  $\text{NH}\cdots\pi$  hydrogen bonds, the ratio and strength of which is determined by the nature of the aromatic system. As follows from Fig. 47, which shows the calculated interaction energies for optimized structures, stacking is most efficient for the imidazolium ion, followed by indole, neutral imidazole, phenol, and benzene. As for  $\text{NH}\cdots\pi$  interactions, they are stronger for indole and phenyl group. Decomposition of the obtained energies into components showed that the attraction of urea to aromatic nuclei is mainly due to dispersion forces (shown in parentheses in the top row), while the electrostatic interaction is slightly repulsive.

### 7.3. $\text{NH}\cdots\pi$ interaction in vitamin $\text{B}_{12}$ coenzyme

The significance of  $\text{NH}\cdots\pi$  interactions is not limited to proteins and such biomolecules as neurotransmitters. Thus, Starikov and Steiner,<sup>187</sup> using neutron diffraction on crystals of cobalamin **131** (a coenzyme of vitamin  $\text{B}_{12}$ ), found an  $\text{NH}\cdots\pi$  bond in it with a length of 2.58 Å and an energy of 4.0  $\text{kcal mol}^{-1}$ . This bond is formed between the proton of

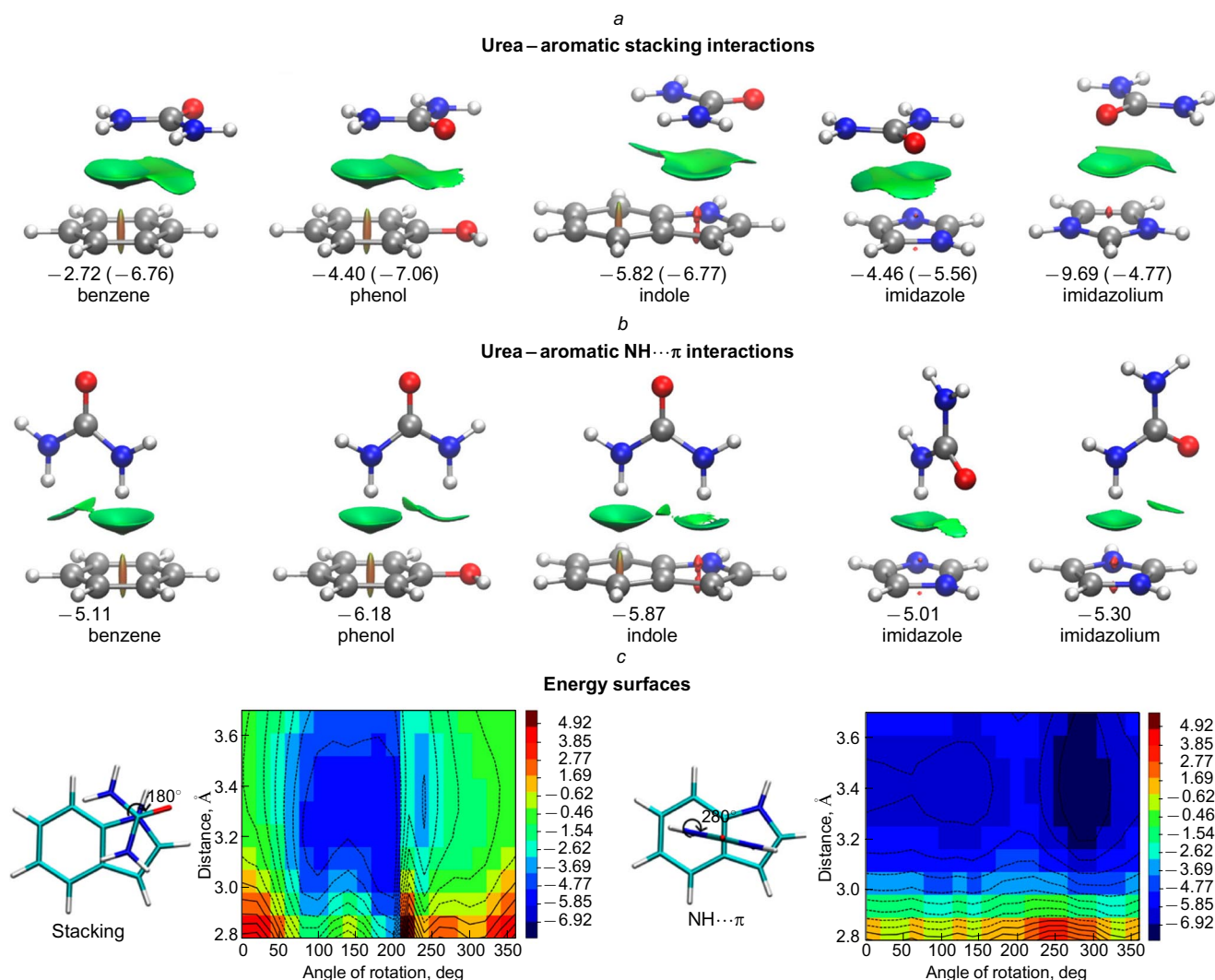


**Figure 47.** Calculated energies of interaction of urea with aromatic rings that make up amino acids. Reproduced from Goyal *et al.*<sup>186</sup> with permission of the American Chemical Society.

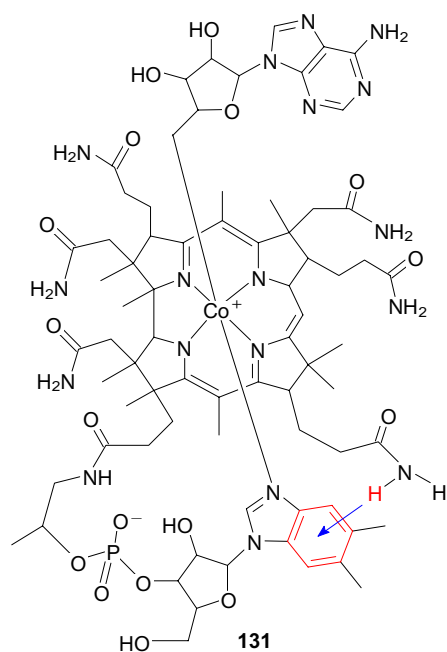


**Figure 48.** NH...π interaction in vitamin B<sub>12</sub> coenzyme. The figure was created by the authors using data of Ref. 187.

one of the propioamide groups and the benzene ring of the 5,6-dimethylbenzimidazole moiety (Fig. 48).

## 8. Practical applications of NH...π interactions

Most of the research on the practical use of NH...π interactions is to some extent related to medicinal chemistry. Thus, it has been proposed to use carbon nanotubes [CNTs (5,0)] functionalized with a non-covalently bound amino acid, for example, alanine, for the targeted delivery of the anti-tuberculosis drug isoniazid (isonicotinic acid hydrazide).<sup>188</sup> The success of such a task depends on the optimal binding energy of the drug with the carrier: it must be sufficiently high so that the drug is not desorbed along the way, but at the same time relatively low so that it is easily detached from the carrier upon reaching the receptor. The proposed combination seems to satisfy these requirements, since the binding energy of isoniazid to the CNT-alanine carrier, according to theoretical calculations, is 8.5 kcal mol<sup>-1</sup>. It is believed that the very binding of isoniazid is provided by a combination of stacking and NH...π interaction, which is facilitated by the planarity of the isoniazid molecule and the graphene-like structure of CNTs.

Another problem associated with the targeted drug delivery is the predominantly lipophilic nature of cell membranes, which hinders the penetration of polar substances into the cell. At the same time, receptors having a protein, *i.e.*, very polar in nature, tend to better interact with polar molecules. To increase the membrane permeability with respect to both polar and low-polar drugs, it was proposed to use polyfunctional macrocyclic compounds with a molecular weight of at least 600–700 Da. It was assumed that due to the high conformational flexibility, macrocycles bearing suitable functional groups can more easily adapt to the environment, including tissue receptors. Such molecules were called ‘chameleons’.

Based on this idea, Tyagi *et al.*<sup>189</sup> synthesized macrocyclic polyamides **132a–e** containing residues of lysine (**132a**), phenylalanine (**132c**), and other amino acids with aromatic nuclei (**132b,d,e**) (Fig. 49). They found that whereas in the <sup>1</sup>H NMR spectrum of the lysine-containing macrocycle **132a** in CDCl<sub>3</sub> the NH proton resonates at  $\delta$  6.3 ppm, in the spectrum of compound **132c** containing a phenylalanine residue, it undergoes a significant paramagnetic shift ( $\Delta\delta_{\text{NH}} \approx -1.6$  ppm), resonating at  $\delta$  4.7 ppm.

This indicates that an NH $\cdots\pi$  bond is formed between the phenyl ring of the benzyl group and the N(I)H proton, which was also confirmed by XRD analysis [structure **132c'**; distances are: N(I)H $\cdots$ C1' = 3.40 Å, N(I) $\cdots$ M = 4.02 Å, N $\cdots$ C1' = 3.45 Å]. As expected, the high-field NH proton shift in the spectra of compounds **132d** and **132e**, due to the absence of the benzyl CH<sub>2</sub> group, is much lower ( $\Delta\delta_{\text{NH}} \approx -0.4$  ppm), and in spectrum of **132b** the corresponding value is intermediate ( $-0.6$  ppm) due to the greater distance of phenyl nuclei from the NH proton. Thus, the NH $\cdots\pi$  interaction in **132c** and the realization of the folded conformation contribute to the shielding of the neighbouring C=O group and a decrease in its polarity. As a result, the lipophilicity of the whole compound increases and its penetration into the cell is facilitated.

As already noted above, NH $\cdots\pi$  interactions are involved in the recognition of various exogenous substances by biological receptors, including drugs. Here is another example on this topic, associated with the transmembrane protein neurokinin-1 (Fig. 50). The attachment to its receptors of a neurotransmitter polypeptide under code-name P, causes pain and neurogenic inflammation in animals. In search of an antidote that prevents the binding of the neurokinin receptor to P, a very effective drug was synthesized under the code CP-96345. It was possible to establish that it binds to the histidine residue (His-197) in the neuro-

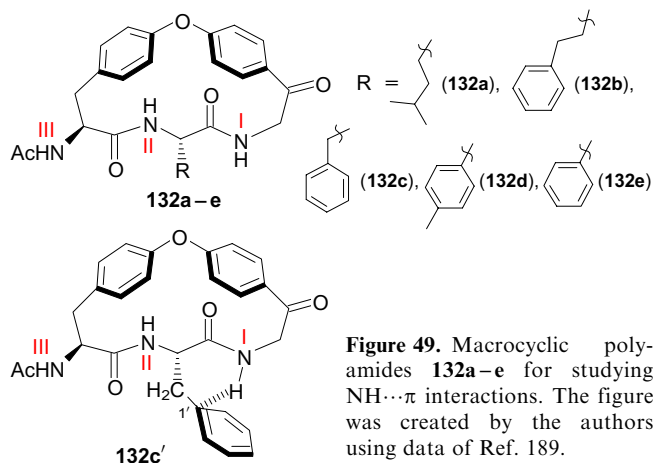


**Figure 49.** Macrocyclic polyamides **132a–e** for studying NH $\cdots\pi$  interactions. The figure was created by the authors using data of Ref. 189.

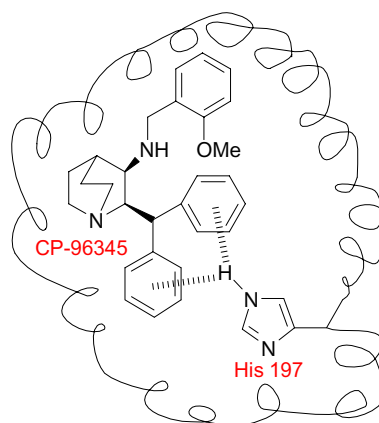


**Figure 50.** Schematic representation of NH $\cdots\pi$  interaction of the neurokinin receptor with the drug CP-96345. The figure was created by the authors using data of Ref. 190.

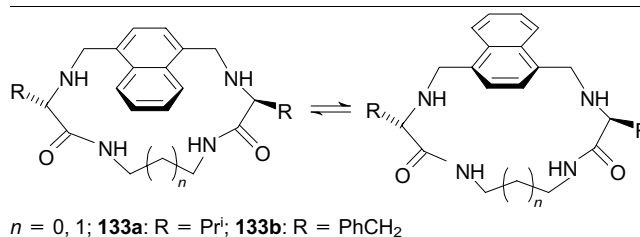
kinin receptor. Based on numerous experiments, it was concluded that the analgesic effect of CP-96345 is due to the presence of a benzhydryl group in its molecule, two benzene rings of which enter NH $\cdots\pi$  interaction with the rather acidic NH proton of the imidazole ring in neurokinin-1 (see Fig. 50).<sup>190</sup>

In connection with the growing interest in molecular machines,<sup>191,192</sup> Alfonso *et al.*<sup>193</sup> synthesized 16- and 17-membered naphthocyclophanes **133a,b** based on valine and phenylalanine (Fig. 51). Investigation of the rotation of the naphthalene ring as a rotor showed that in the case of phenylalanine it slows down significantly. This was attributed to the folding of the amide phenyl groups into a conformation stabilized by NH $\cdots\pi$  interaction.

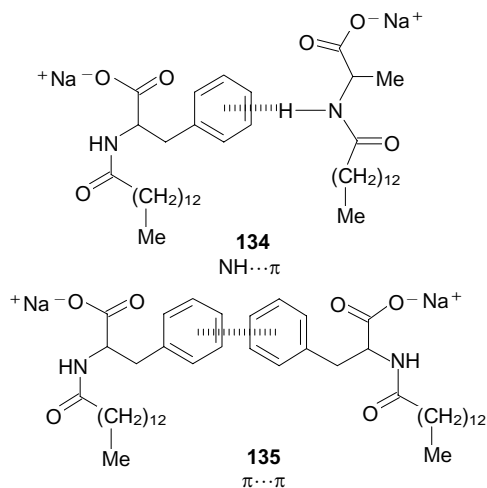
The possibility of using NH $\cdots\pi$  interactions to improve the biocompatibility of surfactants and the quality of cosmetics, detergents, emulsifiers, *etc.*, was investigated.<sup>194</sup> For this, binary mixtures of anionic amphiphilic compounds based on amino acids were taken. It was found that when using mixtures of sodium salts of *N*-tetradecylalanine and *N*-tetradecylphenylalanine, the surface quality and the growth of micelle formation noticeably increase. This was attributed to binding amphiphilic components not only due to hydrophobic forces, but also as a result of NH $\cdots\pi$  and  $\pi\cdots\pi$  binding (Fig. 52, structures **134** and **135**).

Along with other non-covalent forces, NH $\cdots\pi$  interactions play a role in the field of crystal engineering.<sup>195</sup>

Recently, the effect of NH $\cdots\pi$  interactions has been successfully used for the industrially important separation of a mixture of benzene, cyclohexene, and cyclohexane, which is formed by hydrogenation of benzene.<sup>15</sup> Traditional separation methods of this mixture are based on extraction and azeotropic distillation processes and are extremely expensive. Yao *et al.*<sup>15</sup> have developed a much more efficient adsorption method using amide naphthalene-containing nanotubes of the **76–82** types as a solid adsorbent (see



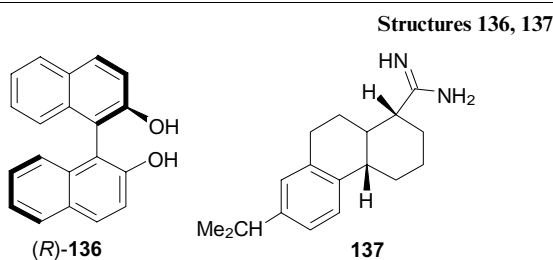
**Figure 51.** Amino acid-based naphthocyclophane molecular rotors. The figure was created by the authors using data of Ref. 193.



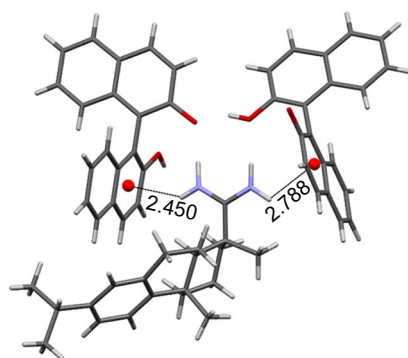
**Figure 53.** Molecular structure of diastereomeric salt of 1,10-bis(2-(2'-hydroxyphenyl)ethyl)ethane-2,2'-diol with dehydroabietyl amidine **138** (ATOFIB, 150 K). The figure was created by the authors using data of Ref. 196.

Table 9). The method is based on the formation of very stable  $\text{NH}\cdots\pi$  clusters by benzene and cyclohexene, and the process can be made highly selective by changing the conditions and choosing a suitable catalyst from this series.

Kodama *et al.*<sup>196</sup> demonstrated that  $\text{NH}\cdots\pi$  interactions can be helpful in chiral recognition processes. Thus, a procedure for the direct enantioseparation of axially chiral 1,1'-biaryl-2,2'-diols was developed. For this purpose, chiral amidines were proposed as resolving agents, for example, compound **137** synthesized from commercially available dehydroabietyl acid. First, when mixing equimolar amounts of optically pure **137** and racemic 1,1'-binaphthyl-2,2'-diol **136**, a mixture of easily separated diastereomeric amidinium salts was obtained as a result of a proton transfer from one of the OH groups on the amidine functionality. Their



**Figure 52.** Stabilizing micelle formation interaction of two amphiphilic molecules:  $\text{NH}\cdots\pi$  interaction between alanyl-based and phenylalanyl-based surfactants (**134**);  $\pi\cdots\pi$  interaction between two phenylalanyl-based surfactants (**135**). The figure was created by the authors using data of Ref. 194.



subsequent acidification and extraction resulted in the isolation of individual diol enantiomers with an optical purity  $ee > 95-97\%$ . The principle of chiral recognition is illustrated by XRD structure **138** (Fig. 53) of one of the obtained salts. It shows how the amidinium group holds two monoanions (*R*)-**138** due to two hydrogen  $\text{N}-\text{H}\cdots\text{O}$  and two  $\text{NH}\cdots\pi$  bonds with modest  $\text{NH}\cdots$ centroid distances.

## 9. Conclusion

To summarize, the present survey shows that the history of  $\text{NH}\cdots\pi$  interactions research is about 30 years old. During this time, more than 170 publications appeared, of which about 120 were published in the 2000s. Whereas in the first years after the emergence of interest in  $\text{NH}\cdots\pi$  forces they were considered exclusively as a factor contributing to the structuring of proteins, then over time it became clear that they also play a significant role in the processes of molecular recognition. Accordingly, it turned out that  $\text{NH}\cdots\pi$  interactions are found not only in proteins, but also in such types of biomolecules as neurotransmitters or vitamin  $\text{B}_{12}$ . In recent years, they have been increasingly considered when solving problems of medicinal chemistry, creating new materials, and even for improving important production technologies. Synthetic reactions have been discovered whose stereochemistry and even the very possibility is determined by  $\text{NH}\cdots\pi$  interactions. Although  $\text{NH}\cdots\pi$  interactions are generally considered weak with energies in the range  $0.5-5 \text{ kcal mol}^{-1}$ , in some cases they can reach  $15-20 \text{ kcal mol}^{-1}$ , *i.e.*, the level of sufficiently strong non-covalent forces. This is especially facilitated by the participation in  $\text{NH}\cdots\pi$  clusters of positively charged NH donors, for example, ammonium salts and electron-rich  $\pi$ -donors such as pyrrole rings. Taking into account the difficulty of studying  $\text{NH}\cdots\pi$  interactions on real living tissues, their modelling by creating simple and accessible synthetic compounds has become widespread. The most convenient and informative models are those in which the positions of the proton-donor and proton-acceptor groups are preliminary pre-organized. These include *peri*-disubstituted naphthalenes and folded or skeletal compounds. Their important advantage lies in the possibility of conducting research in solution and in the solid form. If the necessary conditions are met in the best  $\text{NH}\cdots\pi$  models, the distance between the NH proton and the centroid of the aromatic ring M can reach only  $2.07 \text{ \AA}$ , and the  $\text{NHM}$  angle approaches  $180^\circ$ .

The study was funded by the Russian Foundation for Basic Research (Project No 20-03-00112).

## 10. List of acronyms

- 5-ASA — 5-aminosalicylic acid,
- ATP — adenosine triphosphate,
- BSSE — basis set superposition error,
- CCDC — Cambridge Crystallographic Data Centre,
- CNT — carbon nanotube,
- DABCO — 1,4-diazabicyclo[2.2.2]octane,
- DF — dispersed fluorescence,
- DFT — density functional theory,
- DKP — diketopiperazine,
- $E_{\text{HB}}$  — hydrogen bond energy,
- $E_{\text{int}}$  — interaction energy,
- FTIR — Fourier-transform infrared spectroscopy,
- HB — hydrogen bonding,
- IMPT — intermolecular perturbation theory,

IP<sub>1</sub> — first ionization potential,  
IRMPD — infrared multiple photon dissociation,  
IR/UV — infrared/ultraviolet spectroscopy,  
LIF — laser-induced fluorescence excitation,  
MD — molecular dynamics,  
MeCN — acetonitrile,  
NCI — non-covalent interaction,  
NMR — nuclear magnetic resonance,  
NT — neurotransmitter,  
R2PI — resonant two-photon ionization,  
RE2PI — mass-resolved one-color resonance enhanced  
two-photon ionization,  
REMPI — resonance-enhanced multiphoton ionization,  
UV-UV HB — ultraviolet–ultraviolet hole-burning,  
VDW — van der Waals,  
XRD — X-Ray diffraction,  
ZPE — zero-point energy.

## 11. References

- C.Tanford, J.Reynolds. *Nature's Robots: a History of Proteins*. (Oxford: University Press, 2001)
- C.Branden, J.Toose. *Introduction to Protein Structure*. (2nd Edn). (Taylor & Francis, 1999)
- A.M.Lesk. *Introduction to Protein Architecture — the Structural Biology of Proteins*. (Oxford: Oxford University Press, 2001)
- L.Pauling, R.B.Corey, H.R.Branson. *Proc. Natl. Acad. Sci. USA*, **37**, 205 (1951)
- L.Pauling, R.B.Corey. *J. Am. Chem. Soc.*, **72**, 5349 (1950)
- R.Vargas, J.Garza, R.A.Friesner, H.Stern, B.P.Hay, D.A.Dixon. *J. Phys. Chem. A*, **105**, 4963 (2001)
- L.Regad, J.Martin, G.Nuel, A.-C.Camproux. *BMC Bioinformatics*, **11**, 75 (2010)
- E.Gloaguen, M.Mons, K.Schwing, M.Gerhards. *Chem. Rev.*, **120**, 12490 (2020)
- J.F.Malone, C.M.Murray, M.H.Charlton, R.Docherty, A.J.Lavery. *J. Chem. Soc., Faraday Trans.*, **93**, 3429 (1997)
- S.K.Burley, G.A.Petsko. *FEBS Lett.*, **203**, 139 (1986)
- T.Steiner, G.Koellner. *J. Mol. Biol.*, **305**, 535 (2001)
- J.Fernandez-Recio, A.Romero, J.Sancho. *J. Mol. Biol.*, **290**, 319 (1999)
- M.F.Perutz. *Phil. Trans. R. Soc. A*, **345**, 105 (1993)
- H.Yao, H.Ke, X.Zhang, S.J.Pan, M.S.Li, L.P.Yang, G.Schreckenbach, W.Jiang. *J. Am. Chem. Soc.*, **140**, 13466 (2018)
- H.Yao, Y.M.Wang, M.Quan, M.U.Farooq, L.P.Yang, W.Jiang. *Angew. Chem., Int. Ed.*, **132**, 20117 (2020)
- K.Baskaran, C.W.Wilburn, J.R.Wedell, L.M.I.Koharudin, E.L.Ulrich, A.D.Schuyler, H.R.Eghbalian, A.M.Gronenborn, J.C.Hoch. *Magn. Reson.*, **2**, 765 (2021)
- J.B.O.Mitchell, C.L.Nandi, I.K.McDonald, J.M.Thornton, S.L.Price. *J. Mol. Biol.*, **239**, 315 (1994)
- M.F.Perutz, G.Fermi, D.J.Abraham, C.Poyart, E.Bursaux. *J. Am. Chem. Soc.*, **108**, 1064 (1986)
- A.F.Pozharskii, V.A.Ozeryanskii, E.A.Filatova, O.V.Dyablo, O.G.Pogosova, G.S.Borodkin, A.Filarowski, D.V.Steglenko. *J. Org. Chem.*, **84**, 726 (2019)
- A.F.Pozharskii, O.V.Dyablo, O.G.Pogosova, V.A.Ozeryanskii, A.Filarowski, K.M.Vasilikhina, N.A.Dzhangiryan. *J. Org. Chem.*, **85**, 12468 (2020)
- A.Pérez-Mellor, I.Alata, V.Lepere, A.Zehnacker. *J. Mol. Struct.*, **349**, 71 (2018)
- E.V.Anslin, D.A.Dougherty. *Modern Physical Organic Chemistry*. (Sausalito, California: University Science Book, 2006)
- J.C.Ma, D.A.Dougherty. *Chem. Rev.*, **97**, 1303 (1997)
- A.S.Mahadevi, G.N.Sastry. *Chem. Rev.*, **113**, 2100 (2013)
- D.A.Rodham, S.Suzuki, R.D.Suenram, F.J.Lovas, S.Dasgupta, W.A.Goddard III, G.A.Blake. *Nature*, **362**, 735 (1993)
- S.Tsuzuki. *Struc. Bond.*, **115**, 149 (2005)
- K.Weyers, T.Freudenberg, H.H.Ritze, W.Radlo, V.Stert. *Z. Phys. D*, **39**, 217 (1997)
- M.Mons, I.Dimicoli, B.Tardivel, F.Piuzzi, V.Brenner, Ph.Millié. *Phys. Chem. Chem. Phys.*, **4**, 571 (2002)
- M.Mons, I. Dimicoli, F. Piuzzi. *Rev. Phys. Chem.*, **21**, 101 (2002)
- S.Tsuzuki, K.Honda, T.Uchimaru, M.Mikami, K.Tanabe. *J. Am. Chem. Soc.*, **122**, 11450 (2000)
- S.Vaupel, B.Brutschy, P.Tarakeshwar, K.S.Kim. *J. Am. Chem. Soc.*, **128**, 5416 (2006)
- D.Quñonero, A.Frontera, D.Escudero, P.Ballester, A.Costa, P.M.Deyà. *Theor. Chem. Account*, **120**, 385 (2008)
- X.Wang, P.P.Power. *Angew. Chem., Int. Ed.*, **50**, 10965 (2011)
- L.V.Saloutina, A.Y.Zapevalov, V.I.Saloutin, M.I.Kodess, P.A.Slepukhin. *Russ. J. Org. Chem.*, **45**, 865 (2009)
- Y.Zhang, Y.Zhang, W.Ye, Z.Li, S.Jin, M.Guo, L Bai, D.Wang. *J. Mol. Struct.*, **1241**, 130614 (2021)
- B.M.Giuliano, L.Evangelisti, A.Maris, W.Caminati. *Chem. Phys. Lett.*, **485**, 36 (2010)
- N.M.Tonge, E.C.MacMahon, I.Pugliesi, M.C.R.Cockett. *J. Chem. Phys.*, **126**, 154319 (2007)
- M.P.Gosling, I.Pugliesi, M.C.R.Cockett. *Phys. Chem. Chem. Phys.*, **12**, 132 (2010)
- G.Piani, M.Pasquini, G.Pietraperzia, M.Becucci, A.Armentano, E.Castellucci. *Chem. Phys. Lett.*, **434**, 25 (2007)
- M.C.R.Cockett, M.Miyazaki, K.Tanabe, M.Fujii. *Phys. Chem. Chem. Phys.*, **13**, 15633 (2011)
- B.M.Giuliano, A.Maris, S.Melandri, W.Caminati. *J. Phys. Chem. A*, **113**, 14277 (2009)
- P.C.Singh, G.N.Patwari. *J. Phys. Chem. A*, **112**, 4426 (2008)
- R.Sedlak, P.Hobza, G.N.Patwari. *J. Phys. Chem. A*, **113**, 6620 (2009)
- C.Tanner, D.Henseler, S.Leutwyler, L.L.Connell, P.M.Felker. *J. Chem. Phys.*, **118**, 9157 (2003)
- R.Kanya, Y.Ohshima. *Phys. Chem. Chem. Phys.*, **5**, 3851 (2003)
- A.Pandith, G.Hazra, H.S.Kim. *Spectrochim. Acta Part A: Mol. Biomol. Spectrosc.*, **178**, 151 (2017)
- A.D.Nikolić, N.L.Kobilarov, A.N.Brzić. *J. Mol. Struct.*, **99**, 179 (1983)
- A.D.Nikolić, S.D.Petrović, N.Perišić-Janjić, N.L.Kobilarov. *J. Mol. Struct.*, **143**, 329 (1986)
- A.D.Nikolić, M.Tarjani, N.Perišić-Janjić, S.D.Petrović. *J. Mol. Struct.*, **174**, 129 (1988)
- A.Nikolić, S.Petrović, D.Antonović, L.Gobor. *J. Mol. Struct.*, **408/409**, 355 (1997)
- J.Cheng, C.Kang, W.Zhu, X.Luo, C.M.Puah, K.Chen, J.Shen, H.Jiang. *J. Org. Chem.*, **68**, 7490 (2003)
- A.F.Pozharskii, E.A.Zvezdina. *Russ. Chem. Rev.*, **42**, 37 (1973)
- J.Wu, X.Cui, X.Mi, Y.Li, Y.Wu. *Chem. Commun.*, **46**, 6771 (2010)
- Y.N.Belokon, N.B.Bespalova, T.D.Churkina, I.Císařová, M.G.Ezernitskaya, S.R.Harutyunyan, R.Hrdina, H.B.Kagan, P.Kočovský, K.A.Kochetkov, O.V.Larionov, K.A.Lyssenkov, M.North, M.Poláček, A.S.Peregudov, V.V.Prisyazhnyuk, S.Vyskočil. *J. Am. Chem. Soc.*, **125**, 12860 (2003)
- M.A.Aldamen, M.Sinnokrot. *J. Struct. Chem.*, **55**, 53 (2014)
- J.Jian, R.Hammink, C.J.McKenzie, F.M.Bickelhaupt, J.Poater, J.Mecinovic. *Chem. – Eur. J.*, **27**, 5721 (2021)
- H.Andleeb, I.Khan, A.Franconetti, M.N.Tahir, J.Simpson, S.Hameed, A.Frontera. *CrystEngComm*, **21**, 1780 (2019)
- M.K.Bharty, R.K.Dani, S.K.Kushawaha, O.Prakash, R.K.Singh, V.K.Sharma, R.N.Kharwar, N.K.Singh. *Spectrochim. Acta Part A: Mol. Biomol. Spectrosc.*, **145**, 98 (2015)

59. E.A.Filatova, A.V.Gulevskaya, A.F.Pozharskii, E.A.Ermolenko, V.A.Ozeryanskii, A.D. Misharev. *Chem. Select*, **5**, 9932 (2020)
60. A.F.Pozharskii, A.T.Soldatenkov, A.R.Katritzky. *Heterocycles in Life and Society*. (2nd Ed.). (Wiley, 2011)
61. R.Goddard, O.Heinemann, C.Krüger. *Acta Crystallogr. Sect. C*, **53**, 1846 (1997)
62. L.Pejov. *Chem. Phys. Lett.*, **339**, 269 (2001)
63. A.R.Katritzky, A.F.Pozharskii. *Handbook of Heterocyclic Chemistry*. (2nd Ed.). (Amsterdam: Pergamon, 2000)
64. D.A.Evans, G.Borg, K.A.Scheidt. *Angew. Chem., Int. Ed.*, **41**, 3188 (2002)
65. V.Stefov, L.Pejov, B.Šoptrajanov. *J. Mol. Struct.*, **649**, 231 (2003)
66. I.Dauster, C.A.Rice, P.Zielke, M.A. Suhmet. *Phys. Chem. Chem. Phys.*, **10**, 2827 (2008)
67. C.Pfaffen, D.Infanger, P.Ottiger, H.M.Frey, S.Leutwyler. *Phys. Chem. Chem. Phys.*, **13**, 14110 (2011)
68. H.S.Biswal, E.Gloaguen, M.Mons, S.Bhattacharyya, P.R.Shirhatti, S.Wategaonkar. *J. Phys. Chem. A*, **115**, 9485 (2011)
69. M.A.Trachsel, P.Ottiger, H.M.Frey, C.Pfaffen, A.Bihlmeier, W.Klopper, S.Leutwyler. *J. Phys. Chem. B*, **119**, 7778 (2015)
70. M.Balón, M.A.Muoz, P.Guardado, C.Carmona. *Photochem. Photobiol.*, **64**, 531 (1996)
71. M.Balón, P.Guardado, M.A.Muoz, C.Carmona. *Biospectroscopy*, **4**, 185 (1998)
72. M.A.Muoz, O.Sama, M.Galán, P.Guardado, C.Carmona, M.Balón. *J. Phys. Chem. B*, **103**, 8794 (1999)
73. S.Tsuzuki, M.Mikami, S.Yamada. *J. Am. Chem. Soc.*, **129**, 8656 (2007)
74. P.Ottiger, C.Pfaffen, R.Leist, S.Leutwyler. *J. Phys. Chem. B*, **113**, 2937 (2009)
75. R.Leist, J.A.Frey, P.Ottiger, H.M.Frey, S.Leutwyler, R.A.Bachorz, W.Klopper. *Angew. Chem., Int. Ed.*, **26**, 7449 (2007)
76. R.A.Bachorz, F.A.Bischoff, S.Hofener, W.Klopper, P.Ottiger, R.Leist, J.A.Frey, S.Leutwyler. *Phys. Chem. Chem. Phys.*, **10**, 2758 (2008)
77. R.Leist, J.A.Frey, S.Leutwyler. *J. Phys. Chem. A*, **110**, 4180 (2006)
78. J.A.Frey, R.Leist, S.Leutwyler. *J. Phys. Chem. A*, **110**, 4188 (2006)
79. J.H.Yeh, T.L.Shen, D.G.Nocera, G.E.Leroi, I.Suzuka, H.Ozawa, Y.Namuta. *J. Phys. Chem.*, **100**, 4385 (1996)
80. K.Sugawara, J.Miyawaki, T.Nakanaga, H.Takeo, G.Lembach, D.Djiafari, H.-D.Barth, B.Brutschy. *J. Phys. Chem.*, **100**, 17145 (1996)
81. N.Yamamoto, K.Hino, K.Mogi, K.Ohashi, Y.Sakai, H.Sekiya. *Chem. Phys. Lett.*, **342**, 417 (2001)
82. N.P.Funnell, A.Dawson, W.G.Marshall, S.Parsons. *CrystEngComm*, **15**, 1047 (2013)
83. R.E.Gerkin, W.J.Reppart. *Acta Crystallogr., Sect. C*, **42**, 480 (1986)
84. M.Belloni, M.Manickam, P.R.Ashton, B.M.Kariuki, J.A.Preece, N.Spencer, J.Wilkie. *Mol. Cryst. Liq. Cryst.*, **369**, 17 (2001)
85. C.T.Hu. CCDC 1987990: Experimental Crystal Structure Determination (2020)
86. S.Kato, Y.Nonaka, T.Shimasaki, K.Goto, T.Shinmyozu. *J. Org. Chem.*, **73**, 4063 (2008)
87. H.Jiang, P.Hu, J.Ye, A.Chaturvedi, K.K.Zhang, Y.Li, Y.Long, D.Fichou, C.Kloc, W.Hu. *Angew. Chem., Int. Ed.*, **57**, 8875 (2018)
88. X.Gao, Y.Zhang, Q.Xie, W.Xu, S.Jin, QYe, Y. Yu, B.Chen, H.Liu, D.Wang. *J. Mol. Struct.*, **1236**, 130340 (2021)
89. V.A.Ozeryanskii, A.V.Marchenko, A.F.Pozharskii, A.Filarowski, D.V.Spiridonova. *J. Org. Chem.*, **86**, 3637 (2021)
90. A.L.Llamas-Saiz, C.C.Foces-Foces, J.Elguero. *J. Mol. Struct.*, **328**, 297 (1994)
91. K.Y.Akiba, M.Yamashita, Y.Yamamoto, S.Nagase. *J. Am. Chem. Soc.*, **121**, 10644 (1999)
92. H.Aikawa, Y.Takahira, M.Yamaguchi. *Chem. Commun.*, **47**, 1479 (2011)
93. K.Yamamoto, N.Oyamada, S.Hia, Y.Kobayashi, M.Yamaguchi, H.Maeda, H.Nishihara, T.Uchimaru, E.Kwon. *J. Am. Chem. Soc.*, **135**, 16526 (2013)
94. J.D.Hoefelmeyer, M.Schulte, M.Tschinkl, F.P.Gabba. *Coord. Chem. Rev.*, **235**, 93 (2002)
95. V.Balasubramanian. *Chem. Rev.*, **66**, 567 (1966)
96. G.M.Badger. *Aromatic Character and Aromaticity*. (Cambridge: Cambridge University Press, 1969)
97. J.Zong, J.T.Mague, R.A.Pascal. *J. Am. Chem. Soc.*, **135**, 13235 (2013)
98. P.S.Lakshminarayanan, D.K.Kumar, P.Ghosh. *J. Am. Chem. Soc.*, **128**, 9600 (2006)
99. C.Pariya, C.R.Sparrow, C.K.Back, G.Sandí, F.R.Fronczek, A.W.Maverick. *Angew. Chem., Int. Ed.*, **46**, 6305 (2007)
100. H.Adams, F.J.Carver, C.A.Hunter, N.J.Osborne. *Chem. Commun.*, 2529 (1996)
101. C.A.Ilioudis, M.J.Bearpark, J.W.Steed. *New J. Chem.*, **29**, 64 (2005)
102. P.Lan, A.J.Herlt, A.C.Willis, W.C.Taylor, L.N.Mander. *ACS Omega*, **3**, 1912 (2018)
103. M.Micheloni, M.Formica, V.Fusi, P.Romani, R.Pontellini, P.Dapporto, P.Paoli, P.Rossi, B.Valtancoli. *Eur. J. Inorg. Chem.*, 51 (2000)
104. X.Shi, F.León, Y.Sim, S.Quek, G.Hum, Y.X.J.Khoo, Z.X.Ng, M.Y.Par, H.C.Ong, V.K.Singh, R.Ganguly, J.K.Clegg, J.Díaz, F.García. *Angew. Chem., Int. Ed.*, **59**, 22100 (2020)
105. J.Bachmann, T.S.Teets, D.G.Nocera. *Dalton Trans.*, 4549 (2008)
106. W.J.Westerhaus, O.Knop, M.Falk. *Can. J. Chem.*, **58**, 1355, (1980)
107. P.Tomaszewski, M.Wiszniewski, J.Serwatowski, K.Woźniak, K.Durka, S.Lulinski. *Dalton Trans.*, **47**, 16627 (2018)
108. T.C.Johnstone, A.I.Briceno-Strocchia, D.W.Stephan. *Inorg. Chem.*, **57**, 15299 (2018)
109. S.-L.Zheng, P.Coppens. *CrystEngComm*, **7**, 289 (2005)
110. F.F.Nachtigall, I.Vencato, M.Lazzarotto, F.Nome. *Acta Crystallogr., Sect. C*, **54**, 1007 (1998)
111. Q.Zhao, H.Sun, W.Chen, C.Duan, Y.Liu, Y.Pan, X.You. *Organometallics*, **17**, 156 (1998)
112. A.A.Sidorov, I.G.Fomina, A.E.Malkov, A.V.Reshetnikov, G.G.Aleksandrov, V.M.Novotortsev, S.E.Nefedov, I.L.Eremenko. *Russ. Chem. Bull.*, **49**, 1887 (2000)
113. D.R.Mulford, P.E.Fanwick, I.P.Rothwell. *Polyhedron*, **19**, 35 (2000)
114. I.Fomina, Z.Dobrokhotova, G.Aleksandrov, A.Bogomyakov, M.Fedin, A.Dolganov, T.Magdesieva, V.Novotortsev, I.Eremenko. *Polyhedron*, **29**, 1734 (2010)
115. N.Grüger, H.Wadepohl, L.H.Gade. *Eur. J. Inorg. Chem.*, 5358 (2013)
116. T.Steiner, S.A.Mason. *Acta Crystallogr., Sect. B*, **56**, 254 (2000)
117. H.Adams, K.D.M.Harris, G.A.Hernbury, C.A.Hunter, D.Livingstone, J.F.McCabe. *Chem. Commun.*, 2531 (1996)
118. E.Gloaguen, M.Mons. *Top. Curr. Chem.*, **364**, 225 (2015)
119. K.Schwing, M.Gerhards. *Intern. Rev. Phys. Chem.* **35**, 569 (2016)
120. W.Chin, M.Mons, J.-P.Dognon, F.Piuzzi, B.Tardivel, I.Dimicoli. *Phys. Chem. Chem. Phys.*, **6**, 2700 (2004)
121. W.Chin, M.Mons, J.-P.Dognon, R.Mirasol, G.Chass, I.Dimicoli, F.Piuzzi, P.Butz, B.Tardivel, I.Compagnon, G.von Helden, G.Meijer. *J. Phys. Chem. A*, **109**, 5281 (2005)
122. A.Abo-Riziq, L.Grace, B.Crews, M.P.Callahan, T.van Mourik, M.S.de Vries. *J. Phys. Chem. A*, **115**, 6077 (2011)
123. H.Fricke, G.Schafer, T.Schrader, M.Gerhards. *Phys. Chem. Chem. Phys.*, **9**, 4592 (2007)

124. B.C.Dian, A.Longarte, P.R.Winter, T.S.Zwier. *J. Chem. Phys.*, **120**, 133 (2004)
125. W.Y.Sohn, V.Brenner, E.Gloaguen, M.Mons. *Phys. Chem. Chem. Phys.*, **18**, 29969 (2016)
126. E.Gloaguen, Y.Loquais, J.A.Thomas, D.W.Pratt, M.Mons. *J. Phys. Chem. B*, **117**, 4945 (2013)
127. H.Valdes, V.Spiwok, J.Rezac, D.Reha, A.G.Abo-Riziq, M.S.de Vries, P.Hobza. *Chem. – Eur. J.*, **14**, 4886 (2008)
128. L.C.Snoek, E.G.Robertson, R.T.Kroemer, J.P.Simons. *Chem. Phys. Lett.*, **321**, 49 (2000)
129. S.Dautrey, J.Bodiguel, A.Arrault, B.Jamart-Gregoire. *Tetrahedron*, **68**, 4362 (2012)
130. A.S.Felten, S.Dautrey, J.Bodiguel, R.Vanderesse, C.Didierjean, A.Arrault, B.Jamart-Grégoire. *Tetrahedron*, **64**, 10741 (2008)
131. L.Zhai, M.Nara, Y.Otani, T.Ohwada. *Chem. Commun.*, **57**, 8344 (2021)
132. I.Alata, A.Pérez-Mellor, F.B.Nasr, D.Scuderi, V.Steinmetz, F.Gobert, N.E.Jäidane, A.Zehnacker-Rentien. *J. Phys. Chem. A*, **121**, 7130 (2017)
133. A.Pérez-Mellor, I.Alata, V.Lepère, A.Zehnacker. *J. Phys. Chem. B*, **123**, 6023 (2019)
134. F.BenNasr, A.Pérez-Mellor, I.Alata, V.Lepere, N.E.Jäidane, A.Zehnacker. *Faraday Discuss.*, **212**, 399 (2018)
135. M.Gdaniec, B.Liberek. *Acta Crystallogr., Sect. C*, **42**, 1343 (1986)
136. K.D.Kopple, D.H.Marr. *J. Am. Chem. Soc.*, **89**, 6193 (1967)
137. R.A.Webster. *Neurotransmitters, Drugs and Brain Function*. (New York: Wiley, 2002)
138. B.Chiavarino, M.E.Crestoni, M.Schütz, A.Bouchet, S.Piccirillo, V.Steinmetz, O.Dopfer, S.Fornarini. *J. Phys. Chem. A*, **118**, 7130 (2014)
139. A.Bouchet, M.Schütz, B.Chiavarino, M.E.Crestoni, S.Fornarini, O.Dopfer. *Phys. Chem. Chem. Phys.*, **17**, 25742 (2015)
140. T.Isozaki, H.Iga, T.Suzuki, T.Ichimura. *J. Chem. Phys.*, **126**, 214304 (2007)
141. H.Iga, T.Isozaki, T.Suzuki, T.Ichimura. *J. Phys. Chem. A*, **111**, 5981 (2007)
142. M.Schütz, A.Bouchet, O.Dopfer. *Phys. Chem. Chem. Phys.*, **18**, 26980 (2016)
143. E.Horn, E.R.T.Tiekink, G.P.Jones, B.P.Naiola, L.G.Paleg. *Acta Crystallogr., Sect. C*, **46**, 1575 (1990)
144. B.B.Ivanova. *J. Mol. Struct.*, **1016**, 47 (2012)
145. R.Quevedo, N.Nunez-Dallos, K.Wurst, A.Duarte-Ruiz. *J. Mol. Struct.*, **1029**, 175 (2012)
146. A.M.Andersen. *Acta Chem. Scand.*, **31**, 162 (1977)
147. K.Tamura, A.Wakahara, T.Fujiwara, K.I.Tomita. *Bull. Chem. Soc. Jpn.*, **47**, 2682 (1974)
148. A.Podder, J.K.Dattagupta, N.N.Saha, W.Saenger. *Acta Crystallogr., Sect. B*, **35**, 649 (1979)
149. K.Paxton, T.A.Hamor. *Acta Crystallogr., Sect. B*, **33**, 2143 (1977)
150. L.Cruickshank, A.R.Kennedy, N.Shankland. *J. Mol. Struct.*, **1051**, 132 (2013)
151. J.Giesecke. *Acta Crystallogr., Sect. B*, **36**, 178 (1980)
152. S.Ohba, Y.Ito. *Acta Crystallogr., Sect. E*, **58**, o586 (2002)
153. A.M.Andersen. *Acta Chem. Scand.*, **29**, 871 (1975)
154. D.Carlström, R.Bergin. *Acta Crystallogr.*, **23**, 313 (1967)
155. A.M.Andersen. *Acta Chem. Scand.*, **29**, 239 (1975)
156. D.Carlstrom. *Acta Crystallogr., Sect. B*, **29**, 161 (1973)
157. S.R.Ernst, F.W.J.Cagle. *Acta Crystallogr., Sect. B*, **29**, 1543 (1973)
158. J.J.Bonnet, J.A.Ibers. *J. Am. Chem. Soc.*, **95**, 4829 (1973)
159. K.Kodchakorn, P.Nimmanpipug, S.Phongtamrug, K.Tashiro. *RSC Adv.*, **9**, 19375 (2019)
160. K.Prout, S.R.Critchley, C.R.Ganellin. *Acta Crystallogr. Sect. B*, **30**, 2884 (1974)
161. L.B.Cole, E.M.Holt. *J. Chem. Soc. Perkin Trans. 1*, 151 (1986)
162. M.V.Veidis, G.J.Palenik, R.Schaffrin, J.Trotter. *J. Chem. Soc. A*, 2659 (1969)
163. M.Nardelli, G.Pelizzi, F.Vitali, F.Bordi, P.V.Plazzi, T.Vitali. *Acta Crystallogr. Sect. C*, **43**, 507 (1987)
164. H.Nowell, J.P.Attfield, J.C.Cole. *Acta Crystallogr., Sect. B*, **58**, 835 (2002)
165. A.Wakahara, T.Fujiwara, K.I.Tomita. *Bull. Chem. Soc. Jpn.*, **46**, 2481 (1973)
166. A.Terakita, H.Matsunaga, T.Ueda, T.Eguchi, M.Echigoya, K.Umemoto, M.Godo. *Chem. Pharm. Bull.*, **52**, 546 (2004)
167. G.L.Gartland, G.R.Freeman, C.E.Bugg. *Acta Crystallogr. Sect. B*, **30**, 1841 (1974)
168. A.Amit, L.Mester, B.Klewe, S.Furberg. *Acta Chem. Scand.*, **32**, 267 (1978)
169. D.Rychkov, E.V.Boldyreva, N.A.Tumanov. *Acta Crystallogr. Sect. C*, **69**, 1055 (2013)
170. U.Thewalt, C.E.Bugg. *Acta Crystallogr. Sect. B*, **28**, 82 (1972)
171. R.Venkatraman, F.R.Fronczek. *CCDC 1060080: Experimental Crystal Structure Determination* (2015)
172. W.G.Quarles, D.H.Templeton, A.Zalkin. *Acta Crystallogr. Sect. B*, **30**, 95 (1974)
173. T.Sakaki, A.Sogo, A.Wakahara, T.Kanai, T.Fujiwara, K.I.Tomita. *Acta Crystallogr., Sect. B*, **32**, 3235 (1976)
174. H.Koshima, M.Nagano, T.Asahi. *J. Am. Chem. Soc.*, **127**, 2455 (2005)
175. H.Koshima, S.Honke. *J. Org. Chem.*, **64**, 790 (1999)
176. T.Ishida, M.Inoue, S.Senda, K.I.Tomita. *Bull. Chem. Soc. Jpn.*, **52**, 2953 (1979)
177. T.B.C.Vu, I.Kalkman, W.L.Meerts, C.Brand, Y.N.Svartsov, S.Wiedemann, R.Weinkauff, M.Schmitt. *Phys. Chem. Chem. Phys.*, **11**, 2433 (2009)
178. D.A.Dougherty, D.A.Stauffer. *Science*, **250**, 1558 (1990)
179. R.Shishido, Y.Kawai, A.Fujii. *J. Phys. Chem. A*, **118**, 7297 (2014)
180. A.Frontera, D.Quinonero, P.M.Deya. *Wiley Interdisciplinary Reviews: Computational Molecular Science*, **1**, 440 (2011)
181. W.M.Clark, A.M.Tickner-Eldridge, G.K.Huang, L.N.Pridgen, M.A.Olsen, R.J.Mills, I.Lantos, N.H.Baine. *J. Am. Chem. Soc.*, **120**, 4550 (1998)
182. C.Hedberg, P.G.Andersson. *Adv. Synth. Catal.*, **347**, 662 (2005)
183. D.M.H.Ascough, F.Duarte, R.S.Paton. *J. Am. Chem. Soc.*, **140**, 16740 (2018)
184. A.F.Pozharskii, V.A.Ozeryanskii, O.V.Dyablo, O.G.Pogosova, G.S.Borodkin, A.Filarowski. *Org. Lett.*, **21**, 1953 (2019)
185. S.Blasco, B.Verdejo, C.Bazzicalupi, A.Bianchi, C.Giorgi, C.Soriano, E.García-España. *Org. Biomol. Chem.*, **13**, 843 (2015)
186. S.Goyal, A.Chattopadhyay, K.Kasavajhala, U.D.Priyakumar. *J. Am. Chem. Soc.*, **139**, 14931 (2017)
187. E.Starikov, T.Steiner. *Acta Crystallogr., Sect. B*, **54**, 94 (1998)
188. M.Rajarajeswari, K.Iyakutti, I.Lakshmi, R.Rajeswarapalanichamy, Y.Kawazoe. *Int. J. Computational Mater. Sci. Eng.*, **4**, 1550014 (2015)
189. M.Tyagi, V.Poongavanam, M.Lindhagen, A.Pettersen, P.Sjö, S.Schiesser, J.Kihlberg. *Org. Lett.*, **20**, 5737 (2018)
190. T.M.Fong, M.A.Cascieri, H.Yu, A.Bansal, C.Swain, C.D.Strader. *Nature (London)*, **362**, 350 (1993)
191. S.Kassem, T.van Leeuwen, A.S.Lubbe, M.R.Wilson, B.L.Feringa, D.A.Leigh. *Chem. Soc. Rev.*, **46**, 2592 (2017)
192. R.Iino, K.Kinbara, Z.Bryant. *Chem. Rev.*, **120**, 1 (2020)
193. I.Alfonso, M.I.Burguete, F.Galindo, S.V.Luis, L.Vigara. *J. Org. Chem.*, **72**, 7947 (2007)
194. R.A.Shah, R.Masrat, M.S.Lone, S.Afzal, U.Ashraf, G.M.Rather, A.A.Dar. *J. Mol. Liq.*, **284**, 569 (2019)
195. S.Pramanik, S.Konar, K.Chakraborty, T.Pal, S.Das, S.Chatterjee, M.Dolai, S.Pathak. *J. Mol. Struct.*, **1206**, 127663 (2020)
196. K.Kodama, F.Takase, T.Hirose. *RSC Adv.*, **11**, 18162 (2021)